



ATLAS Note

ATL-COM-PHYS-2019-962

24th March 2021



Draft version 0.1

1

2 WZ + Heavy Flavor Production in pp collisions 3 at $\sqrt{s} = 13$ TeV

4 The ATLAS Collaboration¹, Aaron Webb^a, Peter Onyisi^a, Heather
5 Russell^b, Philip Sommer^c

6 ^a*Univ. of Texas at Austin*

7 ^b*McGill University*

8 ^c*Univ. of Sheffield*

9 A measurement of WZ produced with an associated heavy flavor jet is performed using 140
10 fb^{-1} of proton-proton collision data at $\sqrt{s} = 13 \text{ TeV}$ from the ATLAS experiment at the
11 LHC. The measurement is performed in the fully leptonic decay mode, $\text{WZ} \rightarrow \ell\nu\ell\bar{\nu}$. The
12 cross-section of $\text{WZ} + \text{b-jets}$ is measured to be $X \pm X \pm X$, while the cross-section of $\text{WZ} +$
13 charm is measured as X , with a correlation of X between the two processes.

© 2021 CERN for the benefit of the ATLAS Collaboration.
14 Reproduction of this article or parts of it is allowed as specified in the CC-BY-4.0 license.

15 **Contents**

16	1 Changes and outstanding items	5
17	1.1 Changelog	5
18	1.1.1 Changes relative to v7	5
19	1.1.2 Changes relative to v5	5
20	1.1.3 Changes relative to v4	5
21	1.1.4 Changes relative to v3	6
22	1.1.5 Changes relative to v2	6
23	1.1.6 Changes relative to v1	7
24	1.2 Outstanding Items	7
25	2 Executive Summary	8
26	3 Data and Monte Carlo Samples	9
27	3.1 Data Samples	9
28	3.2 Monte Carlo Samples	10
29	4 Object Reconstruction	11
30	4.1 Trigger	11
31	4.2 Light leptons	12
32	4.3 Jets	13
33	4.4 B-tagged Jets	13
34	4.5 Missing transverse energy	14
35	4.6 Overlap removal	14
36	5 Event Selection and Signal Region Definitions	15
37	5.1 Event Preselection	15
38	5.2 Fit Regions	18
39	5.3 Non-Prompt Lepton Estimation	34
40	5.3.1 $t\bar{t}$ Validation	34
41	5.3.2 Z+jets Validation	38
42	6 tZ Separation Multivariate Analysis	42
43	6.1 Top Mass Reconstruction	43
44	6.2 tZ BDT	43
45	7 Systematic Uncertainties	47
46	8 Results	54
47	9 Conclusion	65
48	A Appendices	68

49	Appendices	68
50	A.1 Non-prompt lepton MVA	68
51	A.2 Non-prompt CR Modelling	71
52	A.3 tZ Interference Studies	76
53	A.4 Alternate tZ Inclusive Fit	80
54	A.5 DSID list	84

55 List of contributions

Aaron Webb	Main analyser. Responsible for ntuple production, fits, and note writing.
Peter Onyisi	Advisor to Aaron Webb. Analysis design and implementation strategy.
Heather Russell	EWK group convener. Note editing, developing analysis strategy.
Philip Sommer	EWK group convener. Note editing, developing analysis strategy.

58 **1 Changes and outstanding items**

59 **1.1 Changelog**

60 This is version 8

61 **1.1.1 Changes relative to v7**

- 62 • Add additional plots of Z+jets and ttbar CRs in Section A.2
63 • Clarified CDI file used, MC ptag, PFlow jet algorithm
64 • Included overlap removal procedure
65 • Included details on PLV

66 **1.1.2 Changes relative to v5**

- 67 • added list of DSIDs to an appendix
68 • included systematics on jet migrations
69 • Updated results section to include simultaneous fit over 1-jet and 2-jet bins, describe
70 unfolding procedure
71 • Updated other sections to account for this change
72 • Included info about migrations in Section 5.2

73 **1.1.3 Changes relative to v4**

- 74 • Fixed various typos, clarified wording
75 • Expanded info about JER uncertainties, electron systematics, theory uncertainties
76 • removed a table on lepton selection, included information in the text instead
77 • Plotted lepton Pt Z and W for Zjet CR, rather than lep 1 and 2
78 • fixed binning in kinematic plots
79 • Included prefit and postfit yield tables
80 • added signal modelling systematics
81 • included alternate fit studies with tZ included in signal

82 **1.1.4 Changes relative to v3**

- 83 • Merged introduction into executive summary, including unblinding details and list of
84 SRs/CRs used
- 85 • listed ptag used (p4133), and release (AB 21.2.127)
- 86 • Included table reftab:xsecUnc listing x-sec uncertainties used
- 87 • Removed selection criteria listed in table ?? (QMisID, AmbiguityType) that were removed
88 from the analysis
- 89 • specified variable used to make truth jet flavor determination (HadronConeExclTruthLa-
90 belIID)
- 91 • fixed bug in MtLepMet calculation, updated selection/fits to account for this
- 92 • Included plots of MtLepMet and PtZ, swapped lep 1 and 2 p_T plots for lep W and lep Z
93 plots
- 94 • updated tZ BDT training to reduce overfitting, updated plots to include error bars, feature
95 importance
- 96 • updated table 8 to clarify selection, fix the tZ_BDT cut used
- 97 • replace a few broken ntuples which included large weight events
- 98 • include DL1r distribution for Z+jets and tt} VRs
- 99 • Expanded section on fakes, included information on derived scale factors from VRs.
- 100 • Changed the kinematic plots to include $p_T(Z)$ and $m_T(W)$, list lepton p_T based on W and
101 Z candidates.

102 **1.1.5 Changes relative to v2**

- 103 • Added alternate VBS samples to include missing b-jet diagrams
- 104 • Included a section on tZ interference effects, ??.
- 105 • Updated to reflect changes for 2018, including the move to PFlow jets, DL1r, updated
106 trigger, and updated AnalysisBase version (now 21.2.127)
- 107 • Revised fit regions, using separate 1-jet and 2-jet fits, with all 2-j regions included
- 108 • updated plots for tZ BDT, added details about the model
- 109 • Included truth jet information

110 **1.1.6 Changes relative to v1**

- 111 • Added GRL list
112 • Fixed latex issue in line 92, typo in line 172
113 • Added tables 6 and ??, summarizing the event and object selection
114 • Added table 2, which includes the DSID of samples used
115 • Included reference to WZ inclusive paper in introduction

116 **1.2 Outstanding Items**

- 117 • Complete interference studies, apply any interference effects observed as a systematic
118 • Update results section with additional studies, possibly including:
119 – Truth jet migration studies
120 – Simultaneous fit over 1j and 2j
121 – Impact of allowing tZ to float
122 • Unblind, update plots and fits to include data
123 • Add cross-section, significance once unblinded

124 2 Executive Summary

125 The production of WZ in association with a heavy flavor jet represents an important background
 126 for many major analyses. This includes any process with leptons and b-jets in the final state,
 127 such as $t\bar{t}H$, $t\bar{t}W$, and $t\bar{t}Z$. While precise measurements have been made of WZ production
 128 [1], $WZ +$ heavy flavor remains poorly understood. This is largely because the QCD processes
 129 involved in the production of the b-jet make it difficult to simulate accurately. This introduces a
 130 large uncertainty for analyses that include this process as a background.

131 Motivated by its relevance to the $t\bar{t}H$ multilepton analysis, we perform a study of the fully
 132 leptonic decay mode of this channel; that is, events where both the W and Z decay leptonically.
 133 Because WZ has no associated jets at leading order, while the major backgrounds for this channel
 134 tend to have high jet multiplicity, events with more than two jets are rejected. This gives a final
 135 state signature of three leptons and one or two jets.

136 Events that meet this selection criteria are sorted into pseudo-continuous b-tagging regions based
 137 on the DL1r b-tag score of their associated jets. This is done to separate $WZ +$ b-jet events from
 138 $WZ +$ charm and $WZ +$ light jets. These regions are fit to data in order make a more accurate
 139 estimate of the contribution of $WZ +$ heavy-flavor, where heavy-flavor jets include b-jets and
 140 charm jets. The full Run-2 dataset collected by the ATLAS detector, representing 139 fb^{-1} of
 141 data from pp collisions at $\sqrt{s} = 13 \text{ TeV}$, is used for this study.

142 All backgrounds are accounted for using Monte Carlo, with the simulation of non-prompt lepton
 143 backgrounds - $Z+jets$ and $t\bar{t}$ - validated using non-prompt Validation Regions.

144 Section 3 details the data and Monte Carlo (MC) samples used in the analysis. The reconstruction
 145 of various physics objects is described in section 4. Section 5 describes the event selection applied
 146 to these samples, along the definitions of the various regions used in the fit. The multivariate
 147 analysis techniques used to separate the tZ background from $WZ +$ heavy flavor are described in
 148 section 6. Section 7 describes the various sources of systematic uncertainties considered in the
 149 fit. Finally, the results of the analysis are summarized in section 8, followed by a brief conclusion
 150 in section 9.

151 The analysis aims to report a cross-section measurement of $WZ+b$ and $WZ+charm$, along with
 152 their correlations, for both 1-jet and 2-jet exclusive regions. The proposed fiducial region for
 153 these measurements includes events with three leptons, where the invariant mass of at least one
 154 opposite charge, same flavor lepton pair falls within 10 GeV of 91.2 GeV , with 1 or 2 associated
 155 jets. An alternate version of the measurement is included in the appendix, which considers tZ as
 156 part of the $WZ+b$ signal.

157 The current state of the analysis shows blinded results for the full Run 2 dataset. Regions
 158 containing $>5\%$ $WZ+b$ events are blinded, and results are from Asimov, MC only fits. Expected
 159 significance and cross-section numbers are reported.

160 3 Data and Monte Carlo Samples

161 Both data and Monte Carlo samples used in this analysis were prepared in the `xAOD` format,
 162 which was used to produce a `DxAOD` sample in the `HIGG8D1` derivation framework. The `HIGG8D1`
 163 framework is designed for the $t\bar{t}H$ multi-lepton analysis, which targets events with multiple
 164 leptons as well as tau hadrons. This framework skims the dataset to remove unneeded variables
 165 as well as entire events. Events are removed from the derivations that do not meet the following
 166 selection:

- 167 • at least two light leptons within a range $|\eta| < 2.6$, with leading lepton $p_T > 15$ GeV and
 168 subleading lepton $p_T > 5$ GeV
- 169 • at least one light lepton with $p_T > 15$ GeV within a range $|\eta| < 2.6$, and at least two hadronic
 170 taus with $p_T > 15$ GeV.

171 Samples were then generated from these `HIGG8D1` derivations with `p-tag` of `p4134` for data
 172 and `p4133` for Monte Carlo using `AnalysisBase` version 21.2.127 modified to include custom
 173 variables.

174 3.1 Data Samples

175 The study uses a sample of proton-proton collision data collected by the ATLAS detector from
 176 2015 through 2018 at an energy of $\sqrt{s} = 13$ TeV, which represents an integrated luminosity of
 177 139 fb^{-1} . This data set was collected with a bunch crossing rate of 25 ns. All data used in this
 178 analysis was verified by data quality checks, having been included in the following Good Run
 179 Lists:

- 180 • `data15_13TeV.periodAllYear_DetStatus-v79-repro20-02_DQDefects-00-02-02`
 181 `_PHYS_StandardGRL_All_Good_25ns.xml`
- 182 • `data16_13TeV.periodAllYear_DetStatus-v88-pro20-21_DQDefects-00-02-04`
 183 `_PHYS_StandardGRL_All_Good_25ns.xml`
- 184 • `data17_13TeV.periodAllYear_DetStatus-v97-pro21-13_Unknown_PHYS_StandardGRL`
 185 `_All_Good_25ns_Triggerno17e33prim.xml`
- 186 • `data18_13TeV.periodAllYear_DetStatus-v102-pro22-04_Unknown_PHYS_StandardGRL`
 187 `_All_Good_25ns_Triggerno17e33prim.xml`

188 Runs included from the AllYear period containers are included.

189 3.2 Monte Carlo Samples

190 Several different generators were used to produce Monte Carlo simulations of the signal and
 191 background processes. For all samples, the response of the ATLAS detector is simulated using
 192 Geant4. The WZ signal samples are simulated using Sherpa 2.2.2 [2]. Specific information
 193 about the Monte Carlo samples being used can be found in Table 1. A list of the specific samples
 194 used by data set ID is shown in Table 2.

Table 1: The configurations used for event generation of signal and background processes, including the event generator, matrix element (ME) order, parton shower algorithm, and parton distribution function (PDF).

Process	Event generator	ME order	Parton Shower	PDF
WZ, VV	SHERPA 2.2.2	MEPS NLO	SHERPA	CT10
tZ	MG5_AMC	LO	PYTHIA 6	CTEQ6L1
t̄tW	MG5_AMC (SHERPA 2.1.1)	NLO (LO multileg)	PYTHIA 8 (SHERPA)	NNPDF 3.0 NLO (NNPDF 3.0 NLO)
t̄t(Z/γ* → ll)	MG5_AMC	NLO	PYTHIA 8	NNPDF 3.0 NLO
t̄tH	MG5_AMC (MG5_AMC)	NLO (NLO)	PYTHIA 8 (HERWIG++)	NNPDF 3.0 NLO [3] (CT10 [4])
tHqb	MG5_AMC	LO	PYTHIA 8	CT10
tHW	MG5_AMC (SHERPA 2.1.1)	NLO (LO multileg)	HERWIG++ (SHERPA)	CT10 (NNPDF 3.0 NLO)
tWZ	MG5_AMC	NLO	PYTHIA 8	NNPDF 2.3 LO
t̄t̄t, t̄t̄t̄t̄	MG5_AMC	LO	PYTHIA 8	NNPDF 2.3 LO
t̄tW+W-	MG5_AMC	LO	PYTHIA 8	NNPDF 2.3 LO
t̄t	POWHEG-BOX v2 [5]	NLO	PYTHIA 8	NNPDF 3.0 NLO
t̄t̄γ	MG5_AMC	LO	PYTHIA 8	NNPDF 2.3 LO
s-, t-channel, Wt single top	POWHEG-BOX v1 [6]	NLO	PYTHIA 6	CT10
qqVV, VVV				
Z → l+l-	SHERPA 2.2.1	MEPS NLO	SHERPA	NNPDF 3.0 NLO

Sample	DSID
WZ	364253, 364739-42
VV	364250, 364254, 364255, 363355-60, 364890
t̄W	410155
t̄Z	410156, 410157, 410218-20
low mass t̄Z	410276-8
Rare Top	410397, 410398, 410399
single Top	410658-9, 410644-5
three Top	304014
four Top	410080
t̄WW	410081
Z + jets	364100-41
low mass Z + jets	364198-215
W + jets	364156-97
Vγ	364500-35
tZ	410560
tW	410013-4
WtZ	410408
VVV	364242-9
VH	342284-5
WtH	341998
t̄tγ	410389
t̄t	410470
t̄tH	345873-5, 346343-5

Table 2: List of Monte Carlo samples by data set ID used in the analysis.

4 Object Reconstruction

All regions defined in this analysis share a common lepton, jet, and overall event preselection. The selection applied to each physics object is detailed here; the event preselection, and the selection used to define the various fit regions, is described in Section 5.

4.1 Trigger

Events are required to be selected by dilepton triggers, as summarized in Table 3.

Dilepton triggers (2015)	
$\mu\mu$ (asymm.)	HLT_mu18_mu8noL1
ee (symm.)	HLT_2e12_lhloose_L12EM10VH
$e\mu, \mu e$ (\sim symm.)	HLT_e17_lhloose_mu14
Dilepton triggers (2016)	
$\mu\mu$ (asymm.)	HLT_mu22_mu8noL1
ee (symm.)	HLT_2e17_lhvloose_nod0
$e\mu, \mu e$ (\sim symm.)	HLT_e17_lhloose_nod0_mu14
Dilepton triggers (2017)	
$\mu\mu$ (asymm.)	HLT_mu22_mu8noL1
ee (symm.)	HLT_2e24_lhvloose_nod0
$e\mu, \mu e$ (\sim symm.)	HLT_e17_lhloose_nod0_mu14
Dilepton triggers (2018)	
$\mu\mu$ (asymm.)	HLT_mu22_mu8noL1
ee (symm.)	HLT_2e24_lhvloose_nod0
$e\mu, \mu e$ (\sim symm.)	HLT_e17_lhloose_nod0_mu14

Table 3: List of lowest p_T -threshold, un-prescaled dilepton triggers used for 2015-2018 data taking.

201 4.2 Light leptons

- 202 Electron candidates are reconstructed from energy clusters in the electromagnetic calorimeter
 203 that are associated with charged particle tracks reconstructed in the inner detector [7]. Electron
 204 candidates are required to have $p_T > 10$ GeV and $|\eta_{\text{cluster}}| < 2.47$. Muon candidates are
 205 reconstructed by combining inner detector tracks with track segments or full tracks in the muon
 206 spectrometer [8]. Muon candidates are required to have $p_T > 10$ GeV and $|\eta| < 2.5$. Candidates
 207 in the transition region between different electromagnetic calorimeter components, $1.37 <$
 208 $|\eta_{\text{cluster}}| < 1.52$, are rejected. A multivariate likelihood discriminant combining shower shape
 209 and track information is used to distinguish real electrons from hadronic showers (fake electrons).
 210 To further reduce the non-prompt electron contribution, the track is required to be consistent
 211 with originating from the primary vertex; requirements are imposed on the transverse impact
 212 parameter significance ($|d_0|/\sigma_{d_0} < 5$) and the longitudinal impact parameter ($|\Delta z_0 \sin \theta_\ell| < 0.5$
 213 mm).
- 214 Muon candidates are reconstructed by combining inner detector tracks with track segments or
 215 full tracks in the muon spectrometer [8]. Muon candidates are required to have $p_T > 10$ GeV
 216 and $|\eta| < 2.5$. The longitudinal impact parameter is the same for both electrons and muons, while
 217 muons are required to pass a slightly tighter transverse impact parameter, $|d_0|/\sigma_{d_0} < 3$.

218 All leptons are required to be isolated, as defined through the standard PLVLoose working point
 219 supported by combined performance groups. Leptons are additionally required to pass a non-
 220 prompt BDT selection described in detail in [9]. Optimized working points and scale factors for
 221 this BDT are taken from that analysis.

222 4.3 Jets

223 Jets are reconstructed from calibrated topological clusters built from energy deposits in the
 224 calorimeters [10], using the anti- k_t algorithm with a radius parameter $R = 0.4$. Particle Flow,
 225 or PFlow, jets are used in the analysis. Jets with energy contributions likely arising from noise
 226 or detector effects are removed from consideration [11], and only jets satisfying $p_T > 25$ GeV
 227 and $|\eta| < 2.5$ are used in this analysis. For jets with $p_T < 60$ GeV and $|\eta| < 2.4$, a jet-track,
 228 association algorithm is used to confirm that the jet originates from the selected primary vertex,
 229 in order to reject jets arising from pileup collisions [12].

230 4.4 B-tagged Jets

231 In order to make a measurement of $WZ +$ heavy flavor it is necessary to distinguish these events
 232 from $WZ +$ light jets. For this purpose, the DL1r b-tagging algorithm is used to distinguish
 233 heavy flavor jets from lighter ones. The DL1r algorithm uses jet kinematics, particularly jet
 234 vertex information, as input for a neural network which assigns each jet a score designed to
 235 reflect how likely that jet is to have originated from a b-quark.

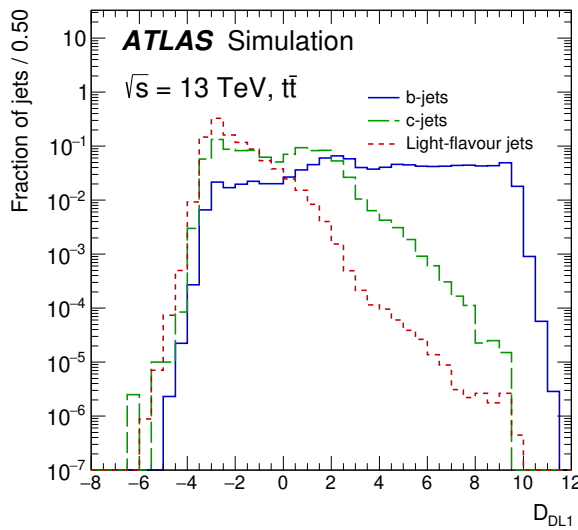


Figure 1: Output distribution of the DL1r algorithm for b-jets, charm jets, and light jets

236 From the output of the BDT, working points (WPs) are developed based on the efficiency of truth
 237 b-jets at particular values of the DL1r algorithm. These WPs are taken from the March 2020 CDI
 238 file, 2020-21-13TeV-MC16-CDI-2020-03-11_v2.root. The working points used in this analysis
 239 are summarized in Table 4.

WP	none	loose	medium	tight	tightest
b eff.	-	85%	77%	70%	60%

Table 4: B-tagging Working Points by tightness and b-jet efficiency

240 A tighter WP will accept fewer b-jets, but reject a higher fraction of charm and light jets.
 241 Generally, analyses that include b-jets will use a fixed working point, for example, requiring that
 242 a jet pass the 70% threshold. By instead treating these working point as bins, e.g. events with
 243 jets that fall between the 85% and 77% WPs fall into one bin, while events with jets passing the
 244 60% WP fall into another, and looking at the full psuedo-continuous DL1r spectrum of the jets,
 245 additional information can be gained. The psuedo-continuous b-tag spectrum is used in this case
 246 to separate out $WZ + b$, $WZ + \text{charm}$, and $WZ + \text{light}$.

247 4.5 Missing transverse energy

248 Missing transverse momentum (E_T^{miss}) is used as part of the event selection. The missing
 249 transverse momentum vector is defined as the inverse of the sum of the transverse momenta of
 250 all reconstructed physics objects as well as remaining unclustered energy, the latter of which is
 251 estimated from low- p_T tracks associated with the primary vertex but not assigned to a hard object,
 252 with object definitions taken from [13]. Light leptons considered in the E_T^{miss} reconstruction are
 253 required to have $p_T > 10$ GeV, while jets are required to have $p_T > 20$ GeV.

254 4.6 Overlap removal

255 To avoid double counting objects and remove leptons originating from decays of hadrons, overlap
 256 removal is performed in the following order: any electron candidate within $\Delta R = 0.1$ of another
 257 electron candidate with higher p_T is removed; any electron candidate within $\Delta R = 0.1$ of a muon
 258 candidate is removed; any jet within $\Delta R = 0.3$ of an electron candidate is removed; if a muon
 259 candidate and a jet lie within $\Delta R = \min(0.4, 0.04 + 10[\text{GeV}] / p_T(\text{muon}))$ of each other, the jet
 260 is kept and the muon is removed.

261 This algorithm is applied to the preselected objects. The overlap removal procedure is summarized
 262 in Table 5.

Keep	Remove	Cone size (ΔR)
electron	electron (low p_T)	0.1
muon	electron	0.1
electron	jet	0.3
jet	muon	$\min(0.4, 0.04 + 10[\text{GeV}]/p_T \text{ (muon)})$
electron	tau	0.2

Table 5: Summary of the overlap removal procedure between electrons, muons, and jets.

263 5 Event Selection and Signal Region Definitions

264 Event are required to pass a preselection described in Section 5.1 and summarized in Table 6.
 265 Those that pass this preselection are divided into various fit regions described in Section 5.2,
 266 based on the number of jets in the event, and the b-tag score of those jets.

267 **5.1 Event Preselection**

268 Events are required to include exactly three reconstructed light leptons passing the requirement
 269 described in 4.2, which have a total charge of ± 1 . As the opposite sign lepton is found to be
 270 prompt the vast majority of the time [9], it is required to be loose and isolated, as defined though
 271 the standard PLVLoose working point supported by combined performance groups. The same
 272 sign leptons are required to be very tightly isolated, as per the recommended PLVTight.

273 The leptons are ordered in the analysis code as 0, 1, and 2. Lepton 0 is the lepton whose charge
 274 is opposite the other two. Lepton 1 is the lepton closest to the opposite charge lepton, i.e. the
 275 smallest ΔR , leaving lepton 2 as the lepton further from the opposite charge lepton. Lepton 0
 276 is required to have $p_T > 10$ GeV, while the same sign leptons, 1 and 2, are required to have
 277 $p_T > 20$ GeV to reduce the contribution of non-prompt leptons.

278 The invariant mass of at least one pair of opposite sign, same flavor leptons is required to fall
 279 within 10 GeV of the mass of the Z boson, 91.2 GeV. Events where one of the opposite sign pairs
 280 have an invariant mass less than 12 GeV are rejected in order to suppress low mass resonances.

281 An additional requirement is placed on the missing transverse energy, $E_T^{\text{miss}} > 20$ GeV, and the
 282 transverse mass of the W candidate, $m(E_T^{\text{miss}} + l_{\text{other}}) > 30$ GeV, where E_T^{miss} is the missing
 283 transverse energy, and l_{other} is the lepton not included in the Z-candidate.

284 Events are required to have one or two reconstructed jets passing the selection described in
 285 Section 4.3. Events with more than two jets are rejected in order to reduce the contribution of
 286 backgrounds such as $t\bar{t}Z$ and $t\bar{t}W$, which tend to have higher jet multiplicity.

Event Selection
Exactly three leptons with charge ± 1
Two tight Iso, tight ID same-charge leptons with $p_T > 20 \text{ GeV}$
One loose Iso, medium ID opposite charge lepton with $p_T > 10 \text{ GeV}$
$m(l^+l^-)$ within 10 GeV of 91.2 GeV
Transverse mass of W-candidate, $m_T(E_T^{\text{miss}} + \text{lep}_{\text{other}}) > 30 \text{ GeV}$
Missing transverse energy, $E_T^{\text{miss}} > 20 \text{ GeV}$
One or two jets with $p_T > 25 \text{ GeV}$

Table 6: Summary of the selection applied to events for inclusion in the fit

287 The event yields in the preselection region for both data and Monte Carlo are summarized in
 288 Table 5.1, which shows good agreement between data and Monte Carlo, and demonstrates that
 289 this region consists primarily of WZ events. The WZ events are split into WZ + b, WZ + c, and
 290 WZ + l based on the truth flavor of the associated jet in the event. Specifically, this determination
 291 is made based on the HadronConeExclTruthLabelID of the jet, as recommended by the b-
 292 tagging working group [14]. In this ordering b-jet supersedes charm, which supersedes light. That
 293 is, WZ + l events contain no charm and no b jets at truth level, WZ + c contain at least one truth
 294 charm and no b-jets, and WZ + b contains at least one truth b-jet.

Process	Events
WZ + b	167.6 ± 6.5
WZ + c	1080 ± 40
WZ + l	7220 ± 310
Other VV	850 ± 140
t̄tW	16.8 ± 2.3
t̄tZ	115 ± 17
rare Top	2.2 ± 0.1
Single top	0.10 ± 0.45
Three top	0.01 ± 0.01
Four top	0.02 ± 0.01
t̄tWW	0.23 ± 0.05
Z + jets	600 ± 260
V + γ	37 ± 54
tZ	190 ± 70
tW	5.5 ± 1.2
WtZ	25.8 ± 1.1
VVV	26.2 ± 0.9
VH	94 ± 7
t̄t	108.68 ± 8
t̄tH	4.3 ± 0.5
Total	10600 ± 530
Data	10574

Table 7: Event yields in the preselection region at 139.0 fb^{-1}

295 Here Other VV represents diboson processes other than WZ, and consists predominantly of
 296 $ZZ \rightarrow ll\bar{l}\bar{l}$ events where one of the leptons is not reconstructed.

297 Simulations are further validated by comparing the kinematic distributions of the Monte Carlo
 298 with data, which are shown in Figure 2. Here, bins with 5% or more WZ+b are blinded.

WZ Fit Region - Inclusive

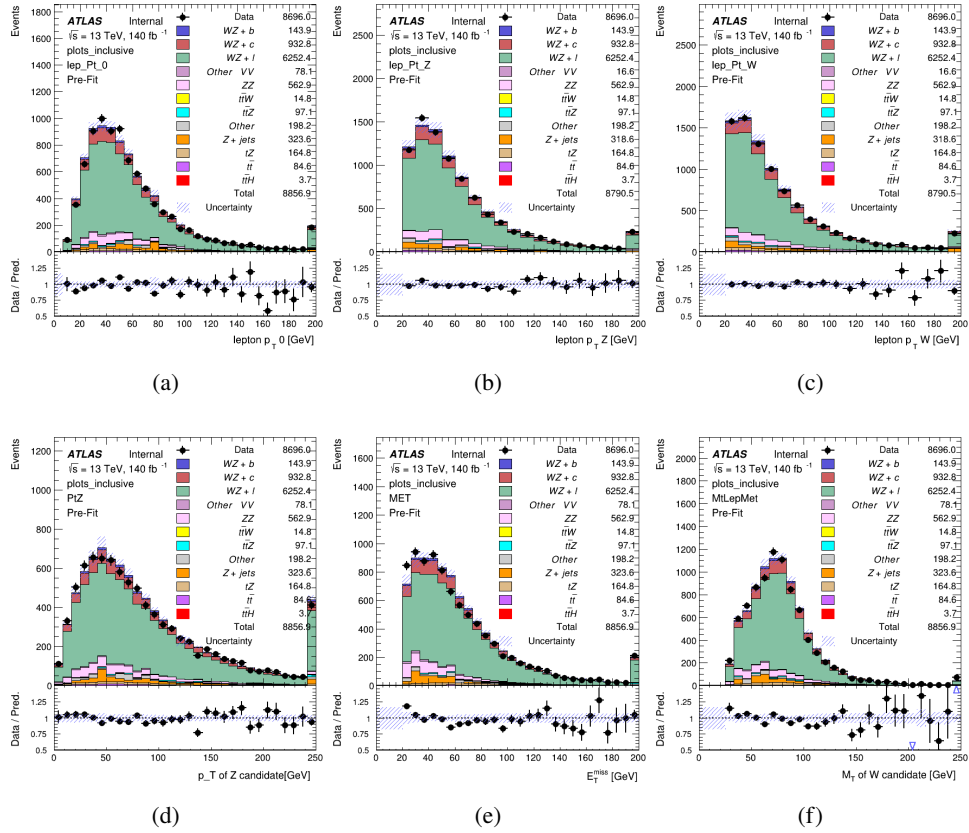


Figure 2: Comparisons between the data and MC distributions in the preselection region for (a) the p_T of the opposite sign lepton, (b) the p_T of the other lepton from the Z candidate, (c) the p_T of the lepton from the W candidate, (d) the p_T of the Z candidate, (e) the E_T^{miss} , and (f) the M_T of the W candidate.

299 5.2 Fit Regions

300 Once preselection has been applied, the remaining events are categorized into one of twelve
 301 orthogonal regions. The regions used in the fit are summarized in Table 8.

Table 8: A list of the regions used in the fit and the selection used for each.

Region	Selection
1j, <85%	$N_{\text{jets}} = 1, n\text{Jets}_{\text{DL1r_85}} = 0$
1j, 85%-77%	$N_{\text{jets}} = 1, n\text{Jets}_{\text{DL1r_85}} = 1, n\text{Jets}_{\text{DL1r_77}} = 0$
1j, 77%-70%	$N_{\text{jets}} = 1, n\text{Jets}_{\text{DL1r_77}} = 1, n\text{Jets}_{\text{DL1r_70}} = 0$
1j, 70%-60%	$N_{\text{jets}} = 1, n\text{Jets}_{\text{DL1r_70}} = 1, n\text{Jets}_{\text{DL1r_60}} = 0$
1j, >60%	$N_{\text{jets}} = 1, n\text{Jets}_{\text{DL1r_60}} = 1, tZ \text{ BDT} > 0.725$
1j tZ CR	$N_{\text{jets}} = 1, n\text{Jets}_{\text{DL1r_60}} = 1, tZ \text{ BDT} < 0.725$
2j, <85%	$N_{\text{jets}} = 2, n\text{Jets}_{\text{DL1r_85}} = 0$
2j, 85%-77%	$N_{\text{jets}} = 2, n\text{Jets}_{\text{DL1r_85}} \geq 1, n\text{Jets}_{\text{DL1r_77}} = 0$
2j, 77%-70%	$N_{\text{jets}} = 2, n\text{Jets}_{\text{DL1r_77}} \geq 1, n\text{Jets}_{\text{DL1r_70}} = 0$
2j, 70%-60%	$N_{\text{jets}} = 2, n\text{Jets}_{\text{DL1r_70}} \geq 1, n\text{Jets}_{\text{DL1r_60}} = 0$
2j, >60%	$N_{\text{jets}} = 2, n\text{Jets}_{\text{DL1r_60}} \geq 1, tZ \text{ BDT} > 0.725$
2j tZ CR	$N_{\text{jets}} = 2, n\text{Jets}_{\text{DL1r_60}} \geq 1, tZ \text{ BDT} < 0.725$

302 The working points discussed in Section 4.4 are used to separate events into fit regions based on
 303 the highest working point reached by a jet in each event. Because the background composition
 304 differs significantly based on the number of b-jets, events are further subdivided into 1-jet and
 305 2-jet regions in order to minimize the impact of background uncertainties.

306 An unfolding procedure is performed to account for differences in the number of reconstructed
 307 jets compared to the number of truth jets in each event. The `AntiKt4TruthDressedWZJets`
 308 truth jet collection is used to make this determination. In order to account for migration of
 309 WZ+1-jet and WZ+2-jet events between the 1-jet and 2-jet bins at reco level, the signal samples
 310 are separated based on the number of truth jets. Events with 0 jets or more than 3 jets at truth
 311 level, yet fall within one of the categories listed in Table 8, are categorized as WZ + other, and
 312 treated as a background. The migration matrix in the number of jets at truth level versus reco
 313 level is shown in Figure 3. The composition of the number of truth jets in each reco jet bin is
 314 taken from MC, with uncertainties in these estimates described in detail in Section 7.

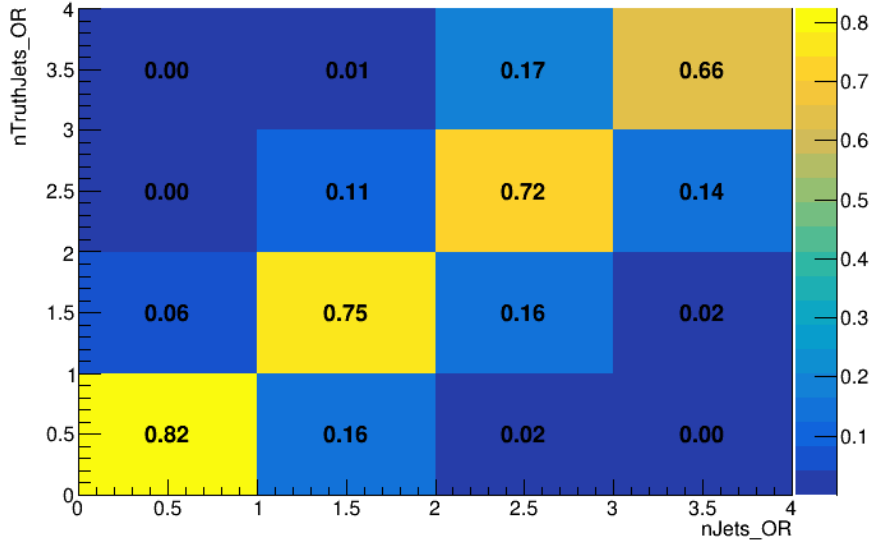


Figure 3: Number of truth jets compared to the number of reconstructed jets in each WZ event falling in the preselection region. Each row is normalized to unity.

315 An additional tZ control region is created based on the BDT described in Section 6. The region
 316 with 1-jet passing the 60% working point is split in two - a signal enriched region of events with
 317 a BDT score greater than 0.03, and a tZ control region including events with less than 0.03. This
 318 cutoff is arrived at by performing an Asimov fit with a variety of cutoffs, and selecting the value
 319 that produces the highest significance for the measurement of WZ + b.

320 The modeling in each region is validated by comparing data and MC predictions for various
 321 kinematic distributions. These plot are shown in Figures 4-17.

WZ Fit Region - 1j Inclusive

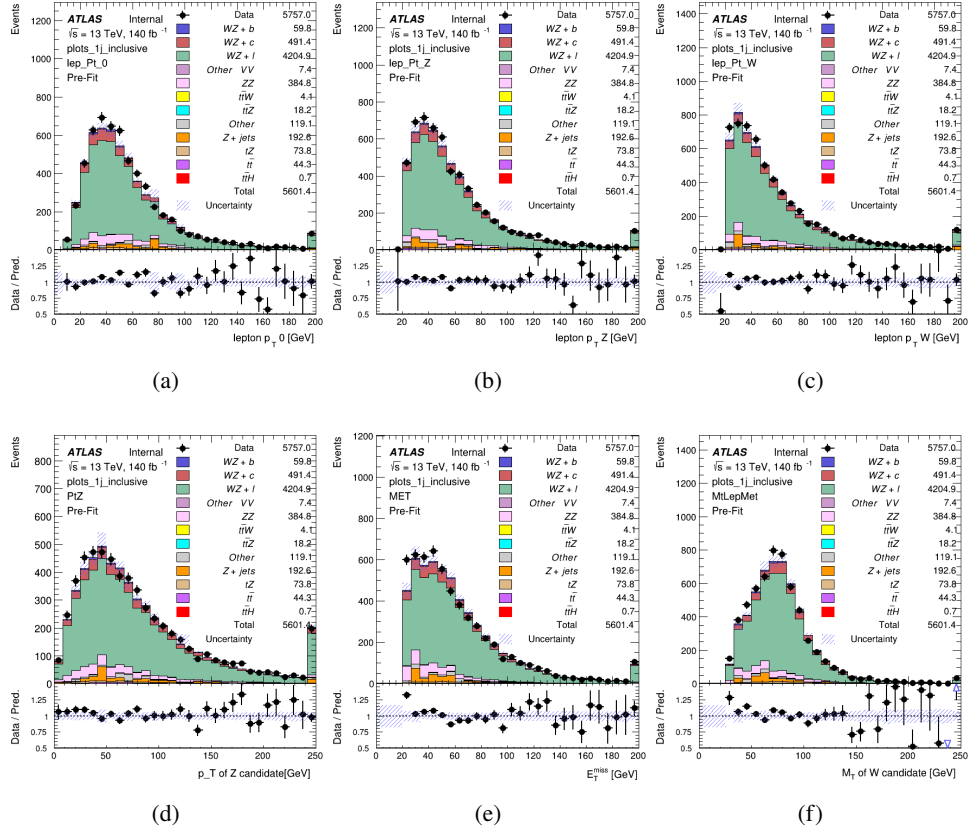


Figure 4: Comparisons between the data and MC distributions in the preselection region for (a) the p_T of the opposite sign lepton, (b) the p_T of the other lepton from the Z candidate, (c) the p_T of the lepton from the W candidate, (d) the p_T of the Z candidate, (e) the E_T^{miss} , and (f) the m_T of the W candidate.

WZ Fit Region - 1j < 85% WP

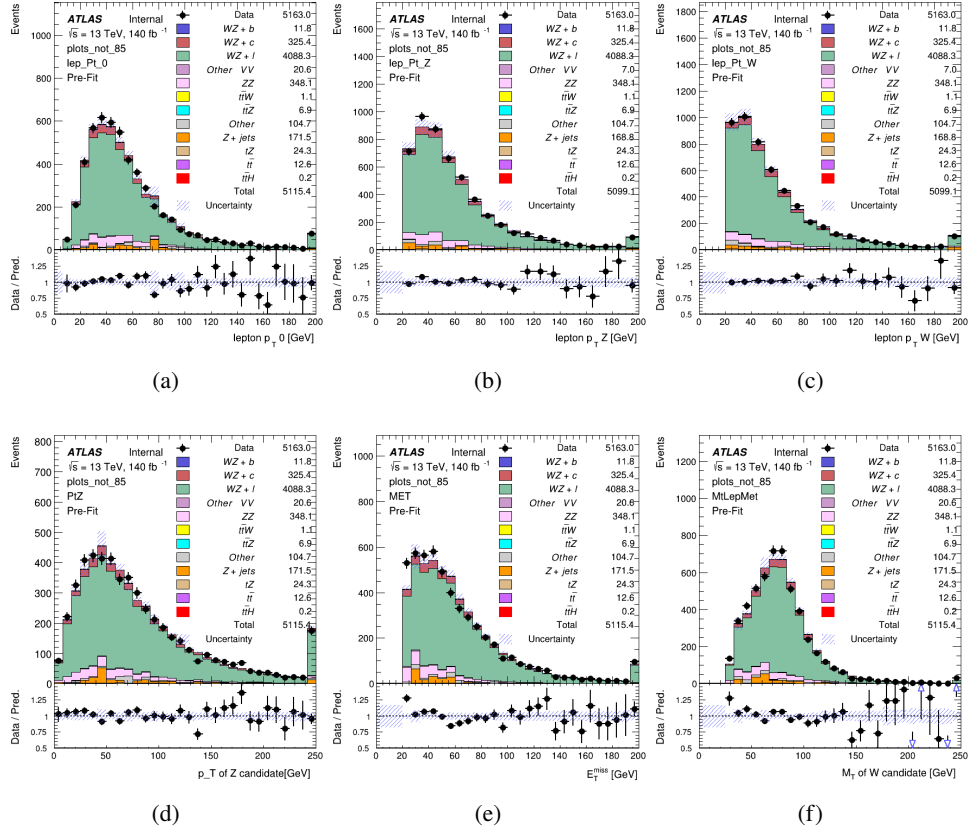


Figure 5: Comparisons between the data and MC distributions in the preselection region for (a) the p_T of the opposite sign lepton, (b) the p_T of the other lepton from the Z candidate, (c) the p_T of the lepton from the W candidate, (d) the p_T of the Z candidate, (e) the E_T^{miss} , and (f) the m_T of the W candidate.

WZ Fit Region - 1j 77-85% WP

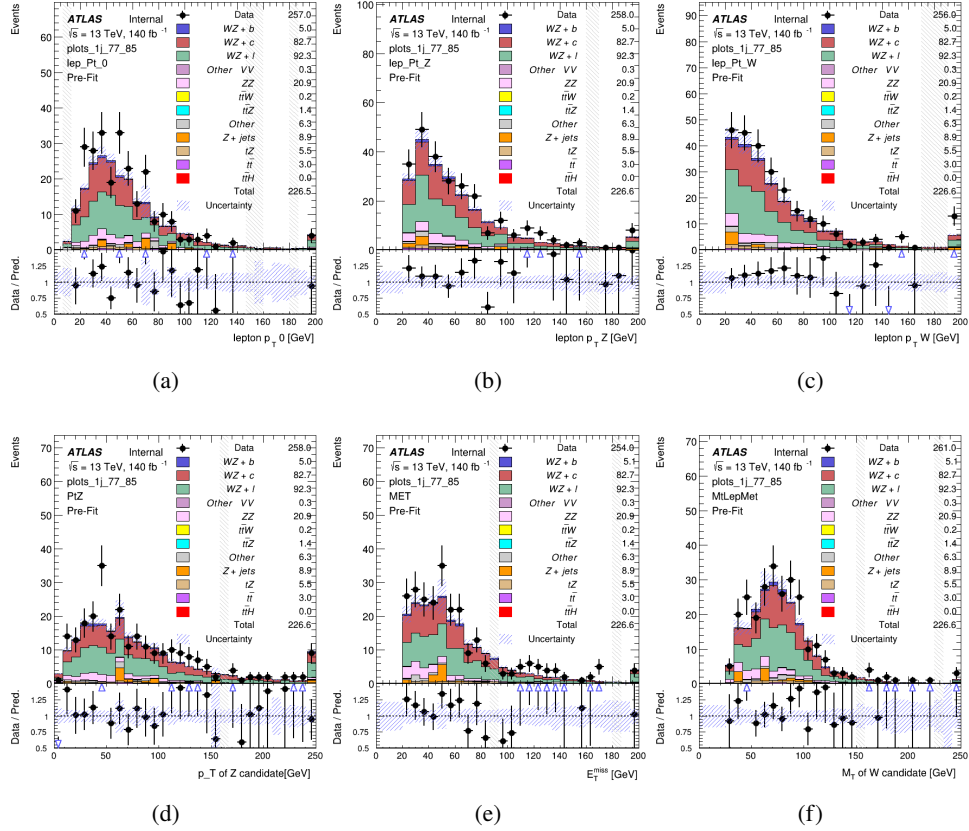


Figure 6: Comparisons between the data and MC distributions in the preselection region for (a) the p_T of the opposite sign lepton, (b) the p_T of the other lepton from the Z candidate, (c) the p_T of the lepton from the W candidate, (d) the p_T of the Z candidate, (e) the E_T^{miss} , and (f) the m_T of the W candidate.

WZ Fit Region - 1j 70-77% WP

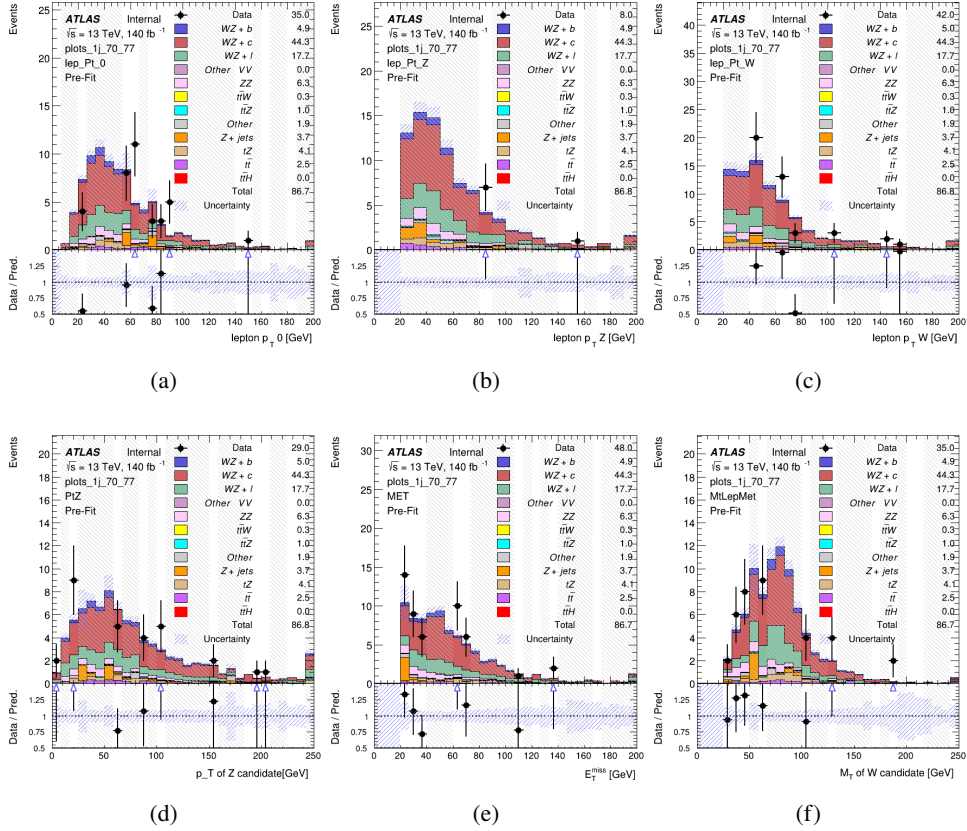


Figure 7: Comparisons between the data and MC distributions in the preselection region for (a) the p_T of the opposite sign lepton, (b) the p_T of the other lepton from the Z candidate, (c) the p_T of the lepton from the W candidate, (d) the p_T of the Z candidate, (e) the E_T^{miss} , and (f) the m_T of the W candidate.

WZ Fit Region - 1j 60-70% WP

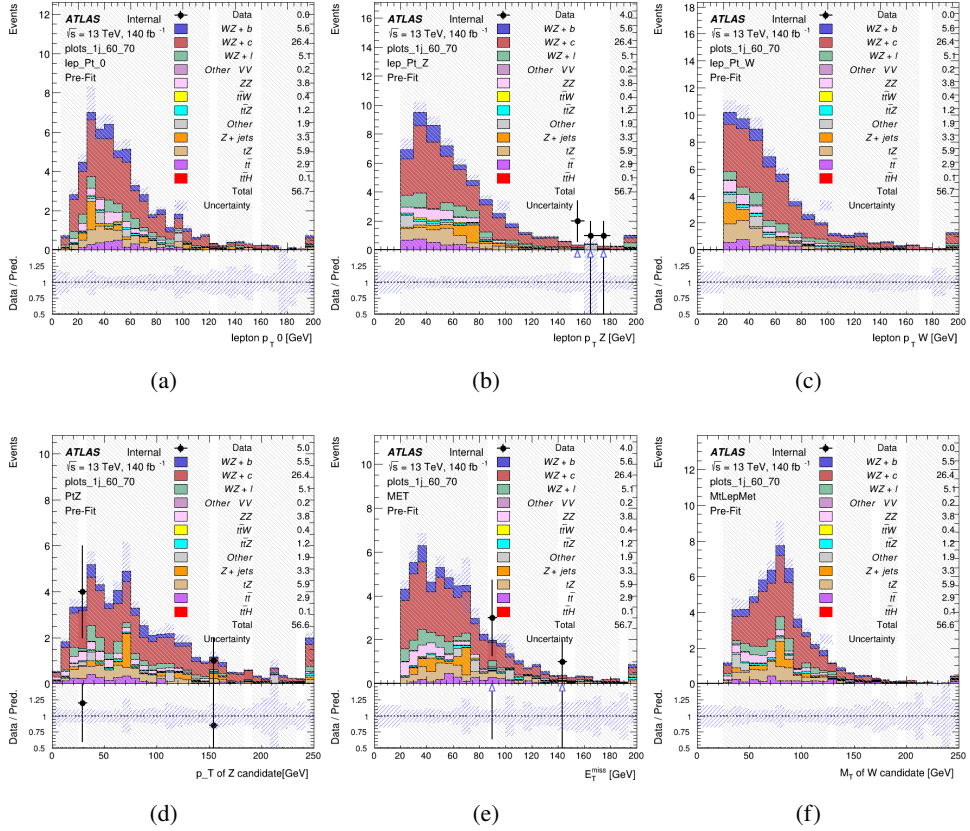


Figure 8: Comparisons between the data and MC distributions in the preselection region for (a) the p_T of the opposite sign lepton, (b) the p_T of the other lepton from the Z candidate, (c) the p_T of the lepton from the W candidate, (d) the p_T of the Z candidate, (e) the E_T^{miss} , and (f) the m_T of the W candidate.

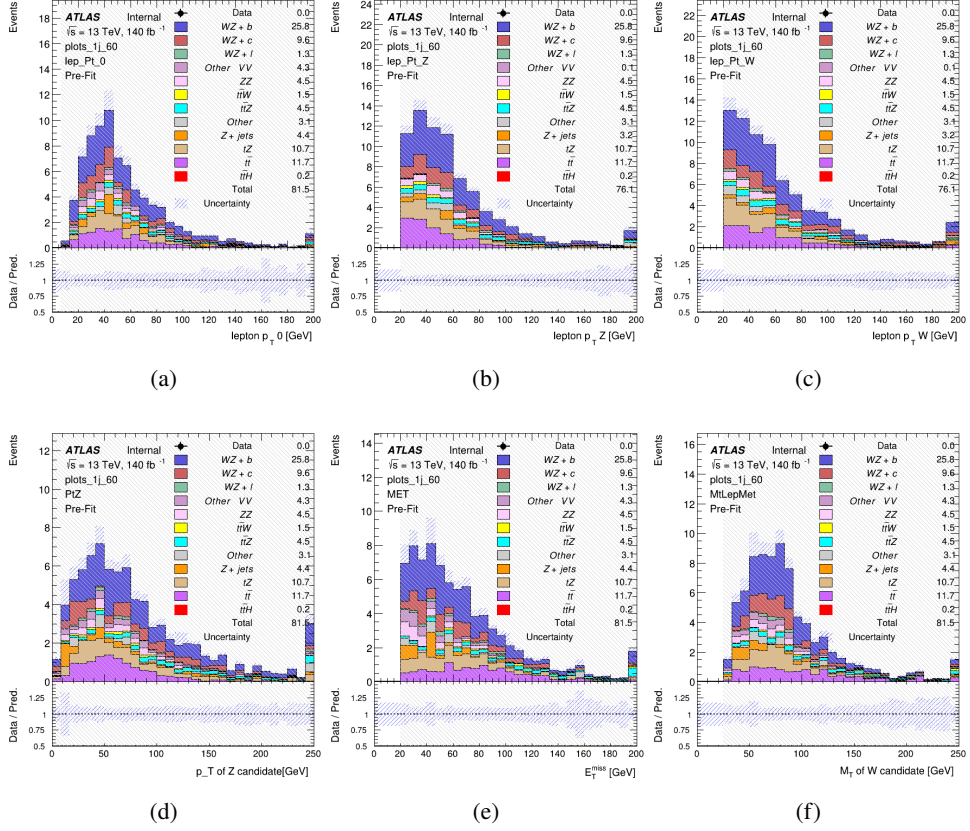
WZ Fit Region - 1j 60% WP

Figure 9: Comparisons between the data and MC distributions in the preselection region for (a) the p_T of the opposite sign lepton, (b) the p_T of the other lepton from the Z candidate, (c) the p_T of the lepton from the W candidate, (d) the p_T of the Z candidate, (e) the E_T^{miss} , and (f) the m_T of the W candidate.

WZ Fit Region - tZ-CR

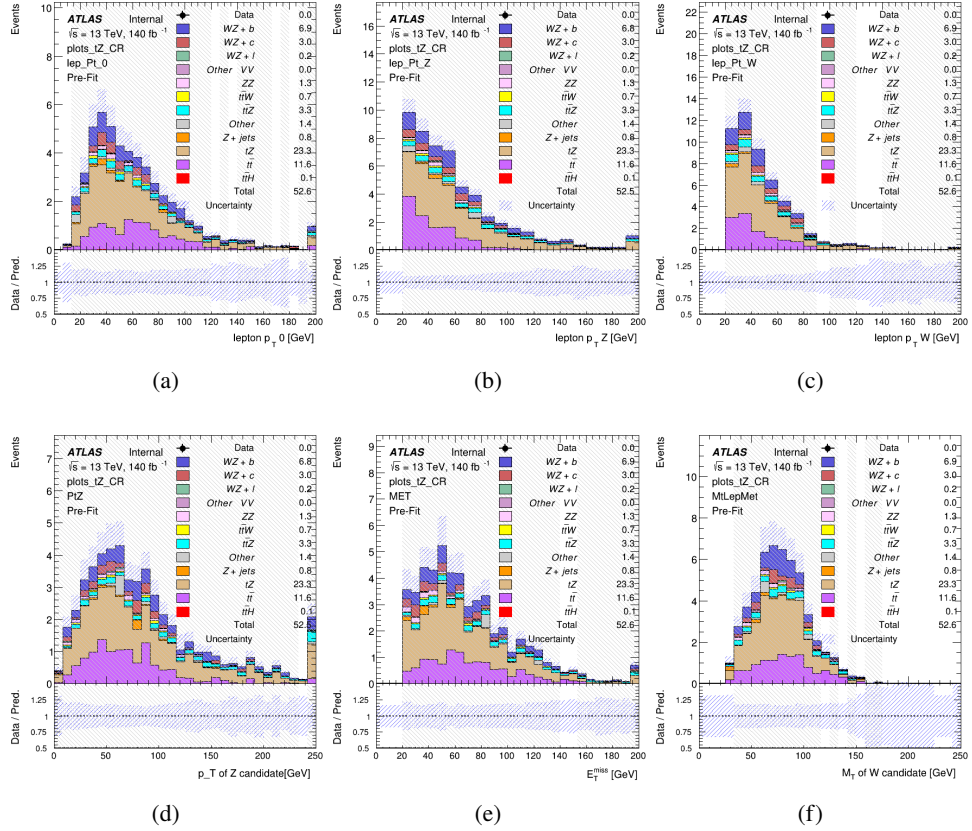


Figure 10: Comparisons between the data and MC distributions in the preselection region for (a) the p_T of the opposite sign lepton, (b) the p_T of the other lepton from the Z candidate, (c) the p_T of the lepton from the W candidate, (d) the p_T of the Z candidate, (e) the E_T^{miss} , and (f) the m_T of the W candidate.

WZ Fit Region - 2j Inclusive

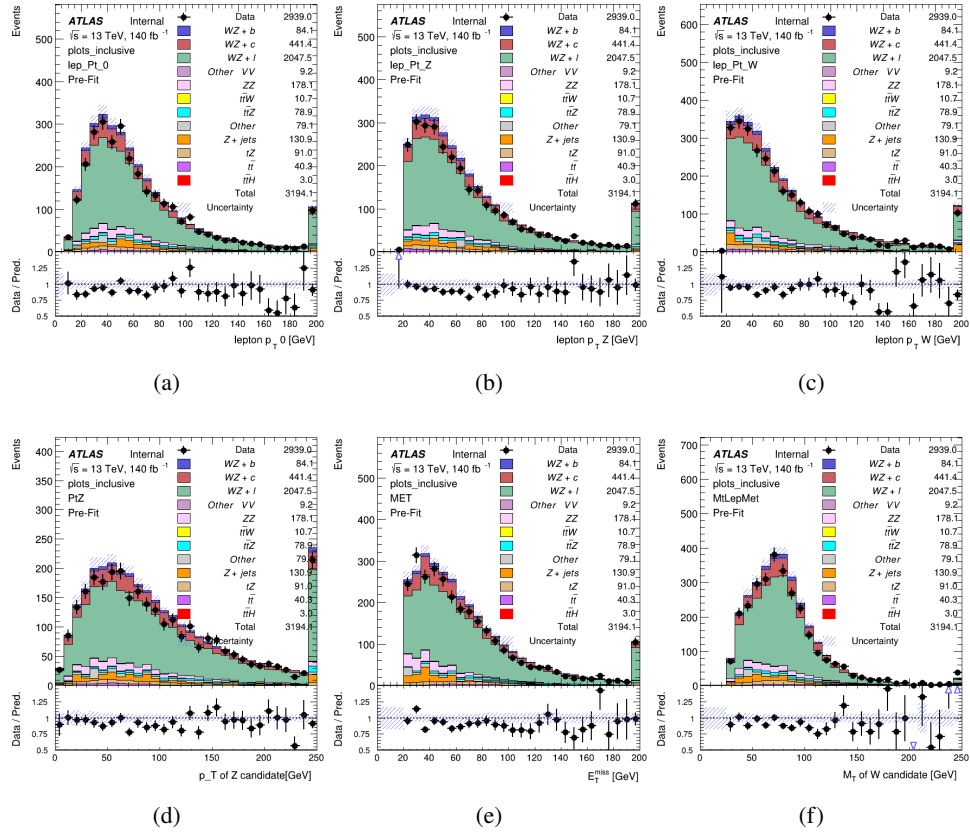


Figure 11: Comparisons between the data and MC distributions in the preselection region for (a) the p_T of the opposite sign lepton, (b) the p_T of the other lepton from the Z candidate, (c) the p_T of the lepton from the W candidate, (d) the p_T of the Z candidate, (e) the E_T^{miss} , and (f) the m_T of the W candidate.

WZ Fit Region - 2j < 85% WP

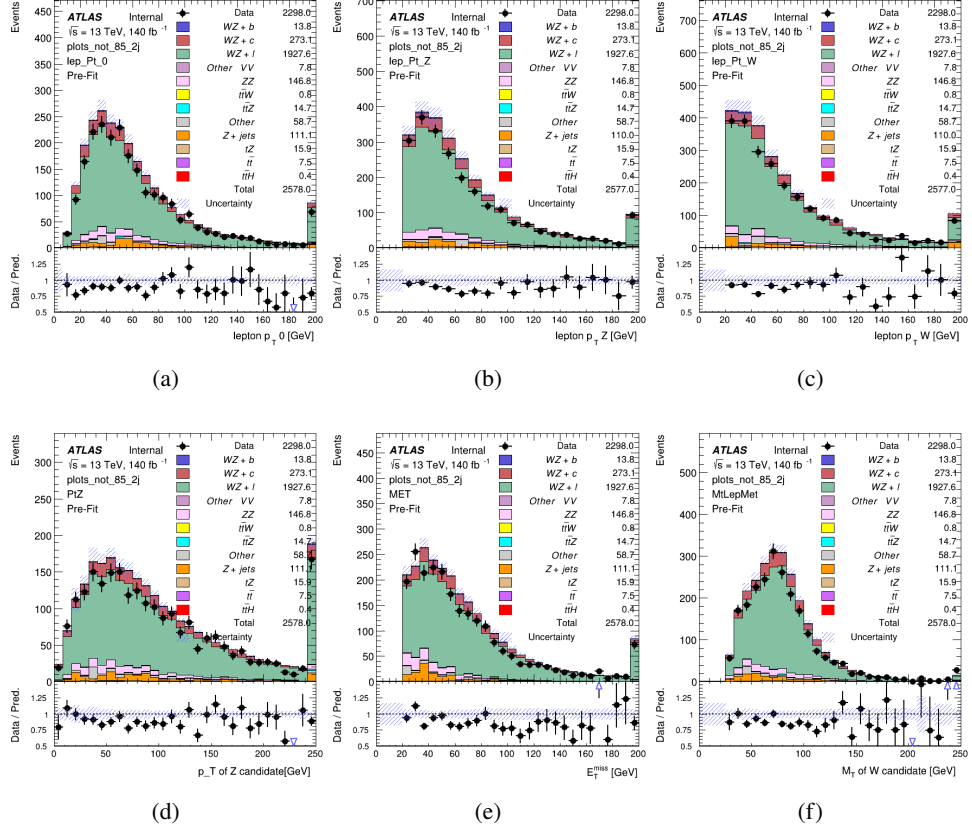


Figure 12: Comparisons between the data and MC distributions in the preselection region for (a) the p_T of the opposite sign lepton, (b) the p_T of the other lepton from the Z candidate, (c) the p_T of the lepton from the W candidate, (d) the p_T of the Z candidate, (e) the E_T^{miss} , and (f) the m_T of the W candidate.

WZ Fit Region - 2j 77-85% WP

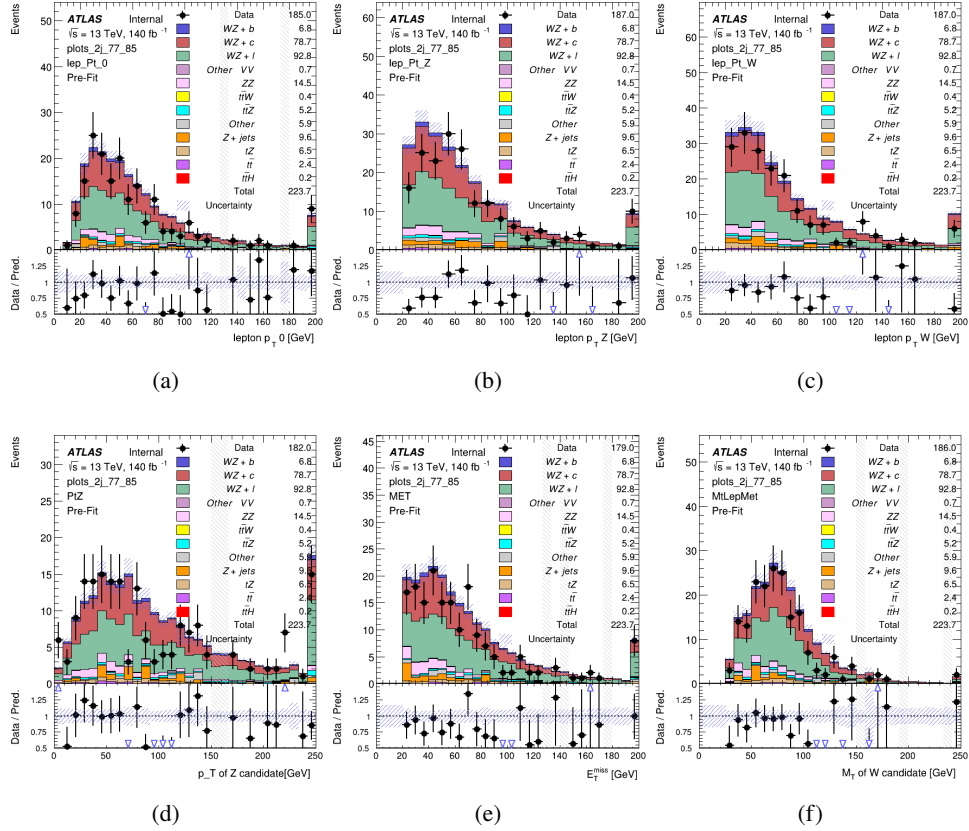


Figure 13: Comparisons between the data and MC distributions in the preselection region for (a) the p_T of the opposite sign lepton, (b) the p_T of the other lepton from the Z candidate, (c) the p_T of the lepton from the W candidate, (d) the p_T of the Z candidate, (e) the E_T^{miss} , and (f) the m_T of the W candidate.

WZ Fit Region - 2j 70-77% WP

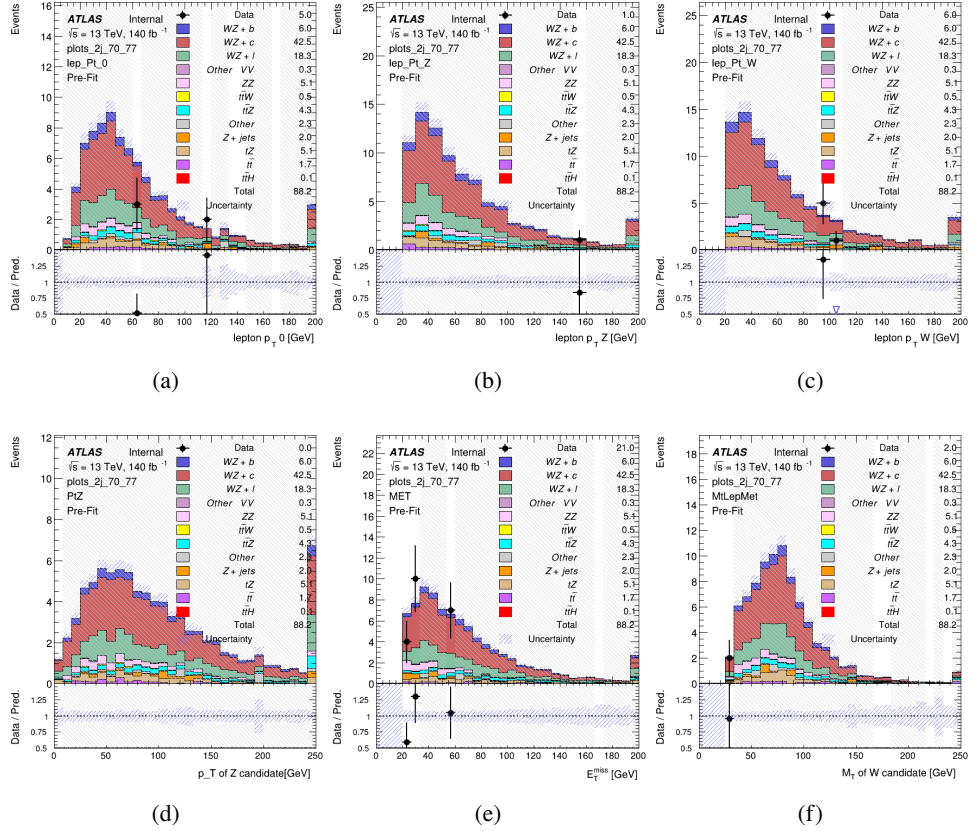


Figure 14: Comparisons between the data and MC distributions in the preselection region for (a) the p_T of the opposite sign lepton, (b) the p_T of the other lepton from the Z candidate, (c) the p_T of the lepton from the W candidate, (d) the p_T of the Z candidate, (e) the E_T^{miss} , and (f) the m_T of the W candidate.

WZ Fit Region - 2j 60-70% WP

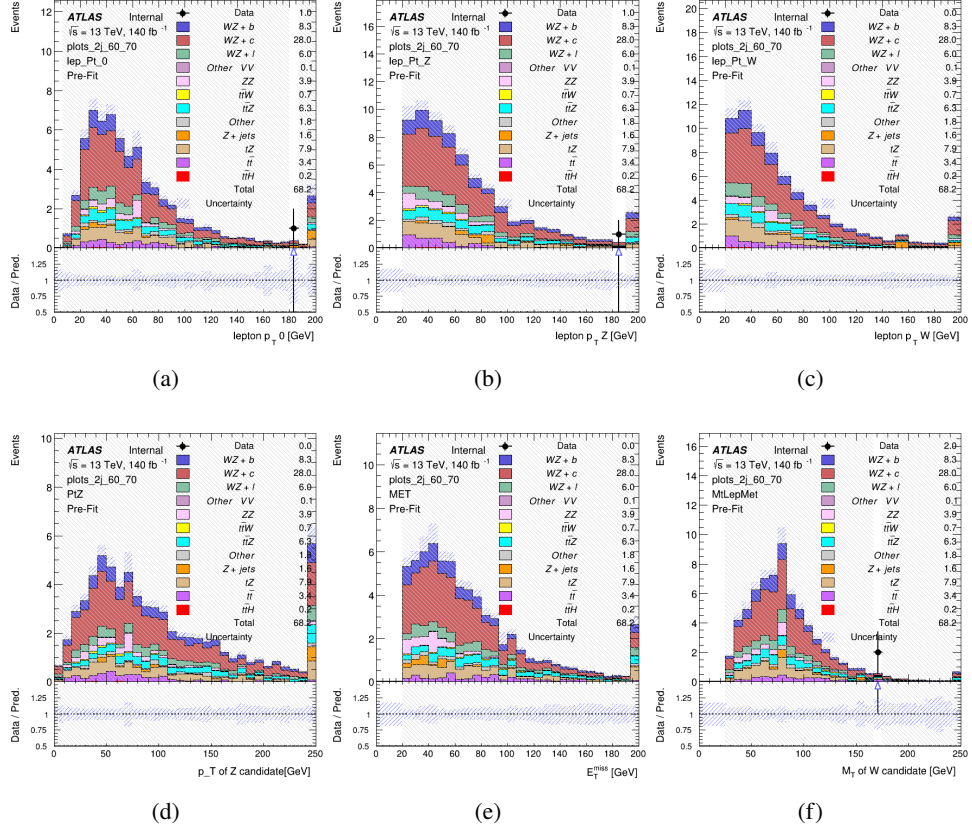


Figure 15: Comparisons between the data and MC distributions in the preselection region for (a) the p_T of the opposite sign lepton, (b) the p_T of the other lepton from the Z candidate, (c) the p_T of the lepton from the W candidate, (d) the p_T of the Z candidate, (e) the E_T^{miss} , and (f) the m_T of the W candidate.

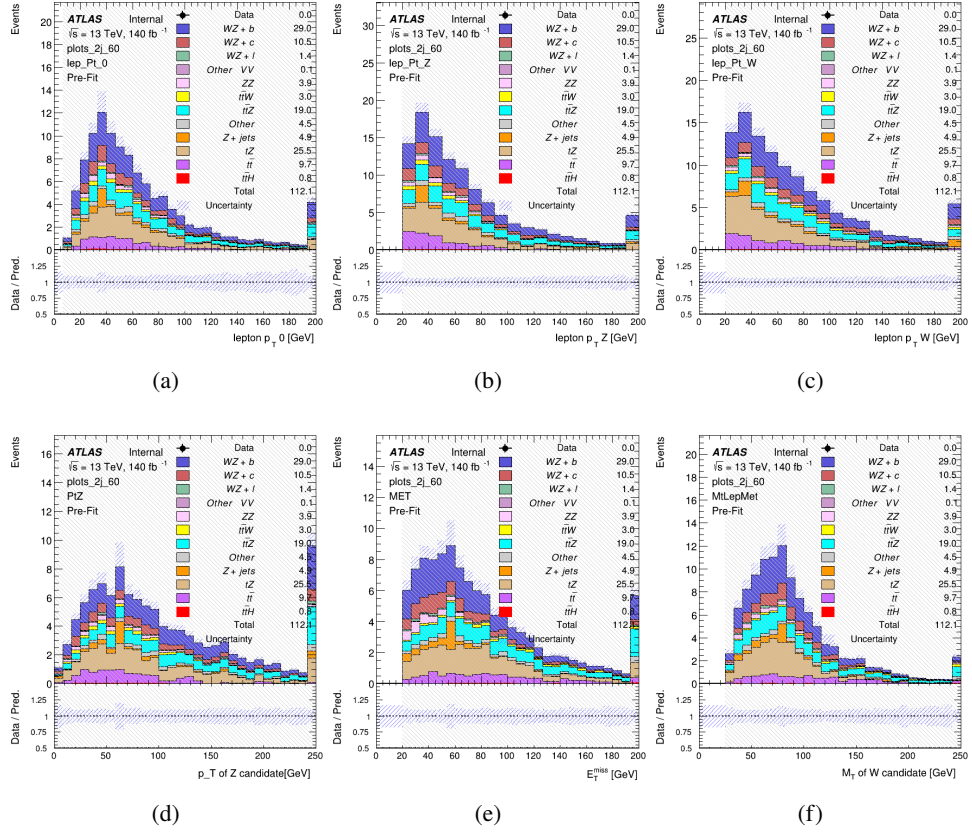
WZ Fit Region - 2j 60% WP

Figure 16: Comparisons between the data and MC distributions in the preselection region for (a) the p_T of the opposite sign lepton, (b) the p_T of the other lepton from the Z candidate, (c) the p_T of the lepton from the W candidate, (d) the p_T of the Z candidate, (e) the E_T^{miss} , and (f) the m_T of the W candidate.

WZ Fit Region - tZ-CR-2j

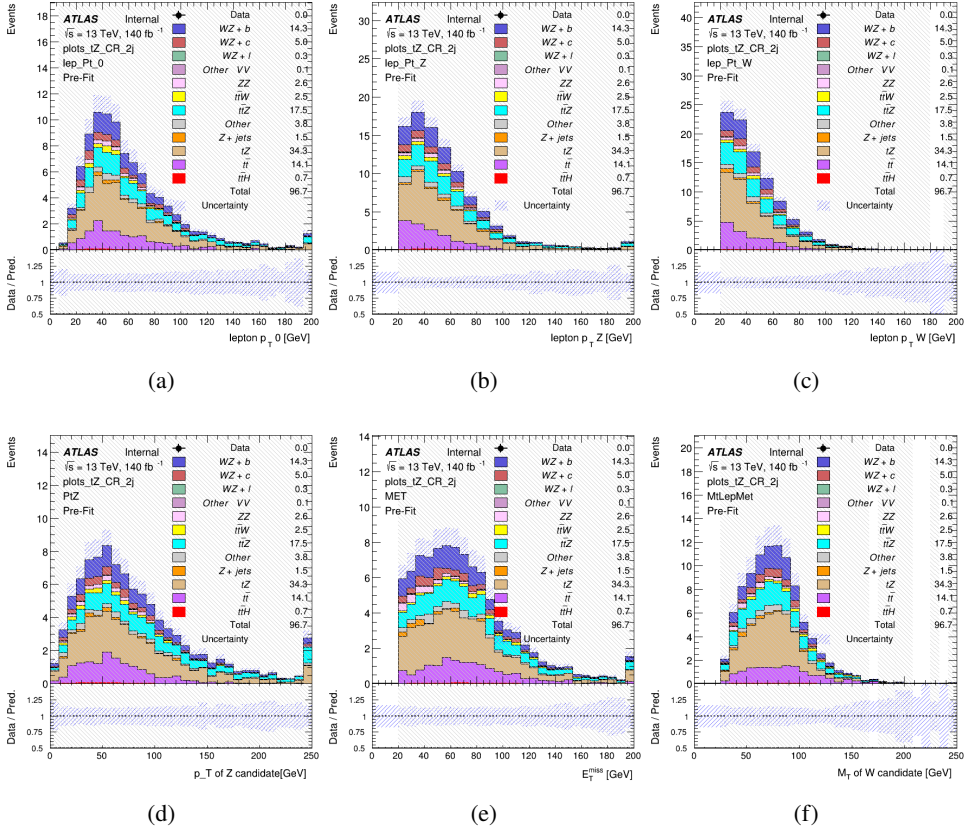


Figure 17: Comparisons between the data and MC distributions in the preselection region for (a) the p_T of the opposite sign lepton, (b) the p_T of the other lepton from the Z candidate, (c) the p_T of the lepton from the W candidate, (d) the p_T of the Z candidate, (e) the E_T^{miss} , and (f) the m_T of the W candidate.

5.3 Non-Prompt Lepton Estimation

Two processes act as sources of non-prompt leptons appear in the analysis: $t\bar{t}$ and $Z+jet$ production both produce two prompt leptons, and each contribute to the 3l region when an additional non-prompt lepton appears in the event. The contribution of these processes is estimated with Monte Carlo simulations, which are validated using enriched control regions.

5.3.1 $t\bar{t}$ Validation

$t\bar{t}$ events can produce two prompt leptons from the decay of each of the tops. These top decays produce two b-quarks, the decay of which can produce additional non-prompt leptons, which occasionally pass the event preselection. In order to validate that the Monte Carlo accurately

331 simulates this process accurately, the MC prediction in a non-prompt $t\bar{t}$ enriched control region
332 is compared to data.

333 The $t\bar{t}$ control region is similar to the preselection region - three leptons meeting the criteria
334 described in Section 5 are required, and the requirements on E_T^{miss} remain the same. However,
335 the selection requiring a lepton pair form a Z-candidate are reversed. Events where the invariant
336 mass of any two opposite sign, same flavor leptons falls within 10 GeV of 91.2 GeV are rejected.
337 This ensures the $t\bar{t}$ control region is orthogonal to the preselection region.

338 Further, because the jet multiplicity of $t\bar{t}$ events tends to be higher than WZ, the number of jets
339 in each event is required to be greater than 1. As b-jets are almost invariably produced from top
340 decays, at least one b-tagged jet passing the 70% DL1r WP in each event is required. Various
341 kinematic plots of this region are shown in Figure 18.

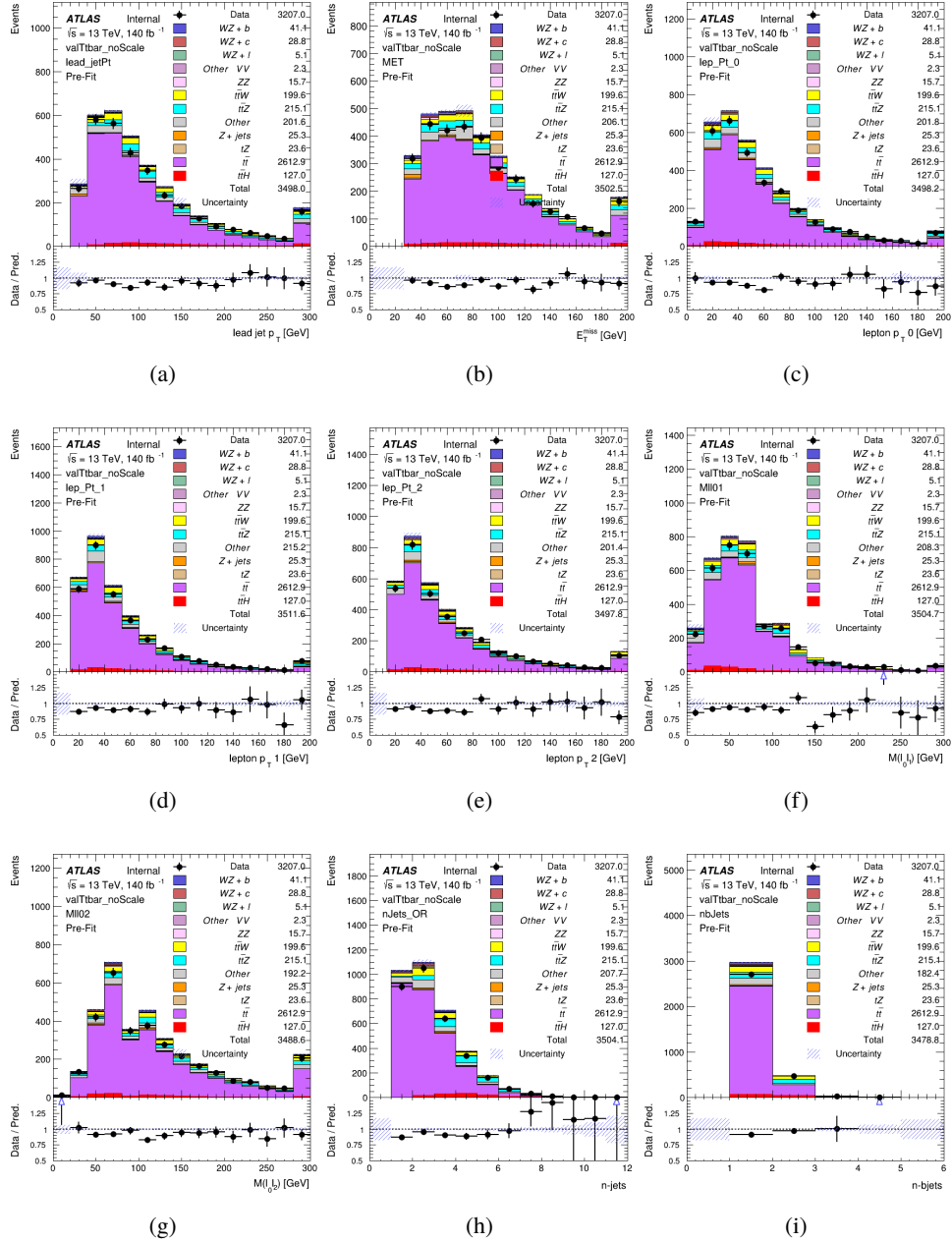


Figure 18: Comparisons between the data and MC distributions in the $t\bar{t}$ control region for (a) the p_T of the leading jet, (b) the missing transverse energy, (c) the p_T of lepton 0, (d) p_T of lepton 1, (e) p_T of lepton 2, (f) the invariant mass of leptons 0 and 1, (g) the invariant mass of leptons 0 and 2, (h) the number of jets, (i) the number of b-tagged jets.

342 The shape of each distribution agrees quite well between data and MC, with a constant offset
 343 between the two. This is accounted for by applying a constant correction factor of 0.883 to the $t\bar{t}$

344 MC prediction. Plots showing the kinematics of the $t\bar{t}$ VR after this correction factor has been
 345 applied are shown in Figure 19.

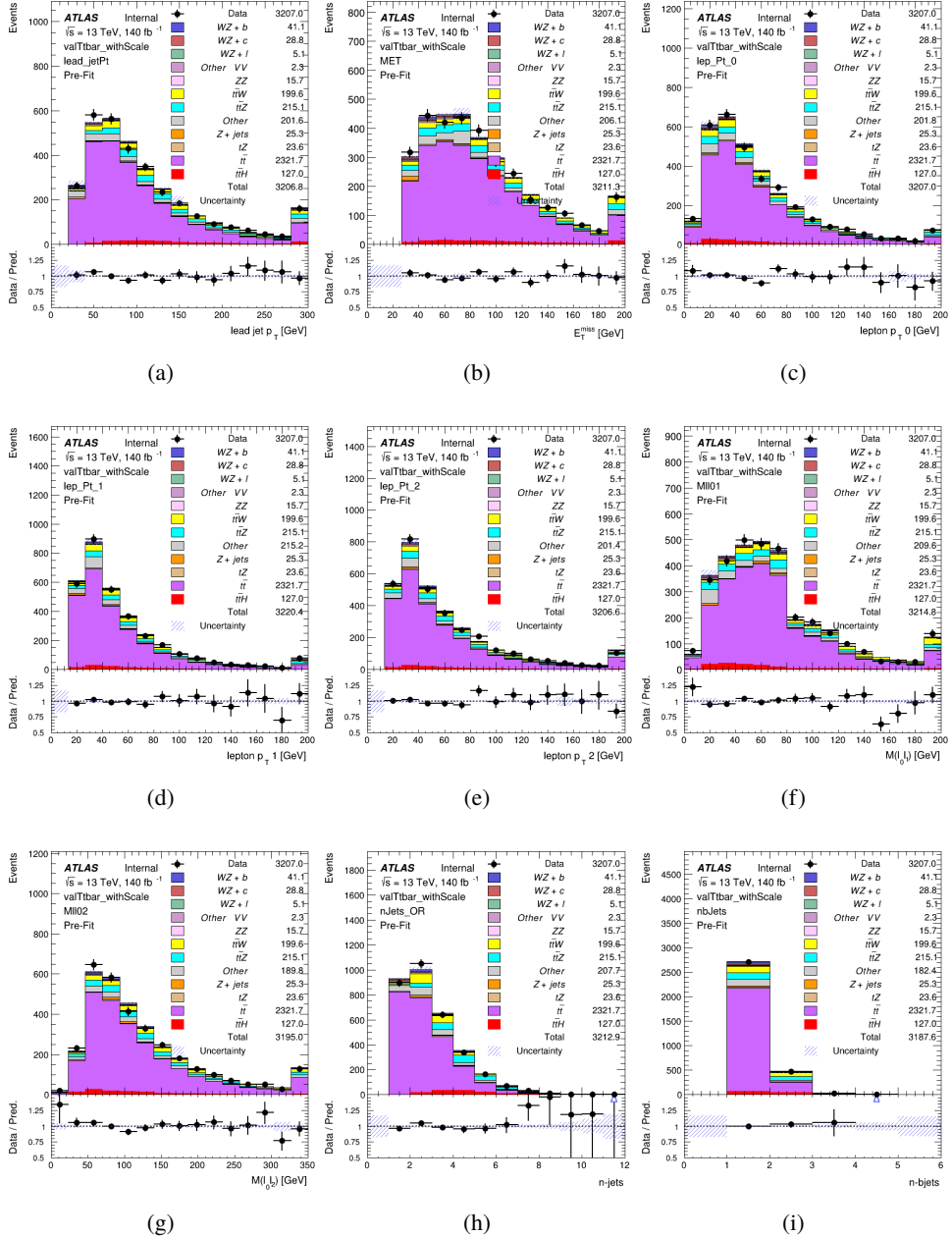


Figure 19: Comparisons between the data and MC distributions in the $t\bar{t}$ control region after the correction factor has been applied for (a) the p_T of the leading jet, (b) the missing transverse energy, (c) the p_T of lepton 0, (d) p_T of lepton 1, (e) p_T of lepton 2, (f) the invariant mass of leptons 0 and 1, (g) the invariant mass of leptons 0 and 2, (h) the number of jets, (i) the number of b-tagged jets.

346 The modeling is further validated by looking at the yield in the $t\bar{t}$ VR for each DL1r WP, giving
 347 a clearer correspondence to the signal regions used in the fit. Each region shown in Figure 20
 348 requires one or more jets pass the listed WP, with no jets passing the next highest WP.

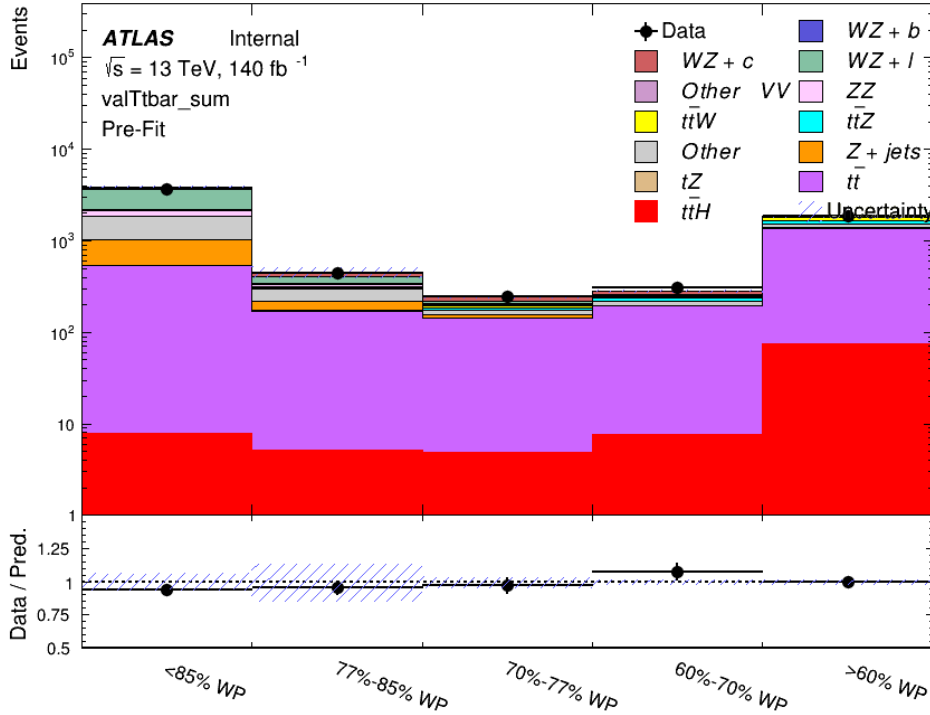


Figure 20: Data and MC comparisons for each DL1r WP for both 1-jet and 2-jet regions, after the $t\bar{t}$ VR selection and correction factor have been applied

349 As data and MC are found to agree within 20% for each of these working points, a 20% systematic
 350 uncertainty on the $t\bar{t}$ prediction is included for the analysis.

351 5.3.2 Z+jets Validation

352 Similar to $t\bar{t}$, a non-prompt $Z+jets$ control region is produced in order to validate the MC
 353 predictions. The lepton requirements remain the same as the preselection region. Because no
 354 neutrinos are present for this process, the E_T^{miss} cut is reversed, requiring $E_T^{\text{miss}} < 30 \text{ GeV}$. This
 355 also ensures this control region is orthogonal to the preselection region. Further, the number of
 356 jets in each event is required to be greater than or equal to one. Various kinematic plots of this
 357 region are shown below. The general agreement between data and MC in each of these suggests
 358 that the non-prompt contribution of $Z+jets$ is well modeled by Monte Carlo.

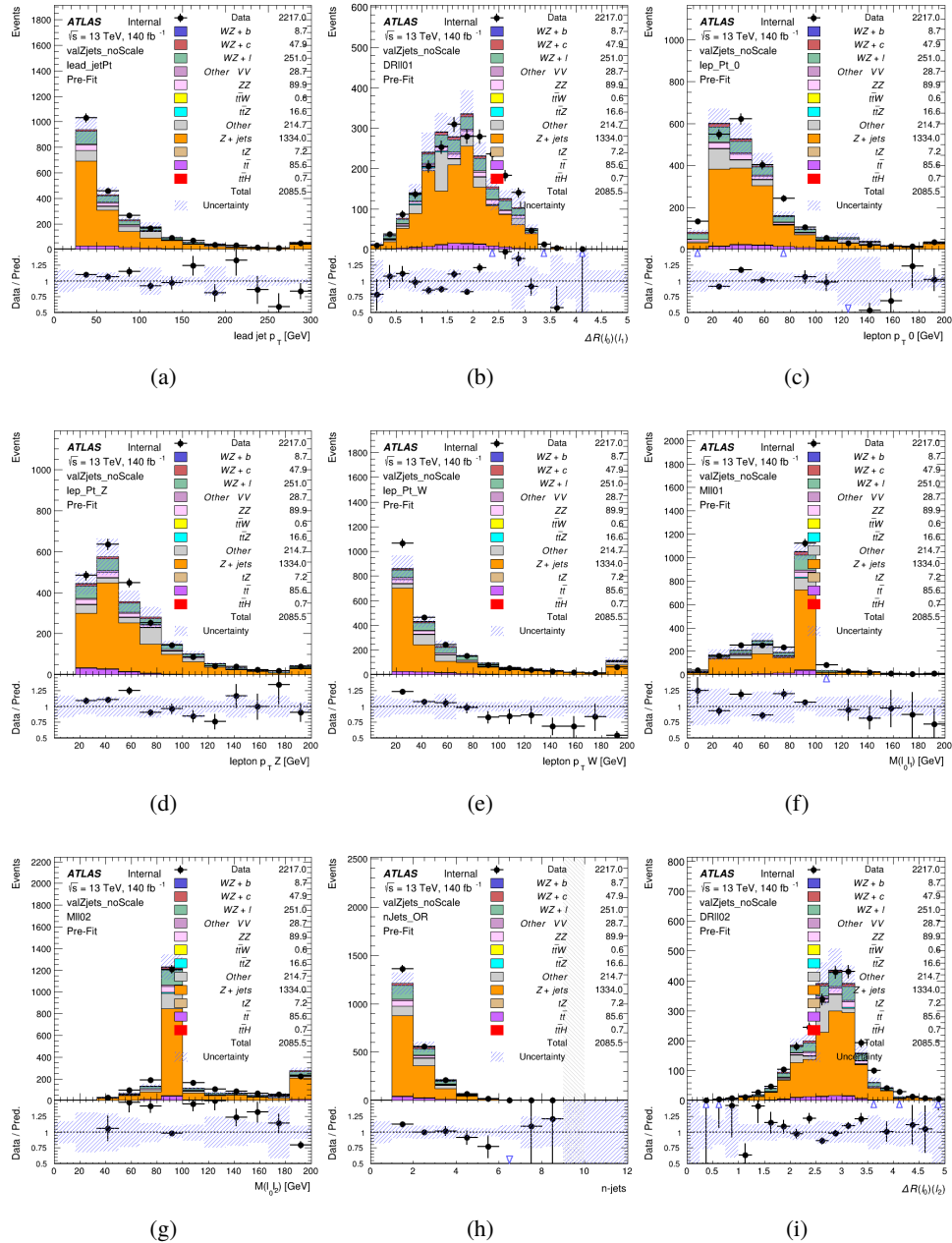


Figure 21: Comparisons between the data and MC distributions in the Z+jets control region for (a) the p_T of the leading jet, (b) ΔR between leptons 0 and 1, (c) the p_T of lepton 0, (d) p_T of SS lepton from the Z candidate, (e) p_T of the SS lepton from the W candidate, (f) the invariant mass of leptons 0 and 1, (g) the invariant mass of leptons 0 and 2, (h) the number of jets, (i) ΔR between leptons 0 and 2. Includes only statistical uncertainties

359 While there is general agreement between data and MC within statistical uncertainty, the shape

³⁶⁰ of the p_T spectrum of the lepton from the W is found to differ. To account for this discrepancy,
³⁶¹ a variable correction factor is applied to Z+jets. χ^2 minimization of the lepton 2 p_T spectrum
³⁶² is performed to derive a correction factor of $1.53 - 6.6 * 10^{-6}(\text{lep_Pt_W})$. Kinematic plots of
³⁶³ the Z + jets control region after this correction factor has been aplied are shown in Figure 22.

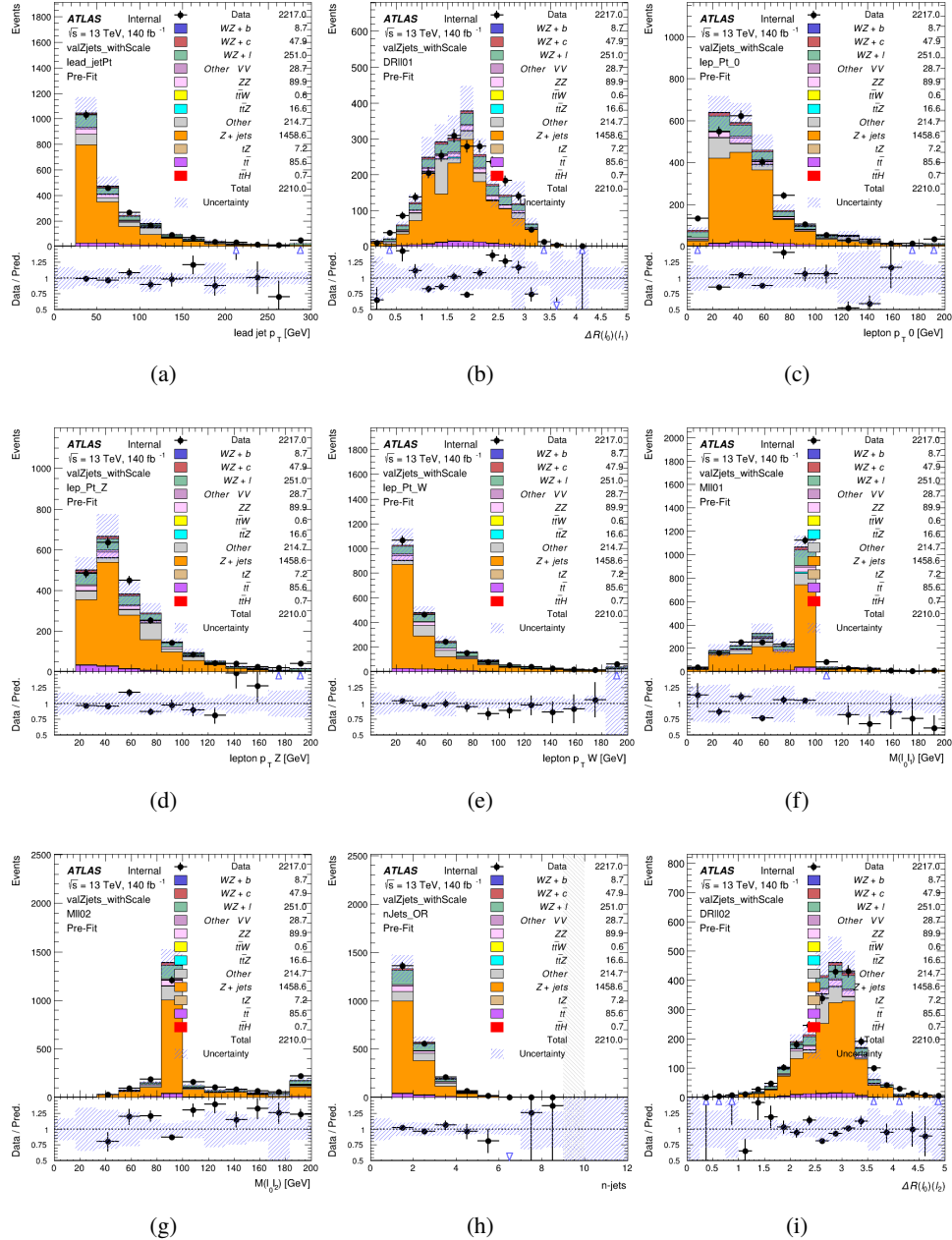


Figure 22: Comparisons between the data and MC distributions in the Z+jets control region after the correction factor has been applied for (a) the p_T of the leading jet, (b) ΔR between leptons 0 and 1, (c) the p_T of lepton 0, (d) p_T of SS lepton from the Z candidate, (e) p_T of the SS lepton from the W candidate, (f) the invariant mass of leptons 0 and 1, (g) the invariant mass of leptons 0 and 2, (h) the number of jets, (i) ΔR between leptons 0 and 2

364 The modeling is further validated by looking at the yield in the Z+jets VR for each DL1r WP,

365 giving a clearer correspondence to the signal regions used in the fit. Each region shown in Figure
 366 23 requires one or more jets pass the listed WP, with no jets passing the next highest WP.

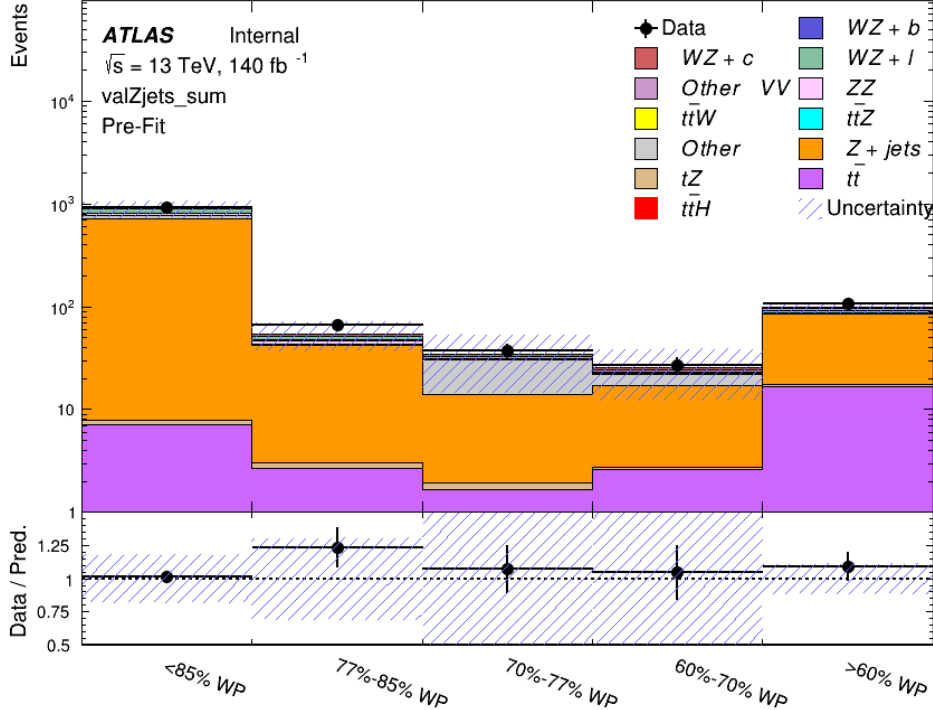


Figure 23: Data and MC comparisons for each DL1r WP for both 1-jet and 2-jet regions, after the Z+jets VR selection and correction factor have been applied

367 For each of the b-tagging working points considered, the data falls within 25% of the MC
 368 prediction once this correction factor has been applied. Therefore, a 25% systematic uncertainty
 369 is applied to Z + jets in the analysis.

370 6 tZ Separation Multivariate Analysis

371 Because tZ produces a final state identical to signal, it represents a predominant background in
 372 the most signal enriched regions. That is, the region with one jet passing the 60% DL1r WP.
 373 Therefore, a boosted decision tree (BDT) algorithm is trained using TMVA [15] to separate WZ
 374 + heavy flavor from tZ.

375 Separation between tZ and WZ + heavy flavor is achieved in part by reconstructing the invariant
 376 mass of the top candidate, which clusters more closely to the top mass for tZ than WZ + heavy
 377 flavor.

378 The result of this BDT is used to create a tZ enriched region in the fit, reducing its impact on the
 379 measurement of WZ + heavy flavor.

380 **6.1 Top Mass Reconstruction**

381 The reconstruction of the top mass follows the procedure described in detail in section 6.1 of
 382 [16]. The mass of the top quark candidate is reconstructed from the jet, the lepton not included
 383 in the Z-candidate, and a reconstructed neutrino. In the case that there is one jet in the event,
 384 there is only possible b-jet candidate. For events with two jets, the jet with the highest DL1r
 385 score is used.

386 The neutrino from the W decay is expected to be the only source of E_T^{miss} . Therefore, the E_T
 387 and ϕ of the neutrino are taken from the E_T^{miss} measurement. This leaves the z-component of
 388 the neutrino momentum, $p_{\nu z}$ as the only unknown.

389 This unknown is solved for by taking the combined invariant mass of the lepton and neutrino to
 390 give the invariant mass of the W boson:

$$391 \quad (p_l + p_\nu)^2 = m_W^2$$

392 Expanding this out into components, this equation gives:

$$393 \quad \sqrt{p_{T\nu}^2 + p_{z\nu}^2} E_l = \frac{m_w^2 - m_l^2}{2} + p_{T\nu}(p_{lx}\cos\phi_\nu + p_{ly}\sin\phi_\nu) + p_{lz}p_{\nu z}$$

394 This equation gives two solutions for $p_{\nu z}$. For cases where only one of these solutions is real,
 395 that is taken as the value of $p_{\nu z}$. For instances with two real solutions, the one which is shown
 396 to be correct in the largest fraction of simulations is taken. For cases when no real solution is
 397 found, often because of detector effects, the value of E_T^{miss} is varied in decreasing increments of
 398 100 MeV until a real solution is found.

399 The reconstructed top mass distribution for tZ and WZ + b can be seen in figure 24.

400 **6.2 tZ BDT**

401 A Boosted Decision Tree (BDT), specifically XGBoost [17], is used to provide separation between
 402 tZ and WZ+b. The following kinematic variables are used as inputs:

- 403 • The invariant mass of the reconstructed top candidate
- 404 • p_T of each of the leptons, jet
- 405 • The invariant mass of each combination of lepton pairs, $M(l\bar{l})$
- 406 • E_T^{miss}

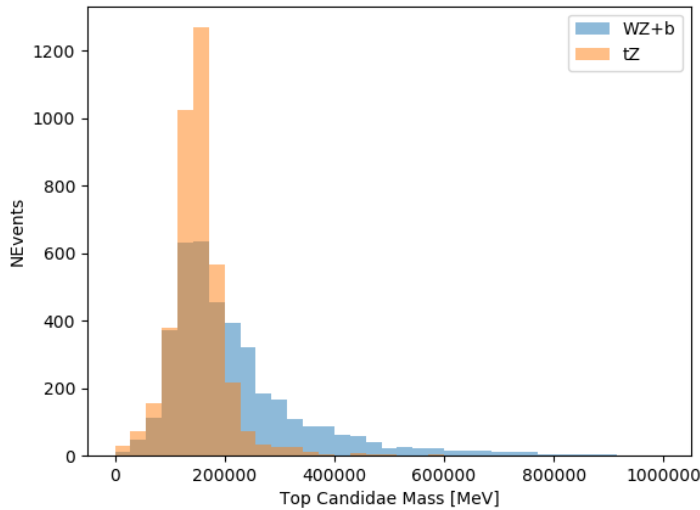


Figure 24: Reconstructed top mass distributions for tZ and WZ + b, measured in MeV.

- 407 • Distance between each combination of leptons, $\Delta R(ll)$
- 408 • Distance between each lepton and the jet, $\Delta R(lj)$

409 The training samples included only events meeting the requirements of the 1-jet, >60% region,
 410 i.e. passing all the selection described in section 5 and having exactly one jet which passes the
 411 tightest (60%) DL1r working point.

412 The distributions of a few of these features for both signal and background is shown in figure
 413 25.

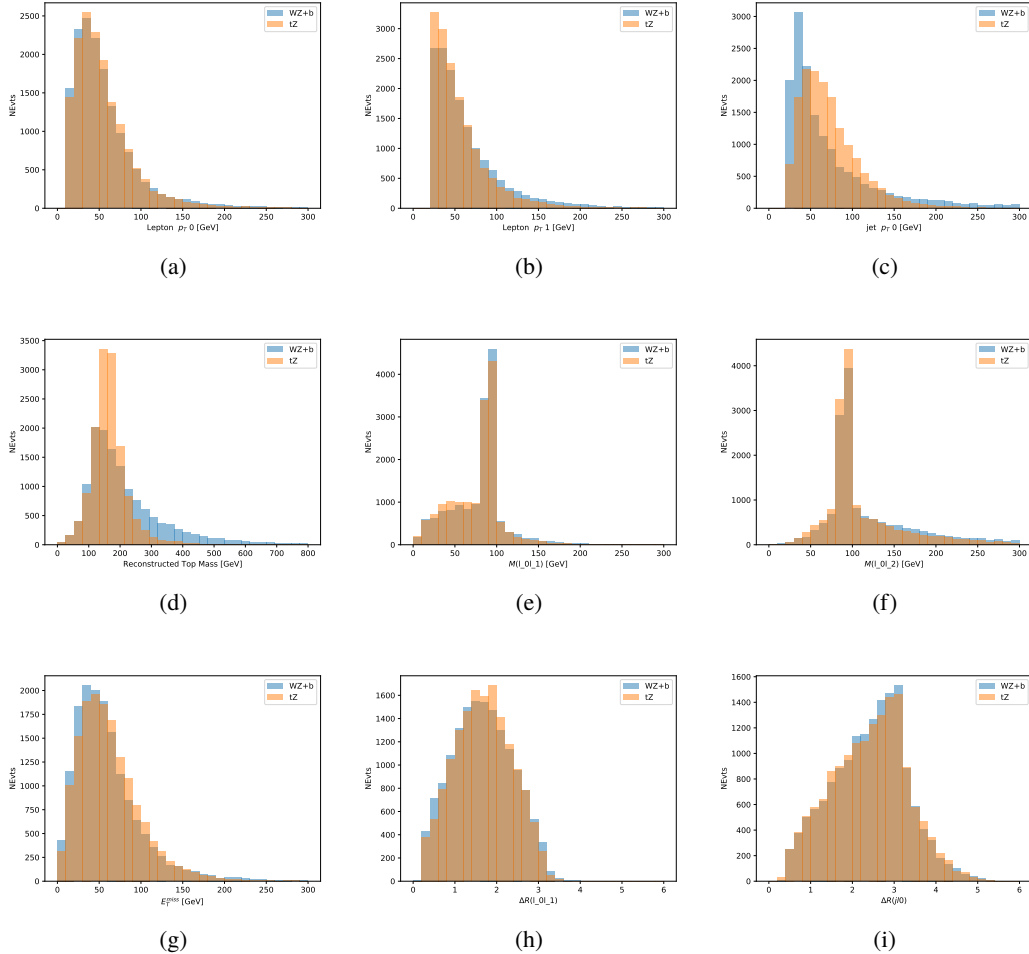


Figure 25: Distribution of input features of the BDT for signal (WZ) and background (tZ). Both are scaled to an equal number of events. (a), (b) and (c) show the p_T of lepton 0, lepton 1, and the jet, (d) show the reconstructed top mass, (e) and (f) show the invariant mass of leptons 0 and 1, leptons 0 and 2. (g) shows the E_T^{miss} of each event. (h) and (i) show the ΔR between lepton 0 and lepton 1, and the jet.

414 A sample of 20,000 background (tZ) and signal (WZ+b) Monte Carlo events are used to train
 415 the BDT. And additional 5,000 events are reserved for testing the model, in order to prevent
 416 over-fitting. A total of 750 decision trees with a maximum depth of 6 branches are used to build
 417 the model. These parameters are chosen empirically, by training several models with different
 418 parameters and selecting the one that gave the best separation for the test sample.

419 The results of the BDT training are shown in figure 26. The output scores for both signal and
 420 background events is shown on the left. The right shows the receiving operating characteristic
 421 (ROC) curve that results from the MVA. The ROC curve represents the background rejection
 422 as a function of signal efficiency, where each point on the curve represents a different response

423 score. The ROC curve of the BDT is compared to the performance of using an optimal set of flat
 424 selections on the same set of input variables.

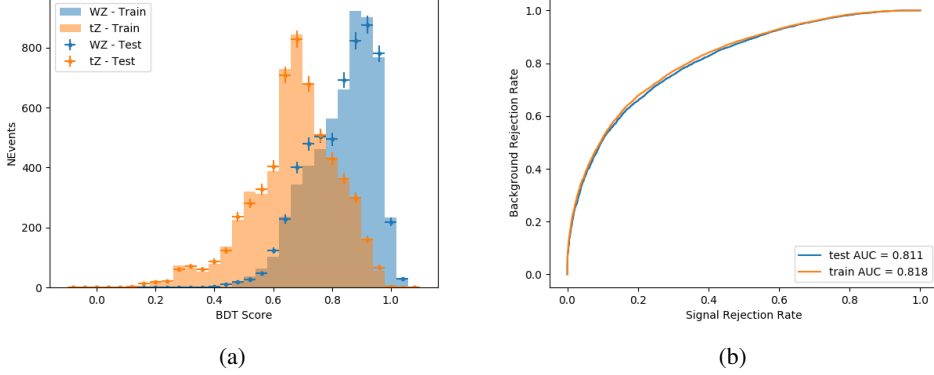


Figure 26: Distribution of the BDT response for signal and background events on the left, the ROC curve for the BDT on the right.

425 The relative important of each input feature in the model, measured by how often they appeared
 426 in the decision trees, is shown in figure 27.

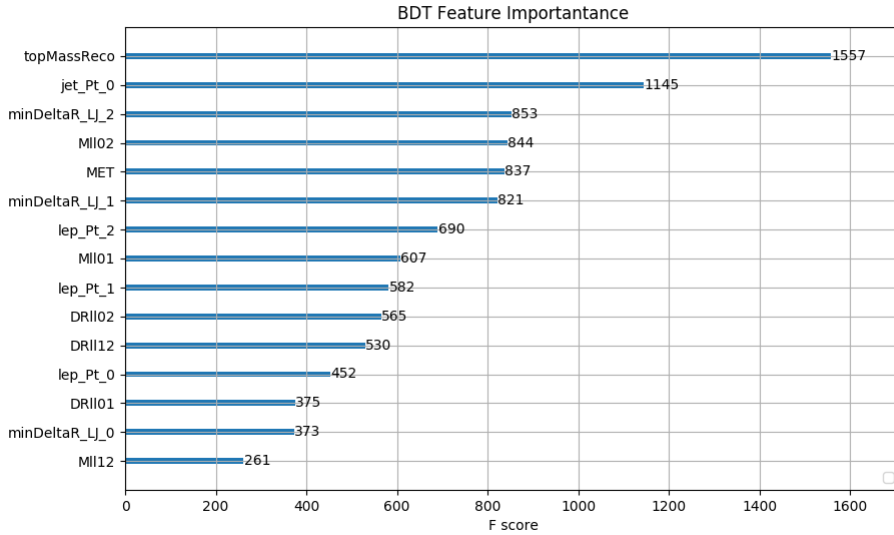


Figure 27: Relative importance of each input feature in the model.

427 These results suggest that some amount of separation can be achieved between these two pro-
 428 cesses, with a high BDT score selecting a set of events that is pure in WZ + b. A BDT score

429 of 0.725 is selected as a cutoff, where events with scores higher than this form a signal enriched
 430 region, and events with scores lower than this form a tZ control region. This cutoff is selected by
 431 varying the value of this cutoff in stat-only Asimov fits, and selecting the value that minimizes
 432 the statistical uncertainty on WZ + b.

433 7 Systematic Uncertainties

434 The systematic uncertainties that are considered are summarized in Table 9. These are imple-
 435 mented in the fit either as a normalization factors or as a shape variation or both in the signal
 436 and background estimations. The numerical impact of each of these uncertainties is outlined in
 437 Section 8.

Table 9: Sources of systematic uncertainty considered in the analysis.

Systematic uncertainty	Components
Luminosity	1
Pileup reweighting	1
Physics Objects	
Electron	6
Muon	15
Jet energy scale	28
Jet energy resolution	8
Jet vertex fraction	1
Jet flavor tagging	131
E_T^{miss}	3
Total (Experimental)	194
Signal Modeling	
Shape modelling	3
Renormalization and factorization scales	5
nJet Migration	4
Background Modeling	
Cross section	15
Renormalization and factorization scales	12
Total (Signal and background modeling)	35
Total (Overall)	229

438 The uncertainty in the combined integrated luminosity is derived from a calibration of the
 439 luminosity scale performed for 13 TeV proton-proton collisions [18], [19].

440 The experimental uncertainties are related to the reconstruction and identification of light leptons
 441 and b-tagging of jets, and to the reconstruction of E_T^{miss} . The TOTAL electron ID correlation

442 model is used, corresponding to 1 electron ID systematic. Electron ID is found to be a subleading
443 systematic that is unconstrained by the fit, making it an appropriate choice for this analysis.

444 The sources which contribute to the uncertainty in the jet energy scale (JES) [20] are decom-
445 posed into uncorrelated components and treated as independent sources in the analysis. The
446 CategoryReduction model is used to account for JES uncertainties, which decomposes the uncer-
447 tainties into 30 nuisance parameters included in the fit. The SimpleJER model is used to account
448 for jet energy resolution (JER) uncertainties, and 8 JER uncertainty components unclued as
449 NPs in the fit.

450 The uncertainties in the b-tagging efficiencies measured in dedicated calibration analyses [21] are
451 also decomposed into uncorrelated components. The large number of components for b-tagging
452 is due to the calibration of the distribution of the MVA discriminant.

453 The full list of systematic uncertainties considered in the analysis is summarized in Tables 10,
454 11 and 12.

455

Experimental Systematics on Leptons and E_T^{miss}			
Type	Description	Systematics Name	Application
Trigger			
Scale Factors	Trigger Efficiency	lepSFTrigTight_MU(EL)_SF_Trigger_STAT(SYST)	Event Weight
Muons			
Efficiencies	Reconstruction and Identification	lepSFObjTight_MU_SF_ID_STAT(SYST)	Event Weight
	Isolation	lepSFObjTight_MU_SF_Isol_STAT(SYST)	Event Weight
	Track To Vertex Association	lepSFObjTight_MU_SF_TTVA_STAT(SYST)	Event Weight
p_T Scale	p_T Scale	MUONS_SCALE	p_T Correction
Resolution	Inner Detector Energy Resolution	MUONS_ID	p_T Correction
	Muon Spectrometer Energy Resolution	MUONS_MS	p_T Correction
Electrons			
Efficiencies	Reconstruction	lepSFObjTight_EL_SF_ID	Event Weight
	Identification	lepSFObjTight_EL_SF_Reco	Event Weight
	Isolation	lepSFObjTight_EL_SF_Isol	Event Weight
Scale Factor	Energy Scale	EG_SCALE_ALL	Energy Correction
Resolution	Energy Resolution	EG_RESOLUTION_ALL	Energy Correction
E_T^{miss}			
Soft Tracks Terms	Resolution	MET_SoftTrk_ResoPerp	p_T Correction
	Resolution	MET_SoftTrk_ResoPara	p_T Correction
	Scale	MET_SoftTrk_ScaleUp	p_T Correction
	Scale	MET_SoftTrk_ScaleDown	p_T Correction

Table 10: Summary of experimental systematics considered for leptons and E_T^{miss} . Includes type, description, name of systematic as used in the fit, and mode of application. The mode of application indicates the systematic evaluation, e.g. as an overall event re-weighting (Event Weight) or rescaling (p_T Correction).

Experimental Systematics on Jets			
Type	Origin	Systematics Name	Application
Jet Vertex Tagger		JVT	Event Weight
Energy Scale	Calibration Method	JET_21NP_ JET_EffectiveNP_1-19	p_T Correction p_T Correction
	η inter-calibration	JET_EtaIntercalibration_Modelling JET_EtaIntercalibration_NonClosure JET_EtaIntercalibration_TotalStat	p_T Correction p_T Correction p_T Correction
	High p_T jets	JET_SingleParticle_HighPt	p_T Correction
	Pile-Up	JET_Pileup_OffsetNPV JET_Pileup_OffsetMu JET_Pileup_PtTerm JET_Pileup_RhoTopology	p_T Correction p_T Correction p_T Correction p_T Correction
	Non Closure	JET_PunchThrough_MC15	p_T Correction
	Flavour	JET_Flavor_Response JET_BJES_Response JET_Flavor_Composition	p_T Correction p_T Correction p_T Correction
Resolution		JET_JER_SINGLE_NP	Event Weight

Table 11: Jet systematics take into account effects of jets calibration method, η inter-calibration, high p_T jets, pile-up, and flavor response. They are all diagonalised into effective parameters.

Experimental Systematics on b-tagging		
Type	Origin	Systematic Name
Scale Factors	DL1r b-tagger efficiency on b originated jets in bins of η	DL1r_Continuous_EventWeight_B0-29
	DL1r b-tagger efficiency on c originated jets in bins of η	DL1r_Continuous_EventWeight_C0-19
	DL1r b-tagger efficiency on light flavoured originated jets in bins of η and p_T	DL1r_Continuous_EventWeight_Light0-79
	DL1r b-tagger extrapolation efficiency	DL1r_Continuous_EventWeight_extrapolation DL1r_Continuous_EventWeight_extrapolation_from_charm

Table 12: Summary of experimental systematics to be included for b-tagging of jets in the analysis, using the continuous DL1r tagging algorithm. All of the b-tagging related systematics are applied as event weights. From left: type, description, and the name of systematic used in the fit.

- 456 Theoretical uncertainties applied to MC predictions, including cross section, PDF, and scale
 457 uncertainties are taken from theory calculations, with the exception of non-prompt and diboson
 458 backgrounds. The cross-section uncertainty on tZ is taken from [22]. Derivation of the non-
 459 prompt background uncertainties, Z+jets and tt}, are explained in detail in Section 5.3.
 460 The other VV + heavy flavor processes (namely VV+b and VV+charm, which primarily consist
 461 of ZZ events) are also poorly understood, because these processes involve the same physics as
 462 WZ + heavy flavor, and have also not been measured. Therefore, a conservative 50% uncertainty
 463 is applied to those samples. While this uncertainty is large, it is found to have little impact on
 464 the significance of the final result.
 465 The theory uncertainties applied to the predominate background estimates are summarized in
 466 Table 13.

Process	X-section [%]
tZ	X-sec: ± 15.2 QCD Scale: $^{+5.2}_{-1.3}$ PDF($+\alpha_S$): ± 1.2
t <bar>t} H (aMC@NLO+Pythia8)</bar>	QCD Scale: $^{+5.8}_{-9.2}$ PDF($+\alpha_S$): ± 3.6
t <bar>t} Z (aMC@NLO+Pythia8)</bar>	QCD Scale: $^{+9.6}_{-11.3}$ PDF($+\alpha_S$): ± 4
t <bar>t} W (aMC@NLO+Pythia8)</bar>	QCD Scale: $^{+12.9}_{-11.5}$ PDF($+\alpha_S$): ± 3.4
VV + b/charm (Sherpa 2.2.1)	± 50
VV + light (Sherpa 2.2.1)	± 6
t <bar>t}</bar>	± 20
Z + jets	± 25
Others	± 50

Table 13: Summary of theoretical uncertainties for MC predictions in the analysis.

467 Additional signal uncertainties are estimated by comparing estimates from the nominal Sherpa
 468 WZ samples with alternate WZ samples generated with Powheg+PYTHIA8 (DSID 361601).
 469 MC/MC scale factors are applied to make these comparisons. The shape of the templates used
 470 in the fit are compared between these two samples for WZ + b, WZ + charm and WZ + light,
 471 as shown in Figures 28 and 29. Each of these plots are normalized to unity in order to capture
 472 differences in shape.

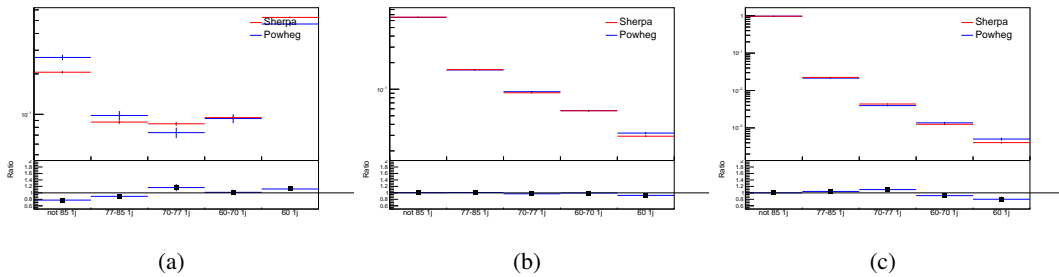


Figure 28: Comparison between Sherpa and Powheg predictions of the distribution of (a) WZ + b, (b) WZ + charm, and (c) WZ + light among the various b-tag WPs used in the 1-jet fit.

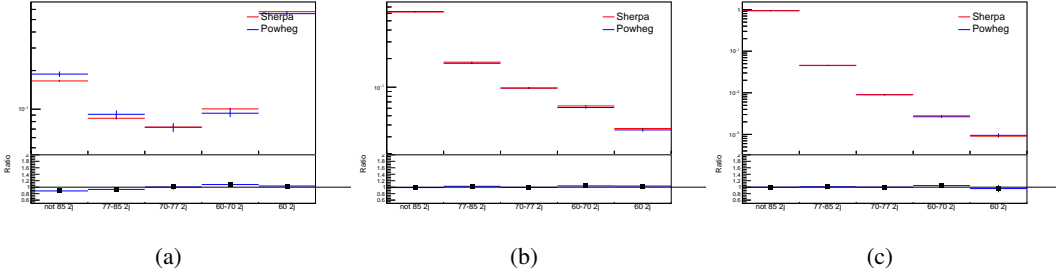


Figure 29: Comparison between Sherpa and Powheg predictions of the distribution of (a) WZ + b, (b) WZ + charm, and (c) WZ + light among the various b-tag WPs used in the 2-jet fit.

473 Separate systematics are included in the fit for WZ + b, WZ + charm and WZ + light, where
 474 the distribution among each of the fit regions is varied based on the prediction of the Powheg
 475 sample.

476 A similar approach is taken to account for uncertainties in migrations between the number of
 477 reco and truth jets. The fraction of events with 1 truth jet which fall into the 1 jet bin versus the
 478 2 jet bin at reco level is compared for Sherpa and Powheg. The same is done for events with 2
 479 truth jets. This comparison is shown in figure 30.

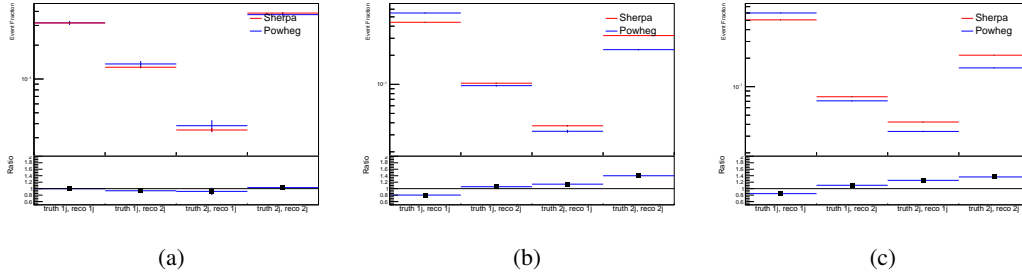


Figure 30: Comparison between Sherpa and Powheg predictions for truth jet migrations between the 1 and 2 jet reco bins for (a) WZ + b, (b) WZ + charm, and (c) WZ + light

480 A systematic is included where events are shifted between the 1-jet and 2-jet regions based on
 481 the differences between these two shapes. This is done independently for each of the WZ + b,
 482 WZ + charm, and WZ + light templates.

483 Additional systematics are included to account for the uncertainty in the contamination of 0 jet
 484 and 3 or more jet events (at truth level) in the 1 and 2 reco jet bins. Because these events fall
 485 outside the scope of this measurement, these events are included as a background. As such, a
 486 normalization, rather than a shape, uncertainty is applied for this background.

487 The number of WZ events with 0-jets and ≥ 3 -jets in the reconstructed 1-jet and 2-jet regions
 488 are compared for Sherpa and Powheg, as seen in figure 31. These differences are taken as separate
 489 normalization systematics on the yield of WZ+0-jet and WZ+ ≥ 3 -jet events.

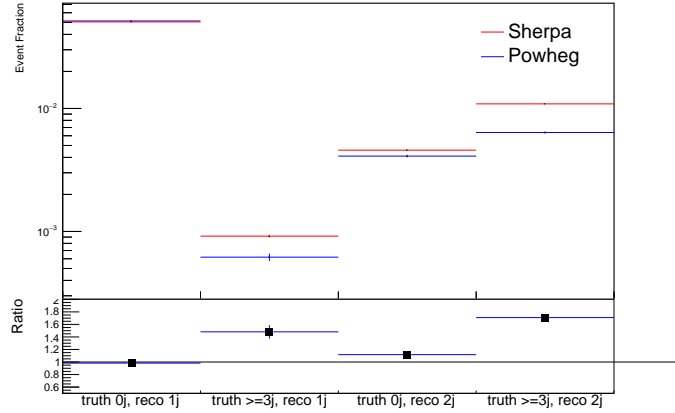


Figure 31: Comparison between Sherpa and Powheg predictions for 0 and ≥ 3 truth jet contributions in the 1 and 2 jet reco bins

490 8 Results

491 A separate maximum-likelihood fit is performed over the various fit regions in order to extract
 492 the best-fit value of the WZ + b-jet and WZ + charm jet contributions for events with both 1 and 2
 493 associated jets. The WZ + b, WZ + charm and WZ + light contributions, are separated into 1-jet
 494 and 2-jet samples at truth level. The signal templates are allowed to float, with the remaining
 495 background contributions are held fixed. The result of the fit is used to extract the cross-section
 496 of WZ + heavy-flavor production.

497 A maximum likelihood fit to data is performed simultaneously in the regions described in Section
 498 5, summarized in figure 32. The parameters $\mu_{WZ+b-1-jet}$, $\mu_{WZ+charm1-jet}$, $\mu_{WZ+light-1-jet}$,
 499 $\mu_{WZ+b-2-jet}$, $\mu_{WZ+charm2-jet}$, $\mu_{WZ+light-2-jet}$, where $\mu = \sigma_{\text{observed}}/\sigma_{\text{SM}}$, are extracted from
 500 the fit. A simultaneous fit is performed over all 1-jet and 2-jet regions.

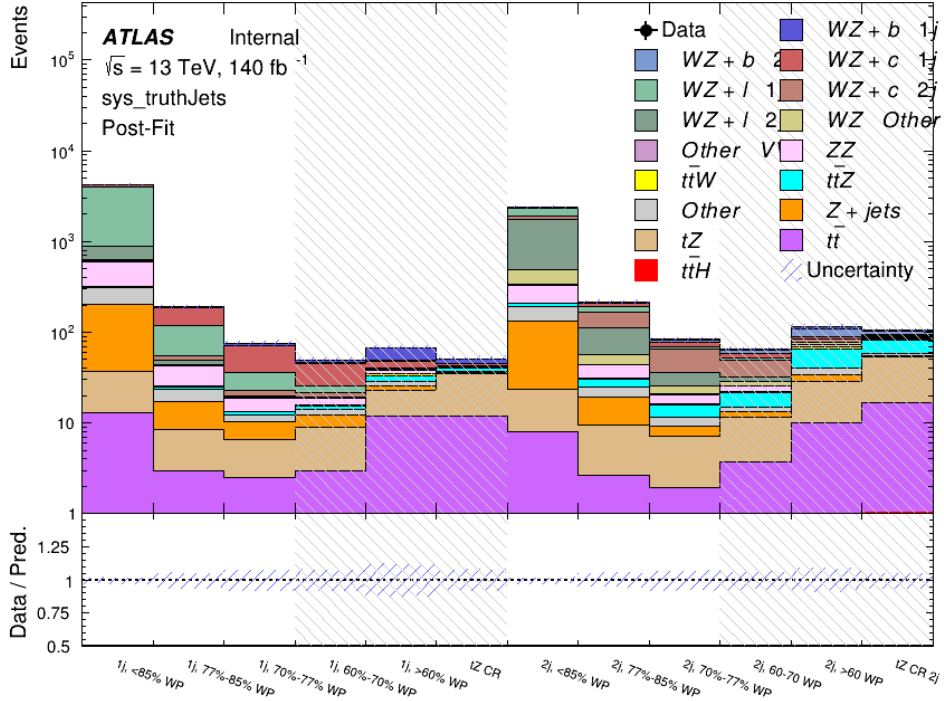


Figure 32: Post-fit summary of the fit regions.

As described in Section 7, there are 229 systematic uncertainties that are considered as NPs in the fit. These NPs are constrained by Gaussian or log-normal probability density functions. The latter are used for normalisation factors to ensure that they are always positive. The expected number of signal and background events are functions of the likelihood. The prior for each NP is added as a penalty term, decreasing the likelihood as it is shifted away from its nominal value. The correlations between these nuisance parameters are summarized in Figure 33.

The Asimov fit for 1-jet events gives an expected μ value of $1.00^{+0.47}_{-0.43}(\text{stat})^{+0.30}_{-0.27}(\text{sys})$ for $WZ + b$. The fitted cross-section modifiers for $WZ + \text{charm}$ and $WZ + \text{light}$ are $1.00 \pm 0.17 \pm 0.17$ and $1.00 \pm 0.06 \pm 0.14$, respectively.

The expected cross-section of $WZ+b$ with 1-jet is $1.74^{+0.82}_{-0.75}(\text{stat})^{+0.53}_{-0.48}(\text{sys})$ fb, and $14.6 \pm 2.5(\text{stat}) \pm 2.3(\text{sys})$ fb for $WZ + \text{charm}$, with a correlation of -0.22 between them. An expected significance of 2.0 is observed for $WZ + b$ in this region.

For 2-jet events, the fit gives an expected μ value of $1.00^{+0.53}_{-0.51}(\text{stat})^{+0.39}_{-0.34}(\text{sys})$ for $WZ + b$. The fitted cross-section modifiers for $WZ + \text{charm}$ and $WZ + \text{light}$ are $1.00 \pm 0.25 \pm 0.21$ and $1.00 \pm 0.06 \pm 0.16$, respectively.

The expected $WZ + b$ cross-section in the 2-jet region is $2.5^{+1.3}_{-1.3}(\text{stat})^{+0.95}_{-0.83}(\text{sys})$ fb with an expected significance of 1.7σ . The 2-jet expected cross-section of $WZ + \text{charm}$ is $12.7 \pm$

518 3.2(stat) \pm 2.7(sys) fb, and the correlation between WZ + charm and WZ + b is -0.26.

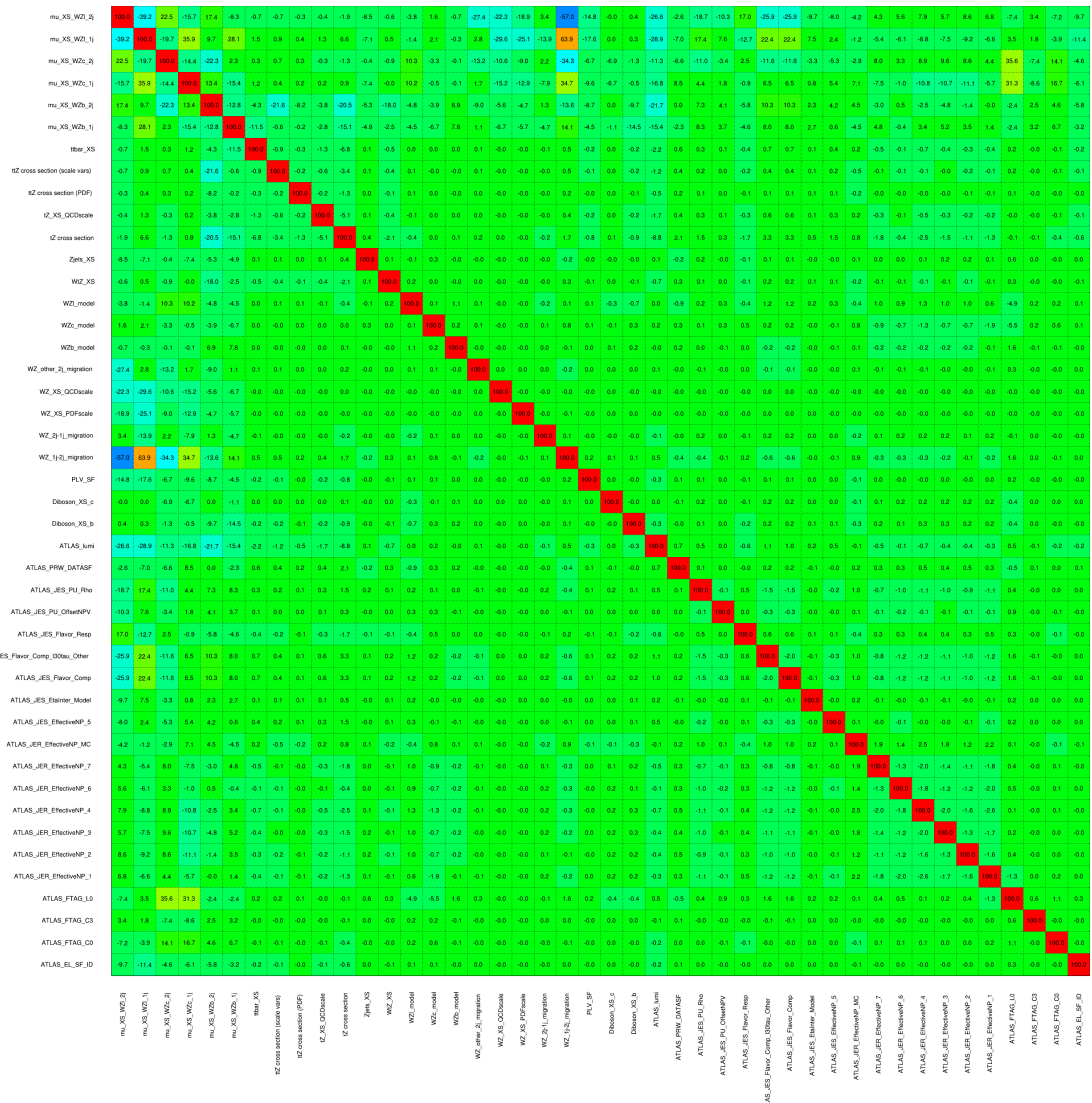


Figure 33: Correlations between nuisance parameters

519 The pre-fit yields in each of the 1-jet regions used in the fit are shown in Table 8.

520

Sample	1j, <85% WP	1j, 77%-85% WP	1j, 70%-77% WP	1j, 60%-70% WP	1j, >60% WP	tZ CR
WZ + b – 1j	8.1 ± 1.6	4.7 ± 0.5	4.6 ± 0.4	5.1 ± 0.4	18.2 ± 2.4	4.8 ± 0.6
WZ + c – 1j	260 ± 22	81 ± 6	43.1 ± 3.6	25.8 ± 2.6	9.4 ± 1.8	2.9 ± 0.6
WZ + l – 1j	3090 ± 250	91 ± 13	17 ± 3	4.9 ± 1.6	1.3 ± 0.4	0.2 ± 0.1
WZ + b – 2j	1.10 ± 0.37	0.44 ± 0.11	0.39 ± 0.06	0.62 ± 0.14	2.1 ± 0.5	0.59 ± 0.14
WZ + c – 2j	21 ± 5	5.6 ± 1.2	3.0 ± 0.7	2.0 ± 0.5	0.70 ± 0.20	0.30 ± 0.08
WZ + l – 2j	250 ± 60	5.7 ± 1.6	0.73 ± 0.53	0.31 ± 0.15	0.07 ± 0.06	0.01 ± 0.01
WZ – Other	13 ± 5	1.4 ± 0.4	0.42 ± 0.08	0.2 ± 0.01	0.30 ± 0.05	0.67 ± 0.15
Other VV	6.2 ± 0.6	0.2 ± 0.4	0.2 ± 0.04	0.07 ± 0.1	0.1 ± 0.1	0.1 ± 0.2
ZZ	336 ± 26	17.8 ± 2.1	4.3 ± 0.6	1.7 ± 0.5	0.36 ± 0.08	0.10 ± 0.03
t <bar>t>W</bar>	1.1 ± 0.2	0.2 ± 0.1	0.3 ± 0.1	0.4 ± 0.1	1.5 ± 0.3	0.7 ± 0.2
t <bar>t>Z</bar>	6.8 ± 1.2	1.4 ± 0.3	1.0 ± 0.2	1.2 ± 0.2	4.4 ± 0.8	3.2 ± 0.6
Z + jets	169 ± 38	8.9 ± 1.9	3.7 ± 0.8	3.3 ± 0.7	3.2 ± 0.7	0.8 ± 0.17
V + γ	45 ± 28	1.9 ± 2.4	0.1 ± 0.1	0.02 ± 0.01	1.0 ± 0.9	0.02 ± 0.03
tZ	24.3 ± 4.3	5.5 ± 1.1	4.1 ± 0.8	5.9 ± 1.1	10.7 ± 2.0	23 ± 4
tW	1.4 ± 0.8	0.2 ± 0.5	0.0 ± 0.2	0.7 ± 0.6	0.26 ± 0.42	0.39 ± 0.41
WtZ	2.3 ± 1.2	0.6 ± 0.3	0.3 ± 0.21	0.27 ± 0.2	1.1 ± 0.7	0.6 ± 0.5
VVV	12.4 ± 0.5	0.93 ± 0.06	0.35 ± 0.03	0.13 ± 0.02	0.14 ± 0.03	0.02 ± 0.01
VH	40 ± 6	2.6 ± 1.4	0.9 ± 0.8	0.7 ± 0.8	0.5 ± 0.6	0.0 ± 0.0
t <bar>t></bar>	12.1 ± 1.6	2.9 ± 0.6	2.5 ± 0.5	2.8 ± 0.5	11.2 ± 1.4	10.9 ± 1.5
t <bar>t>H</bar>	0.24 ± 0.03	0.05 ± 0.01	0.04 ± 0.01	0.06 ± 0.01	0.20 ± 0.03	0.13 ± 0.02
Total	5010 ± 260	227 ± 24	88 ± 12	57 ± 8	76 ± 16	53 ± 8

Table 14: Pre-fit yields in each of the 1-jet regions.

521 The post-fit yields in each region are summarized in Figure 8.

522

	1j, <85% WP	1j, 77%-85% WP	1j, 70%-77% WP	1j, 60%-70% WP	1j, >60% WP	tZ CR
WZ + b	8.1 ± 4.9	4.7 ± 2.0	4.6 ± 2.0	5.1 ± 2.1	18 ± 10	5.0 ± 2.5
WZ + c	260 ± 60	80 ± 14	43 ± 7	26 ± 5	9.4 ± 2.3	2.9 ± 0.7
WZ + l	3090 ± 130	90 ± 11	17.3 ± 2.8	4.9 ± 1.6	1.3 ± 0.4	0.23 ± 0.13
WZ + b - 2j	1.10 ± 0.37	0.44 ± 0.11	0.39 ± 0.06	0.62 ± 0.14	2.1 ± 0.5	0.59 ± 0.14
WZ + c - 2j	21 ± 5	5.6 ± 1.2	3.0 ± 0.7	2.0 ± 0.5	0.70 ± 0.20	0.30 ± 0.08
WZ + l - 2j	250 ± 60	5.7 ± 1.6	0.73 ± 0.53	0.31 ± 0.15	0.07 ± 0.06	0.01 ± 0.01
WZ - Other	13 ± 5	1.4 ± 0.4	0.42 ± 0.08	0.2 ± 0.01	0.30 ± 0.05	0.67 ± 0.15
Other VV	6.2 ± 0.6	0.92 ± 0.07	0.02 ± 0.01	0.01 ± 0.01	0.01 ± 0.01	0.01 ± 0.01
ZZ	346 ± 57	19 ± 5	4.3 ± 0.8	2.7 ± 0.5	2.4 ± 0.1	2.1 ± 0.6
t̄W	1.09 ± 0.21	0.2 ± 0.1	0.1 ± 0.1	0.4 ± 0.1	1.5 ± 0.3	0.1 ± 0.2
t̄Z	6.8 ± 1.2	1.4 ± 0.3	1.0 ± 0.2	1.2 ± 0.2	4.4 ± 0.7	3.2 ± 0.5
rare Top	0.14 ± 0.04	0.04 ± 0.02	0.04 ± 0.0	0.1 ± 0.03	0.14 ± 0.04	0.15 ± 0.05
t̄WW	0.04 ± 0.03	0.01 ± 0.02	0.01 ± 0.01	0.01 ± 0.01	0.01 ± 0.02	0.01 ± 0.01
Z + jets	169 ± 37	8.9 ± 1.9	3.7 ± 0.8	3.3 ± 0.7	3.2 ± 0.7	0.8 ± 0.2
W + jets	0.01 ± 0.01					
V + γ	46 ± 28	1.9 ± 2.4	0.1 ± 0.1	0.0 ± 0.2	1.0 ± 0.9	0.0 ± 0.0
tZ	24 ± 4	5.5 ± 1.0	4.1 ± 0.8	5.9 ± 1.1	10.7 ± 1.8	23.3 ± 3.7
tW	1.37 ± 0.82	0.18 ± 0.26	0.01 ± 0.12	0.67 ± 0.64	0.26 ± 0.42	0.39 ± 0.41
WtZ	2.3 ± 1.2	0.6 ± 0.3	0.3 ± 0.2	0.3 ± 0.2	1.1 ± 0.6	0.6 ± 0.3
VVV	12.4 ± 0.4	0.9 ± 0.1	0.4 ± 0.1	0.13 ± 0.02	0.14 ± 0.03	0.02 ± 0.01
VH	40 ± 6	2.6 ± 1.4	0.9 ± 0.8	0.7 ± 0.8	0.4 ± 0.6	0.01 ± 0.01
t̄t	12.1 ± 1.6	2.9 ± 0.6	2.5 ± 0.5	2.8 ± 0.5	11.2 ± 1.5	10.9 ± 1.4
t̄tH	0.24 ± 0.03	0.05 ± 0.01	0.04 ± 0.01	0.06 ± 0.01	0.20 ± 0.03	0.13 ± 0.02
Total	5100 ± 110	227 ± 12	87 ± 6	56.7 ± 4.4	76 ± 9	52.5 ± 4.2

Table 15: Post-fit yields in each of the 1-jet regions.

523 The impact of each NP is calculated by performing the fit with the parameter of interest held
 524 fixed, varied from its fitted value by its uncertainty, and calculating $\Delta\mu$ relative to the baseline
 525 fit. The impact of the most significant sources of systematic uncertainties on WZ + b with one
 526 associated jet is summarized in Table 16.

Uncertainty Source	$\Delta\mu$	
WZ + 1-jet light XS	0.13	-0.18
WZ + charm cross-section	-0.10	0.12
Jet Energy Scale	0.1	-0.13
tZ cross-section	-0.10	0.10
WZ 1-jet/2-jet Migration	0.08	-0.07
Jet Energy Resolution	-0.10	0.10
Luminosity	-0.08	0.09
Other Diboson + b cross-section	-0.07	0.07
Flavor tagging	0.05	0.05
t <bar>t} cross-section</bar>	-0.05	0.05
Total Systematic Uncertainty	0.29	0.34

Table 16: Summary of the most significant sources of systematic uncertainty on the measurement of WZ + b with exactly one associated jet.

⁵²⁷ The ranking and impact of those nuisance parameters with the largest contribution to the overall
⁵²⁸ uncertainty is shown in Figure 34.

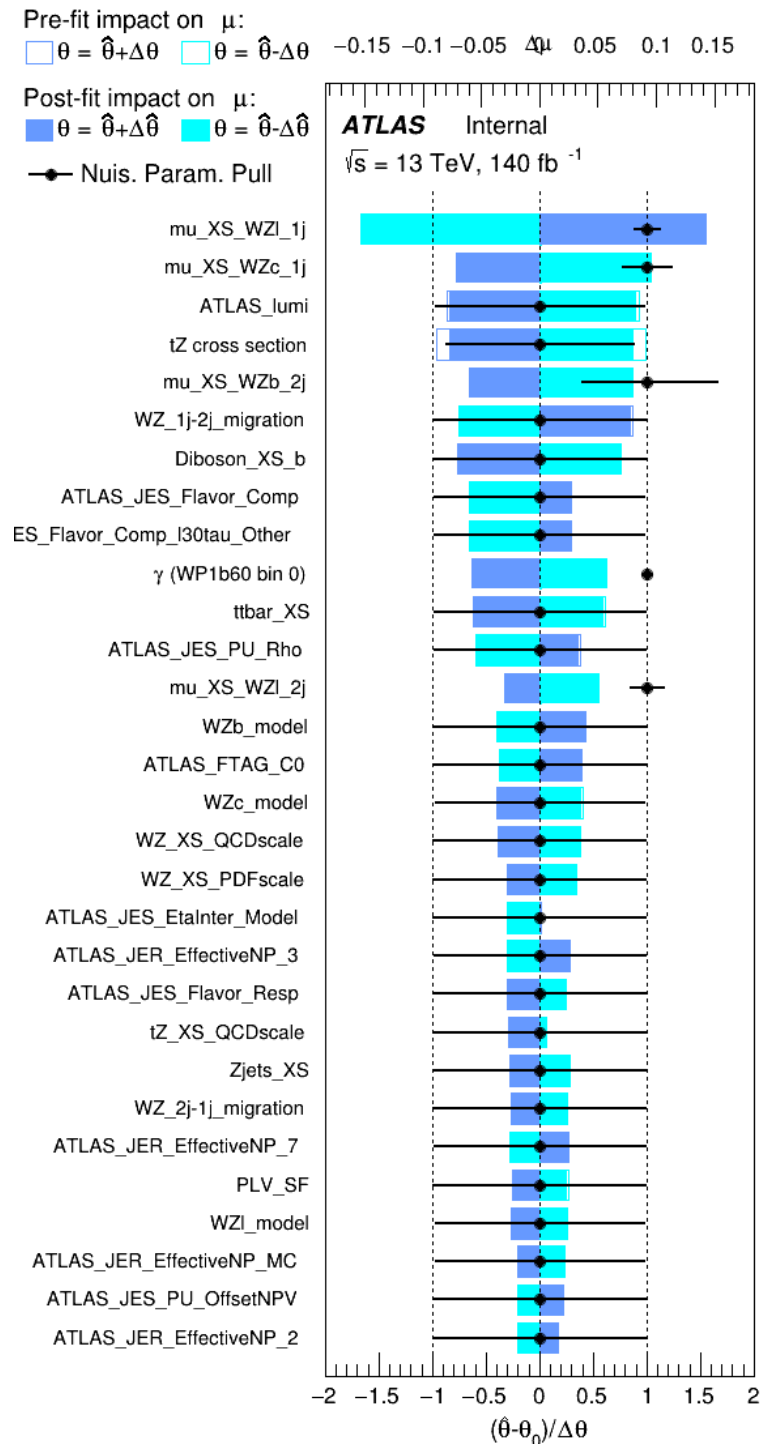


Figure 34: Impact of systematic uncertainties on the signal-strength of $WZ + b$ for events with exactly one jet

529 The large impact of the Jet Energy Scale and Jet Flavor Tagging is unsurprising, as the shape of
 530 the fit regions depends heavily on the modeling of the jets. The other major sources of uncertainty
 531 come from background modelling and cross-section uncertainty.

532 Pre-fit yields in each of the 2-jet fit are shown in Figure 8.

	2j, <85% WP	2j, 77%-85% WP	2j, 70%-77% WP	2j, 60%-70% WP	2j, >60% WP	tZ CR 2j
WZ + b - 2j	3.1 ± 1.6	6.7 ± 0.5	5.6 ± 0.4	8.0 ± 0.6	31 ± 2	14 ± 1
WZ + c - 2j	180 ± 20	54 ± 6	41 ± 3	24 ± 3	11 ± 2	4.8 ± 0.6
WZ + l - 2j	1250 ± 150	90 ± 14	18 ± 3	5.8 ± 1.4	1.4 ± 0.4	0.25 ± 0.15
WZ + b - 1j	3.4 ± 0.6	1.52 ± 0.35	1.58 ± 0.23	1.95 ± 0.39	6.7 ± 1.1	1.9 ± 0.6
WZ + c - 1j	56 ± 14	17.6 ± 4.0	8.6 ± 2.2	6.3 ± 1.8	3.0 ± 0.9	0.7 ± 0.2
WZ + l - 1j	427 ± 120	24 ± 7	4.7 ± 2.3	1.6 ± 0.7	0.3 ± 0.2	0.01 ± 0.01
WZ - Other	129 ± 29	6.1 ± 4.6	1.2 ± 0.3	0.3 ± 0.2	2.9 ± 0.5	3.6 ± 0.6
Other VV	7.63 ± 0.63	0.6 ± 0.5	0.16 ± 0.03	0.01 ± 0.01	0.1 ± 0.1	0.1 ± 0.1
ZZ	135 ± 20	14.1 ± 3.2	4.7 ± 0.8	4.0 ± 0.6	4.1 ± 0.7	3.1 ± 0.5
t̄tW	0.8 ± 0.2	0.4 ± 0.1	0.5 ± 0.1	0.7 ± 0.2	4.3 ± 0.6	3.9 ± 0.6
t̄tZ	14.7 ± 2.2	5.6 ± 0.8	4.5 ± 0.7	6.5 ± 1.1	25.4 ± 4.0	21.9 ± 3.4
rare Top	0.14 ± 0.04	0.07 ± 0.03	0.03 ± 0.02	0.09 ± 0.03	0.37 ± 0.07	0.6 ± 0.1
t̄tWW	0.04 ± 0.03	0.02 ± 0.02	0.01 ± 0.01	0.01 ± 0.00	0.03 ± 0.03	0.01 ± 0.01
Z + jets	110.0 ± 22.9	9.6 ± 2.0	2.1 ± 0.50	1.6 ± 0.4	5.1 ± 1.1	1.5 ± 0.3
W + jets	0.0 ± 0.0	0.0 ± 0.0	0.0 ± 0.0	0.0 ± 0.0	0.0 ± 0.0	0.0 ± 0.0
V + γ	25 ± 18	0.5 ± 0.2	0.1 ± 0.1	0.1 ± 0.1	0.0 ± 0.02	0.05 ± 0.07
tZ	15.9 ± 2.9	6.9 ± 1.3	5.1 ± 1.0	8.0 ± 1.5	18.7 ± 3.2	36.4 ± 6.1
tW	0.9 ± 0.7	0.2 ± 0.3	0.0 ± 0.1	0.0 ± 0.0	0.8 ± 0.6	0.2 ± 0.2
WtZ	4.9 ± 2.5	1.5 ± 0.8	1.1 ± 0.6	1.3 ± 0.7	4.6 ± 2.4	3.3 ± 1.7
VVV	7.4 ± 0.3	1.0 ± 0.1	0.4 ± 0.1	0.2 ± 0.1	0.13 ± 0.03	0.04 ± 0.01
VH	19.5 ± 4.2	2.8 ± 1.6	0.7 ± 0.7	0.1 ± 0.2	0.0 ± 0.0	0.0 ± 0.0
t̄t	0.7 ± 0.4	0.1 ± 0.1	0.05 ± 0.06	0.15 ± 0.13	0.8 ± 0.5	2.3 ± 1.2
t̄t̄	6.8 ± 1.0	2.4 ± 0.5	1.8 ± 0.4	3.3 ± 0.6	8.4 ± 1.2	13.6 ± 1.7
t̄tH	0.4 ± 0.1	0.2 ± 0.1	0.16 ± 0.02	0.23 ± 0.03	0.94 ± 0.11	1.03 ± 0.12
Total	2580 ± 160	229 ± 24	89 ± 13	69 ± 11	120 ± 15	108 ± 11

Table 17: Pre-fit yields in each of the 2-jet regions.

533 The post-fit yields in each region are summarized in Figure 8.

	2j, <85% WP	2j, 77%-85% WP	2j, 70%-77% WP	2j, 60%-70% WP	2j, >60% WP	tZ CR 2j
WZ + b	13 ± 6	6.7 ± 2.9	5.8 ± 2.5	8.0 ± 3.5	31 ± 13	14 ± 5
WZ + c	260 ± 60	77 ± 15	41 ± 8	26 ± 5	10.9 ± 2.4	4.8 ± 1.1
WZ + l	1860 ± 90	90 ± 12	17.6 ± 2.8	5.8 ± 1.3	1.4 ± 0.4	0.3 ± 0.2
WZ + b - 1j	3.4 ± 0.6	1.52 ± 0.35	1.58 ± 0.23	1.95 ± 0.39	6.7 ± 1.1	1.9 ± 0.6
WZ + c - 1j	56 ± 14	17.6 ± 4.0	8.6 ± 2.2	6.3 ± 1.8	3.0 ± 0.9	0.7 ± 0.2
WZ + l - 1j	427 ± 120	24 ± 7	4.7 ± 2.3	1.6 ± 0.7	0.3 ± 0.2	0.01 ± 0.01
WZ - Other	129 ± 29	6.1 ± 4.6	1.2 ± 0.3	0.3 ± 0.2	2.9 ± 0.5	3.6 ± 0.6
Other VV	7.6 ± 0.6	0.3 ± 0.3	0.3 ± 0.1	0.1 ± 0.06	0.03 ± 0.02	0.1 ± 0.1
ZZ	145 ± 30	11.3 ± 4.4	2.7 ± 1.6	1.0 ± 0.3	4.0 ± 0.1	2.4 ± 0.1
t̄tW	0.8 ± 0.2	0.4 ± 0.1	0.54 ± 0.12	0.74 ± 0.15	4.3 ± 0.6	3.9 ± 0.6
t̄tZ	14.7 ± 2.2	5.6 ± 0.8	4.5 ± 0.7	6.5 ± 1.0	25.4 ± 3.9	21.9 ± 3.3
rare Top	0.14 ± 0.04	0.07 ± 0.03	0.03 ± 0.02	0.09 ± 0.03	0.4 ± 0.1	0.6 ± 0.1
t̄tWW	0.04 ± 0.03	0.02 ± 0.02	0.01 ± 0.01	0.01 ± 0.01	0.03 ± 0.03	0.01 ± 0.01
Z + jets	110 ± 23	9.6 ± 2.0	2.1 ± 0.5	1.6 ± 0.4	5.1 ± 1.1	1.5 ± 0.3
W + jets	0.0 ± 0.0					
V + γ	25 ± 19	0.5 ± 0.2	0.1 ± 0.1	0.13 ± 0.14	0.0 ± 0.02	0.05 ± 0.07
tZ	15.9 ± 2.7	6.9 ± 1.2	5.1 ± 0.9	8.0 ± 1.4	18.7 ± 3.0	36 ± 6
tW	0.1 ± 0.7	0.2 ± 0.3	0.0 ± 0.1	0.0 ± 0.0	0.8 ± 0.6	0.2 ± 0.2
WtZ	4.9 ± 2.5	1.5 ± 0.8	1.1 ± 0.6	1.3 ± 0.7	4.6 ± 2.3	3.3 ± 1.7
VVV	7.4 ± 0.3	1.0 ± 0.1	0.36 ± 0.03	0.19 ± 0.03	0.13 ± 0.03	0.04 ± 0.01
VH	19 ± 4	2.8 ± 1.6	0.7 ± 0.7	0.1 ± 0.2	0.0 ± 0.0	0.0 ± 0.0
t̄t	6.8 ± 1.0	2.4 ± 0.5	1.8 ± 0.4	3.3 ± 0.6	8.4 ± 1.2	13.6 ± 1.7
t̄tH	0.40 ± 0.05	0.19 ± 0.03	0.16 ± 0.02	0.23 ± 0.03	0.94 ± 0.11	1.03 ± 0.11
Total	2580 ± 60	229 ± 11	89 ± 6	69.1 ± 4.1	120 ± 10	108 ± 6

Table 18: Post-fit yields in each of the 2-jet regions.

⁵³⁴ The same set of systematic uncertainties consider for the 1-jet fit are included in the 2-jet fit as well. The impact of the most significant systematic uncertainties is summarized in Table 19.

Uncertainty Source	$\Delta\mu$	
WZ + c 2-jet cross-section	0.19	0.15
WZ 0-jet, $>=3$ -jet cross-section	0.14	-0.14
Luminosity	-0.11	0.12
tZ cross-section	-0.11	0.11
Jet Energy Scale	-0.11	0.11
ttZ cross-section - QCD scale	-0.08	0.09
WZ + l cross-section	0.08	-0.07
WtZ cross-section	-0.07	0.07
Flavor tagging	0.05	0.05
Other VV + b cross-section	-0.05	0.05
Total	0.32	0.36

Table 19: Summary of the most significant sources of systematic uncertainty on the measurement of WZ + b 2-jet events.

⁵³⁶ The ranking and impact of those nuisance parameters with the largest contribution to the overall
⁵³⁷ uncertainty is shown in Figure 35.

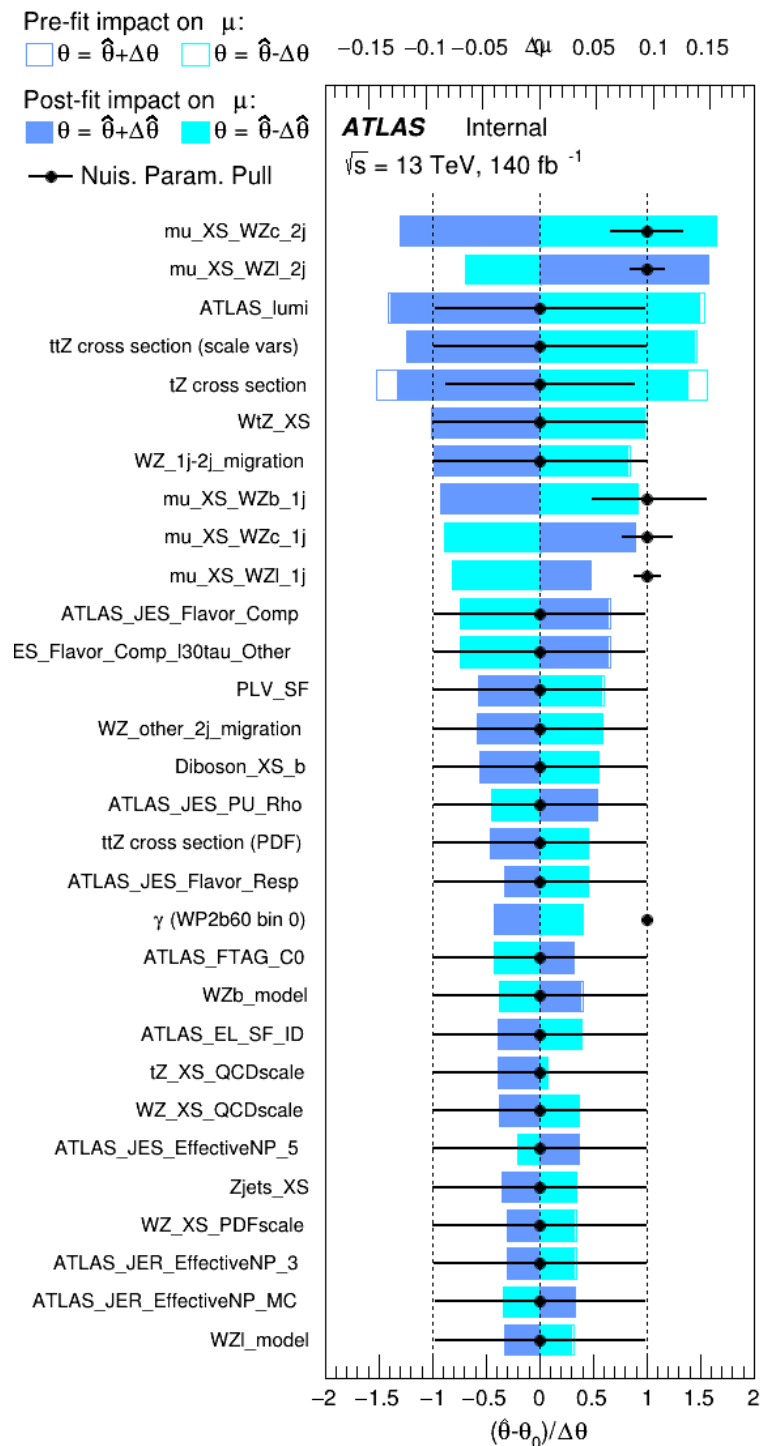


Figure 35: Impact of systematic uncertainties on the signal-strength of $WZ + b$ in 2-jet events.

538 The large impact of the Jet Energy Scale and Jet Flavor Tagging is unsurprising, as the shape of
 539 the fit regions depends heavily on the modeling of the jets. The other major sources of uncertainty
 540 come from background modelling and cross-section uncertainty.

541 9 Conclusion

542 A measurement of $WZ +$ heavy flavor is performed using 140 fb^{-1} of $\sqrt{s} = 13 \text{ TeV}$ proton-
 543 proton collision data collected by the ATLAS detector at the LHC. The expected cross-section
 544 of $WZ+b$ with 1-jet is $1.74^{+0.82}_{-0.75}(\text{stat})^{+0.53}_{-0.48}(\text{sys}) \text{ fb}$, and $14.6 \pm 2.5(\text{stat}) \pm 2.3(\text{sys}) \text{ fb}$ for WZ
 545 + charm, with a correlation of -0.22 between them. An expected significance of 2.0 is observed
 546 for $WZ + b$ in this region.

547 For the 2-jet regions, an expected significance of 1.7 is observed for $WZ + b$, with an ex-
 548 pected cross-section of $2.5^{+1.3}_{-1.3}(\text{stat})^{+0.95}_{-0.83}(\text{sys}) \text{ fb}$. For $WZ +$ charm, a cross-section of
 549 $12.7 \pm 3.2(\text{stat}) \pm 2.7(\text{sys}) \text{ fb}$ is expected for 2-jet events. A correlation of -0.26 is observed
 550 for $WZ+b$ and $WZ +$ charm.

551 **This section will be include final results once unblinded.**

552 References

- 553 [1] M. Aaboud et al. ‘Observation of electroweak $W^\pm Z$ boson pair production in association
 554 with two jets in pp collisions at $\sqrt{s} = 13 \text{ TeV}$ with the ATLAS detector’. In: *Phys.
 555 Lett.* B793 (2019), pp. 469–492. doi: [10.1016/j.physletb.2019.05.012](https://doi.org/10.1016/j.physletb.2019.05.012). arXiv:
 556 [1812.09740 \[hep-ex\]](https://arxiv.org/abs/1812.09740).
- 557 [2] T. Gleisberg et al. ‘Event generation with SHERPA 1.1’. In: *JHEP* 02 (2009), p. 007. doi:
 558 [10.1088/1126-6708/2009/02/007](https://doi.org/10.1088/1126-6708/2009/02/007). arXiv: [0811.4622 \[hep-ph\]](https://arxiv.org/abs/0811.4622).
- 559 [3] R. D. Ball et al. ‘Parton distributions for the LHC Run II’. In: *JHEP* 04 (2015), p. 040.
 560 doi: [10.1007/JHEP04\(2015\)040](https://doi.org/10.1007/JHEP04(2015)040). arXiv: [1410.8849 \[hep-ph\]](https://arxiv.org/abs/1410.8849).
- 561 [4] H.-L. Lai et al. ‘New parton distributions for collider physics’. In: *Phys. Rev. D* 82 (2010),
 562 p. 074024. doi: [10.1103/PhysRevD.82.074024](https://doi.org/10.1103/PhysRevD.82.074024). arXiv: [1007.2241 \[hep-ph\]](https://arxiv.org/abs/1007.2241).
- 563 [5] S. Frixione, G. Ridolfi and P. Nason. ‘A positive-weight next-to-leading-order Monte Carlo
 564 for heavy flavour hadroproduction’. In: *JHEP* 09 (2007), p. 126. doi: [10.1088/1126-6708/2007/09/126](https://doi.org/10.1088/1126-

 565 6708/2007/09/126). arXiv: [0707.3088 \[hep-ph\]](https://arxiv.org/abs/0707.3088).
- 566 [6] E. Re. ‘Single-top Wt-channel production matched with parton showers using the POWHEG
 567 method’. In: *Eur. Phys. J. C* 71 (2011), p. 1547. doi: [10.1140/epjc/s10052-011-1547-z](https://doi.org/10.1140/epjc/s10052-011-

 568 1547-z). arXiv: [1009.2450 \[hep-ph\]](https://arxiv.org/abs/1009.2450).
- 569 [7] ATLAS Collaboration. *Electron efficiency measurements with the ATLAS detector using
 570 the 2015 LHC proton–proton collision data*. ATLAS-CONF-2016-024. 2016. url: <https://cds.cern.ch/record/2157687>.

- 572 [8] ATLAS Collaboration. ‘Measurement of the muon reconstruction performance of the
 573 ATLAS detector using 2011 and 2012 LHC proton–proton collision data’. In: *Eur. Phys.*
 574 *J. C* 74 (2014), p. 3130. doi: [10.1140/epjc/s10052-014-3130-x](https://doi.org/10.1140/epjc/s10052-014-3130-x). arXiv: [1407.3935](https://arxiv.org/abs/1407.3935)
 575 [[hep-ex](#)].
- 576 [9] *Evidence for the associated production of the Higgs boson and a top quark pair with the*
 577 *ATLAS detector*. Tech. rep. ATLAS-CONF-2017-077. Geneva: CERN, Nov. 2017. URL:
 578 <https://cds.cern.ch/record/2291405>.
- 579 [10] ATLAS Collaboration. *Jet Calibration and Systematic Uncertainties for Jets Reconstructed in the ATLAS Detector at $\sqrt{s} = 13$ TeV*. ATL-PHYS-PUB-2015-015. 2015. URL:
 580 <https://cds.cern.ch/record/2037613>.
- 582 [11] ATLAS Collaboration. *Selection of jets produced in 13 TeV proton–proton collisions with*
 583 *the ATLAS detector*. ATLAS-CONF-2015-029. 2015. URL: <https://cds.cern.ch/record/2037702>.
- 585 [12] ATLAS Collaboration. ‘Performance of pile-up mitigation techniques for jets in pp col-
 586 lisions at $\sqrt{s} = 8$ TeV using the ATLAS detector’. In: *Eur. Phys. J. C* 76 (2016), p. 581.
 587 doi: [10.1140/epjc/s10052-016-4395-z](https://doi.org/10.1140/epjc/s10052-016-4395-z). arXiv: [1510.03823](https://arxiv.org/abs/1510.03823) [[hep-ex](#)].
- 588 [13] ATLAS Collaboration. *Performance of missing transverse momentum reconstruction with*
 589 *the ATLAS detector in the first proton–proton collisions at $\sqrt{s} = 13$ TeV*. ATL-PHYS-
 590 PUB-2015-027. 2015. URL: <https://cds.cern.ch/record/2037904>.
- 591 [14] 2021. URL: https://twiki.cern.ch/twiki/bin/view/AtlasProtected/BTagCalibrationRecommendationsRelease21#Tools_for_Flavor_Tagging_Calibra.
- 594 [15] P. S. A. Hoecker. ‘TMVA 4 Toolkit for Multivariate Data Analysis with ROOT’. In:
 595 *arXiv:physics/0703039* (2013).
- 596 [16] F. Cardillo et al. ‘Measurement of the fiducial and differential cross-section of a top quark
 597 pair in association with a Z boson at 13 TeV with the ATLAS detector’. In: ATL-COM-
 598 PHYS-2019-334 (Apr. 2019). URL: <https://cds.cern.ch/record/2672207>.
- 599 [17] T. Chen and C. Guestrin. ‘XGBoost: A Scalable Tree Boosting System’. In: *Proceedings*
 600 *of the 22nd ACM SIGKDD International Conference on Knowledge Discovery and Data*
 601 *Mining*. KDD ’16. San Francisco, California, USA: ACM, 2016, pp. 785–794. ISBN: 978-
 602 1-4503-4232-2. doi: [10.1145/2939672.2939785](https://doi.org/10.1145/2939672.2939785). URL: <http://doi.acm.org/10.1145/2939672.2939785>.
- 604 [18] ATLAS Collaboration. ‘Luminosity determination in pp collisions at $\sqrt{s} = 7$ TeV using
 605 the ATLAS detector at the LHC’. In: *Eur. Phys. J. C* 71 (2011), p. 1630. doi: [10.1140/epjc/s10052-011-1630-5](https://doi.org/10.1140/epjc/s10052-011-1630-5). arXiv: [1101.2185](https://arxiv.org/abs/1101.2185) [[hep-ex](#)].
- 607 [19] G. Avoni et al. ‘The new LUCID-2 detector for luminosity measurement and monitoring in
 608 ATLAS’. In: *JINST* 13.07 (2018), P07017. doi: [10.1088/1748-0221/13/07/P07017](https://doi.org/10.1088/1748-0221/13/07/P07017).

- 609 [20] G. Aad et al. ‘Jet energy resolution in proton-proton collisions at $\sqrt{s} = 7$ TeV recorded
610 in 2010 with the ATLAS detector’. In: *The European Physical Journal C* 73.3 (Mar.
611 2013), p. 2306. ISSN: 1434-6052. DOI: [10.1140/epjc/s10052-013-2306-0](https://doi.org/10.1140/epjc/s10052-013-2306-0). URL:
612 <https://doi.org/10.1140/epjc/s10052-013-2306-0>.
- 613 [21] A. Collaboration. ‘Performance of b -jet identification in the ATLAS experiment’. In:
614 *Journal of Instrumentation* 11.04 (2016), P04008. URL: <http://stacks.iop.org/1748-0221/11/i=04/a=P04008>.
- 616 [22] ‘Observation of the associated production of a top quark and a Z boson at 13 TeV with
617 ATLAS’. In: (July 2020). URL: <https://cds.cern.ch/record/2722504>.

⁶¹⁸ **A Appendices**

⁶¹⁹ **A.1 Non-prompt lepton MVA**

620 A lepton MVA has been developed to better reject non-prompt leptons than standard cut
 621 based selections based upon impact parameter, isolation and PID. The name of this MVA is
 622 `PromptLeptonIso`. The full set of studies and detailed explanation can be found in REFER-
 623 ENCE PAPER.

624 The decays of W and Z bosons are commonly selected by the identification of one or two electrons
 625 or muons. The negligible lifetimes of these bosons mean that the leptons produced in the decay
 626 originate from the interaction vertex and are thus labelled “prompt”. Analyses using these
 627 light leptons impose strict reconstruction quality, isolation and impact parameter requirements
 628 to remove “fake” leptons. A significant source of the fake light leptons are non-prompt leptons
 629 produced in decays of hadrons that contain bottom (b) or charm (c) quarks. Such hadrons
 630 typically have microscopically significant lifetimes that can be detected experimentally.

631 These non-prompt leptons can also pass the tight selection criteria. In analyses that involve top (t)
 632 quarks, which decay almost exclusively into a W boson and a b quark, non-prompt leptons from
 633 the semileptonic decay of bottom and charm hadrons can be a significant source of background
 634 events. This is particularly the case in the selection of same-sign dilepton and multilepton final
 635 states. Even after the application of very tight isolation requirements, the dominant background
 636 and uncertainty in the 2ℓ and 3ℓ signal regions in the Run 2 multilepton $t\bar{t}H$ analysis is due to a
 637 non-prompt light lepton contribution from the $t\bar{t}$ process. The non-prompt lepton background
 638 yield and uncertainty on its normalization are limiting factors for the observation of the $t\bar{t}H$
 639 process in the multilepton final states in Run 2.

640 The main idea is to identify non-prompt light leptons using lifetime information associated with a
 641 track jet that matches the selected light lepton. This lifetime information is computed using tracks
 642 contained within the jet. Typically, lepton lifetime is determined using the impact parameter of the
 643 track reconstructed by the inner tracking detector which is matched to the reconstructed lepton.
 644 Using additional reconstructed charged particle tracks increases the precision of identifying the
 645 displaced decay vertex of bottom or charm hadrons that produced a non-prompt light lepton.
 646 The MVA also includes information related to the isolation of the lepton to reject non-prompt
 647 leptons. `PromptLeptonIso` is a gradient boosted BDT. The training of the BDT is performed on
 648 leptons selected from the PowHEG+PYTHIA6 non-allhad $t\bar{t}$ MC sample. Eight variables are used
 649 to train the BDT in order to discriminate between prompt and non-prompt leptons. The track
 650 jets that are matched to the non-prompt leptons correspond to jets initiated by b or c quarks, and
 651 may contain a displaced vertex. Consequently, three of the selected variables are used to identify
 652 b-tag jets by standard ATLAS flavour tagging algorithms. Two variables use the relationship
 653 between the track jet and lepton: the ratio of the lepton p_T with respect to the track jet p_T and
 654 ΔR between the lepton and the track jet axis. Finally three additional variables test whether the
 655 reconstructed lepton is isolated: the number of tracks collected by the track jet and the lepton
 656 track and calorimeter isolation variables. Table 20 describes the variables used to train the BDT
 657 algorithm. The choice of input variables has been extensively discussed with Egamma, Muon,
 658 Tracking, and Flavour Tagging CP groups.

659 The optimised working point of `PromptLeptonIso` < -0.50 allows to double the signal accept-
 660 ance in the dilepton channel while keeping a similar S/B compared to the ICHEP16 yields, if

Variable	Description
N_{track} in track jet	Number of tracks collected by the track jet
$\text{IP2 log}(P_b/P_{\text{light}})$	Log-likelihood ratio between the b and light jet hypotheses with the IP2D algorithm
$\text{IP3 log}(P_b/P_{\text{light}})$	Log-likelihood ratio between the b and light jet hypotheses with the IP3D algorithm
N_{TrkAtVtx} SV + JF	Number of tracks used in the secondary vertex found by the SV1 algorithm in addition to the number of tracks from secondary vertices found by the JetFitter algorithm with at least two tracks
$p_T^{\text{lepton}}/p_T^{\text{track jet}}$	The ratio of the lepton p_T and the track jet p_T
$\Delta R(\text{lepton}, \text{track jet})$	ΔR between the lepton and the track jet axis
$p_T^{\text{VarCone30}}/p_T$	Lepton track isolation, with track collecting radius of $\Delta R < 0.3$
$E_T^{\text{TopoCone30}}/p_T$	Lepton calorimeter isolation, with topological cluster collecting radius of $\Delta R < 0.3$

Table 20: A table of the variables used in the training of `PromptLeptonIso`.

661 additionally $N_{\text{jets}} \geq 4$ jets (instead of 5) and the transverse momentum of the second lead-
 662 ing lepton is required to be > 15 GeV (instead of 25 GeV). In the trilepton channel, if the
 663 the two same-signed leptons are required to pass that same `PromptLeptonIso` working point,
 664 non-prompt lepton background gets reduced by 40% while keeping the same signal efficiency
 665 as in ICHEP16. The optimisation of this working point is performed on top of the 95% signal
 666 efficiency charge misidentification BDT cut on electrons in dilepton events.

 667 The modelling of `PromptLeptonIso` for prompt leptons is studied with the opposite-sign 2ℓ
 668 CR, with one electron and one muon. The modelling of the overall efficiency of selecting prompt
 669 leptons in data and MC with $\text{PromptLeptonIso} < -0.5$ is within 2%.

 670 The modelling of `PromptLeptonIso` for non-prompt leptons is studied with in the tight 2ℓ
 671 same-sign control region, where the sub-leading lepton in p_T is more likely to be the non-prompt
 672 lepton. In all subregions, the data and MC agreement is excellent. The number of data and
 673 simulation events that are rejected by the `PromptLeptonIso` selection are similar, with the data
 674 to simulation ratio remaining stable to within a percent.

 675 The efficiency of the tight `PromptLeptonIso` working point is measured using the tag and probe
 676 method with $Z \rightarrow \ell^+\ell^-$ events. Such calibration are performed by analysers from this analysis
 677 in communication with the Egamma and Muon combined performance groups. The scale factor
 678 are approximately 0.92 for $10 < p_T < 15$ GeV, and averaging at 0.98 to 0.99 for higher p_T
 679 leptons. An extra systematic is applied to muons within $\Delta R < 0.6$ of a calorimeter jet, since
 680 there is a strong dependence on the scale factor due to the presence of these jets. For electrons,
 681 the dominant systematics is coming from pile-up dependence. Overall the systematics are at
 682 maximum of 3% at low p_T and decreasing at a function of p_T .

683 **A.2 Non-prompt CR Modelling**

684 In order to further validate the modeling in each of the non-prompt CRs, additional kinematic
 685 plots are made in the Z+jets CR and $t\bar{t}$ CR in each of the continuous b-tag regions.

686 In the case of the Z+jets CR, the p_T spectrum of the lepton originating from the W candidate is
 687 shown, as this is the distribution used to extract the scale factor applied to Z+jets. These plots
 688 are shown in Figures 36 and 37.

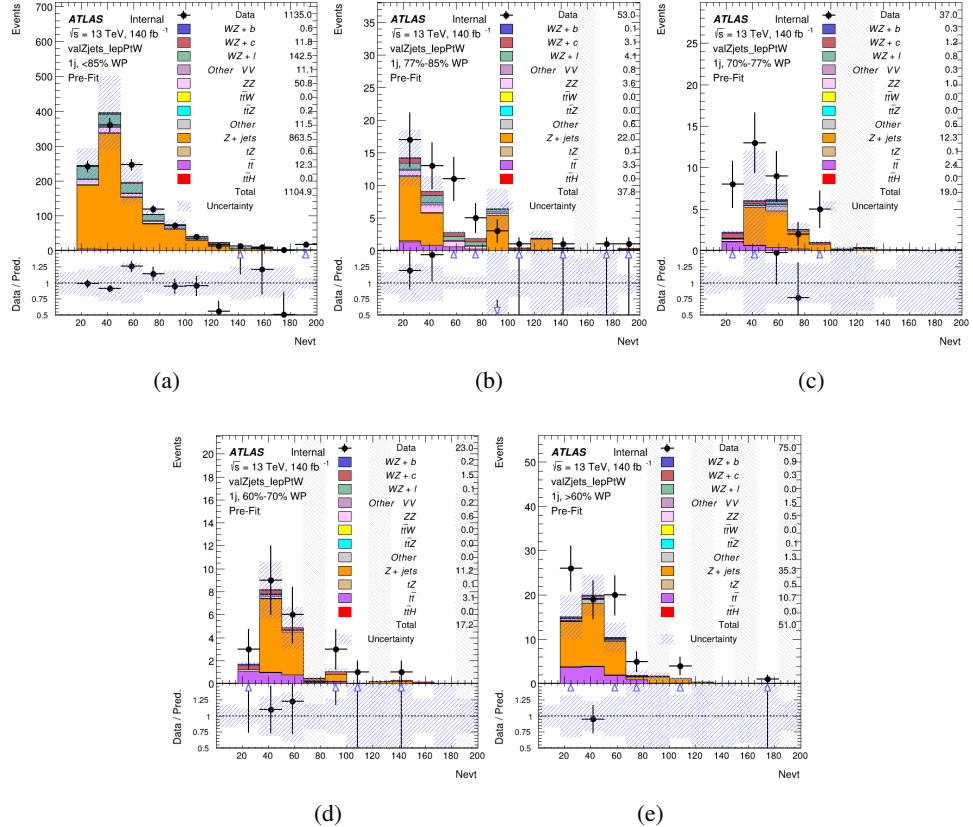


Figure 36: Comparisons between the data and MC distributions in the Z+jets CR for each of the 1-jet b-tag working point regions

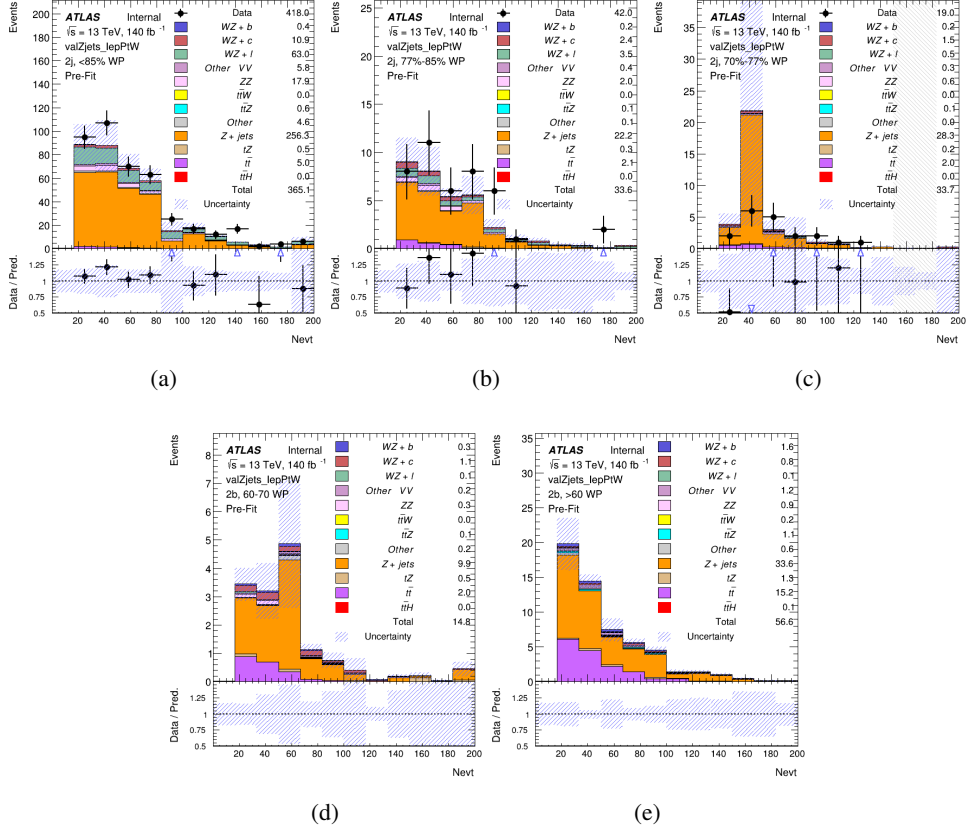


Figure 37: Comparisons between the data and MC distributions in the Z+jets CR for each of the 2-jet b-tag working point regions

689 The same is shown for the $t\bar{t}$ CR, but the p_T of the OS lepton is used instead as a representation
690 of the modeling, as the lepton from the W is not well defined for $t\bar{t}$ events. These plots are shown
691 in Figures 38 and 39.

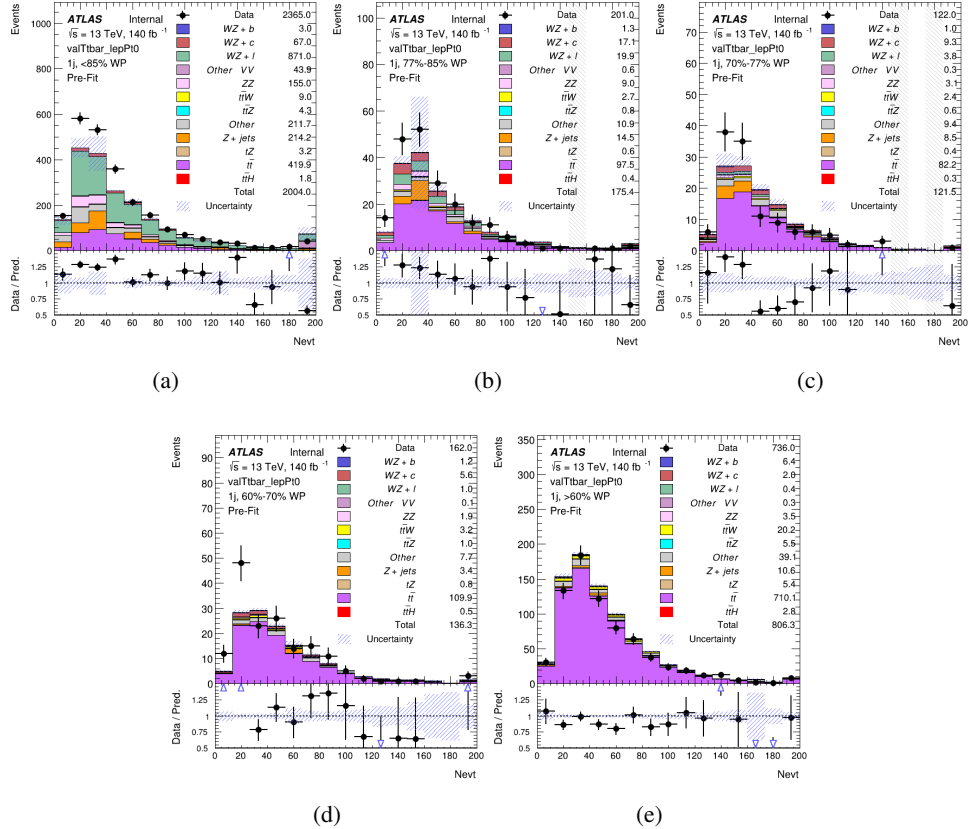


Figure 38: Comparisons between the data and MC distributions in the $t\bar{t}$ CR for each of the 1-jet b-tag working point regions

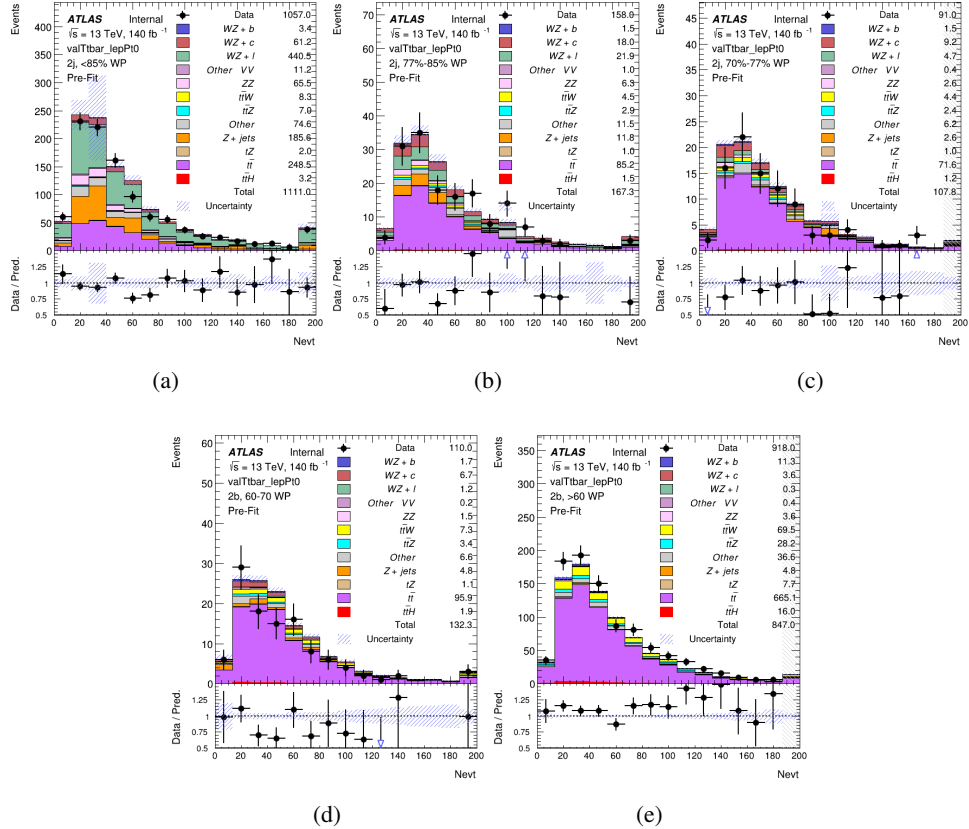


Figure 39: Comparisons between the data and MC distributions in the $t\bar{t}$ CR for each of the 2-jet b-tag working point regions

692 **A.3 tZ Interference Studies**

693 Because it includes an on-shell Z boson as well as a b-jet and W from the top decay, tZ
694 production represents an identical final state to WZ + b-jet. This implies the possibility of matrix
695 level interference between these two processes not accounted for in the Monte Carlo simulations,
696 which consider the two processes independently. Truth level studies are performed in order to
697 estimate the impact of these interference effects.

698 In order to estimate the matrix level interference effects between tZ and WZ + b-jet, two different
699 sets of simulations are produced using MadGraph 5 [**Madgraph**] - one which simulates these
700 two processes independently, and another where they are produced simultaneously, such that
701 interference effects are present. These two sets of samples are then compared, and the difference
702 between them can be taken to represent any interference effects.

703 MadGraph simulations of 10,000 tZ and 10,000 WZ + b-jet events are produced, along with
704 20,000 events where both are present, in the fiducial region where three leptons and at least one
705 jet are produced.

706 A selection mimicking the preselection used in the main analysis is applied to the samples: The
707 SS leptons are required to have $p_T > 20$ GeV, and > 10 GeV is required for the OS lepton. The
708 associated b-jet is required to have $p_T > 25$ GeV, and all physics objects are required to fall in a
709 range of $|\eta| < 2.5$.

710 The kinematics of these samples after the selection has been applied are shown below:

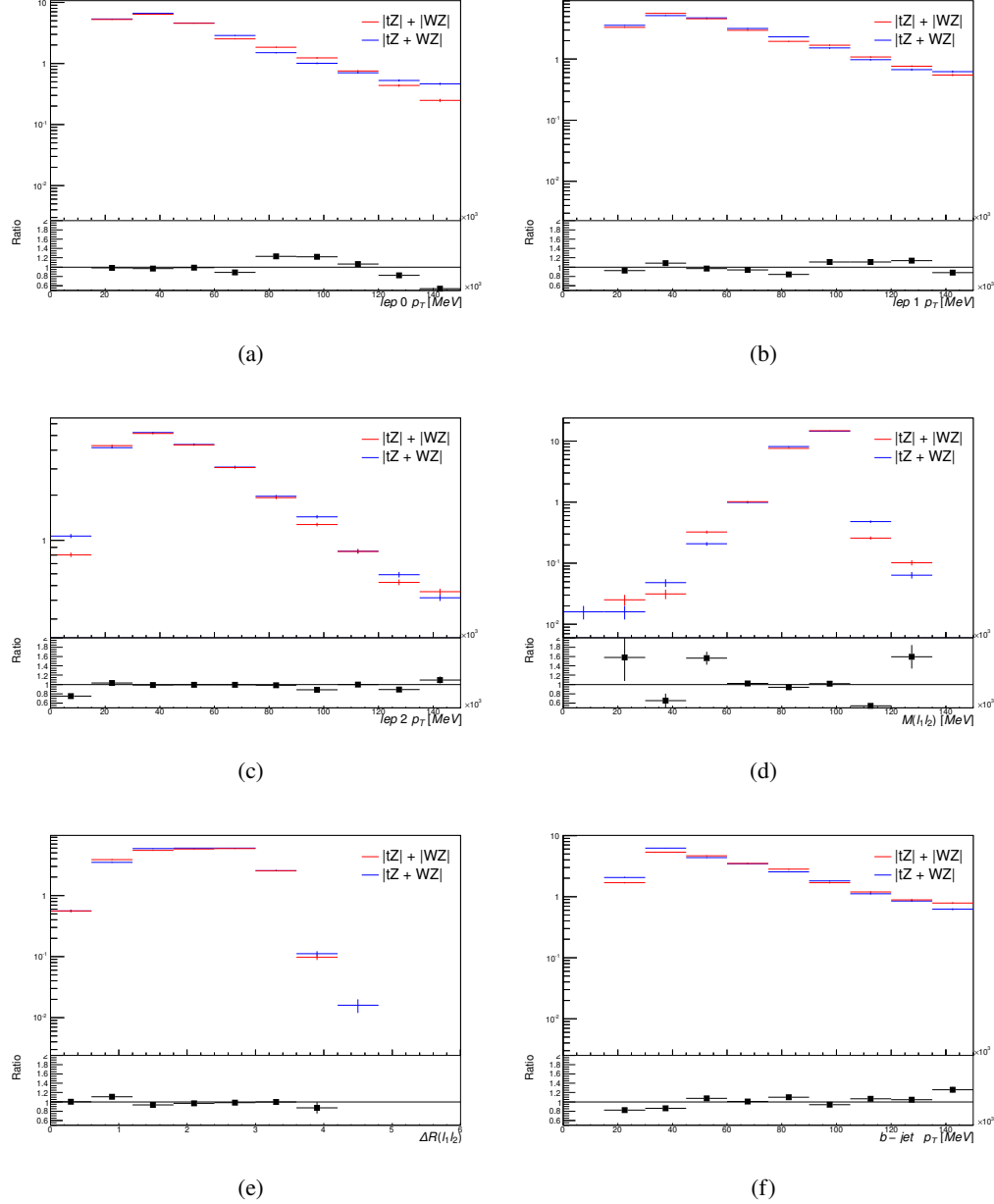


Figure 40: Comparisons between (a) the p_T of the lepton from the W, (b) and (c) show the p_T of the lepton from the Z, (d) the invariant mass of the Z-candidate, (e) ΔR of the leptons from the Z, and (f) the p_T of the b-jet, for WZ and tZ events generated with interference effects (blue) and without interference effects (red).

711 The overall cross-section of the two methods agree within error, and no significant differences
 712 in the kinematic distributions are seen. It is therefore concluded that interference effects do not

₇₁₃ significantly impact the results.

714 **A.4 Alternate tZ Inclusive Fit**

715 While tZ is often considered as a distinct process from WZ + b, this could also be considered part
 716 of the signal. Alternate studies are performed where, using the same framework as the nominal
 717 analysis, a measurement of WZ + b is performed that includes tZ as part of WZ+b.

718 Because of this change, the tZ CR is no longer necessary, and only the five pseudo-continuous
 719 b-tag regions are used in the fit. Further, systematics related to the tZ cross-section are removed
 720 from the fit, as they are now encompassed by the normalization measurement of WZ + b. All
 721 other systematic uncertainties are carried over from the nominal analysis.

722 A post-fit summary of the 1-jet regions used in the fit are shown in Figure 41.

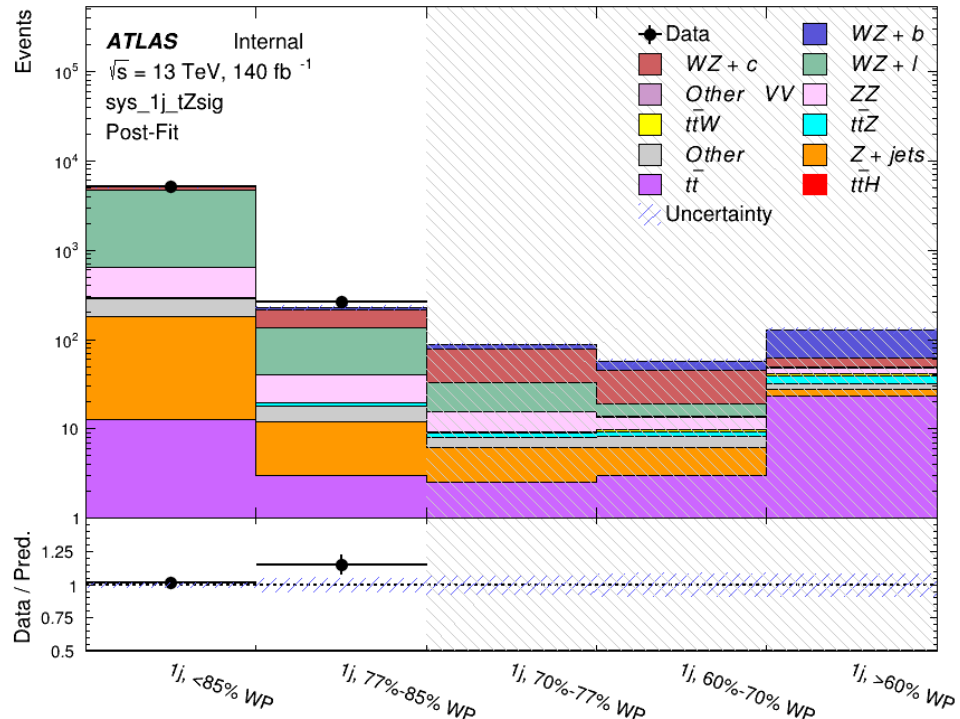


Figure 41: Post-fit summary of the 1-jet fit regions.

723 An expected WZ + b cross-section of $4.1^{+0.78}_{-0.74}(\text{stat})^{+0.53}_{-0.52}(\text{sys}) \text{ fb}$ is extracted from the fit, with
 724 an expected significance of 4.0σ .

725 The impact of the predominate systematics are summarized in Table 21.

Uncertainty Source	$\Delta\mu$	
WZ + light cross-section	0.08	-0.08
Jet Energy Scale	-0.06	0.08
Luminosity	-0.05	0.06
WZ + charm cross-section	-0.04	0.05
Other Diboson + b cross-section	-0.04	0.04
WZ cross-section - QCD scale	-0.04	0.03
t <bar>t</bar>	-0.03	0.03
Jet Energy Resolution	-0.03	0.03
Flavor tagging	-0.03	0.03
Z+jets cross section	-0.02	0.02
Total Systematic Uncertainty	-0.15	0.16

Table 21: Summary of the most significant sources of systematic uncertainty on the measurement of WZ + b with exactly one associated jet.

726 A post-fit summary of the 2-jet regions used in the fit are shown in Figure 42.

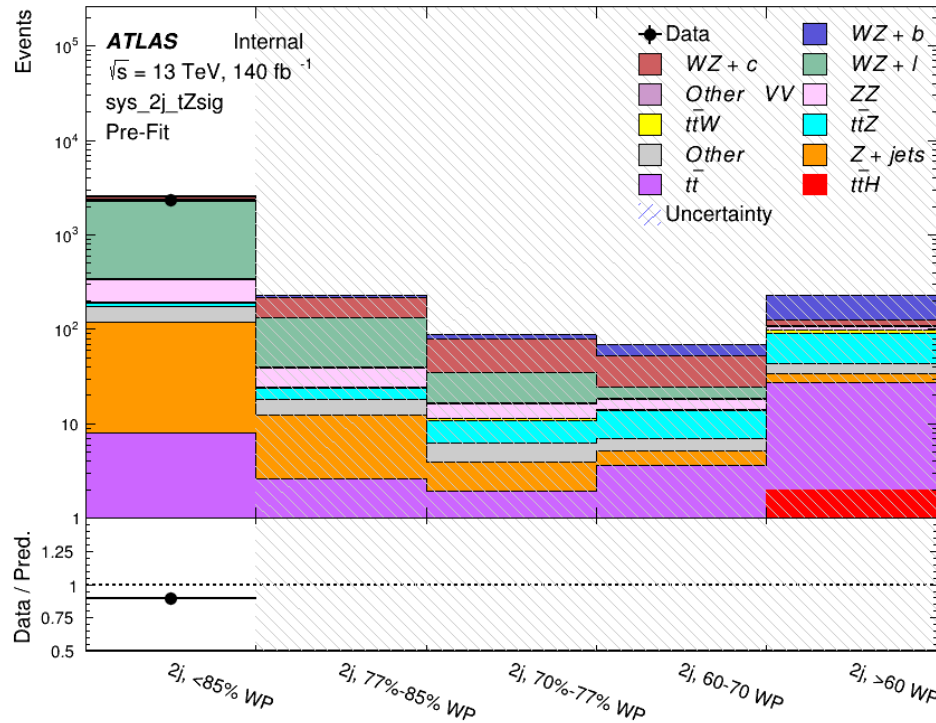


Figure 42: Post-fit summary of the 2-jet fit regions.

727 An expected WZ + b cross-section of $5.9^{+0.9}_{-0.9}(\text{stat})^{+0.9}_{-0.8}(\text{sys}) \text{ fb}$ is extracted from the fit, with an

⁷²⁸ expected significance of 5.3σ .

⁷²⁹ The impact of the predominate systematics are summarized in Table 22.

Uncertainty Source	$\Delta\mu$	
Luminosity	-0.07	0.07
Jet Energy Scale	0.06	0.05
ttZ cross-section - QCD scale	-0.05	0.05
WZ+l cross-section	0.05	-0.05
WZ+c cross-section	-0.03	0.05
WtZ cross-section	-0.03	0.03
WZ cross-section QCDscale	-0.03	0.03
Diboson cross-section b	-0.03	0.03
WZ cross-section - PDF	-0.03	0.03
Flavor Tagging	0.03	0.02
Total Systematic Uncertainty	-0.14	0.16

Table 22: Summary of the most significant sources of systematic uncertainty on the measurement of WZ + b with exactly one associated jet.

730 **A.5 DSID list**

Data:

```

data15_13TeV.AllYear.physics_Main.PhysCont.DAOD_HIGG8D1.grp15_v01_p4134
data16_13TeV.AllYear.physics_Main.PhysCont.DAOD_HIGG8D1.grp16_v01_p4134
data17_13TeV.AllYear.physics_Main.PhysCont.DAOD_HIGG8D1.grp17_v01_p4134
data18_13TeV.AllYear.physics_Main.PhysCont.DAOD_HIGG8D1.grp18_v01_p4134

mc16a:
mc16_13TeV.361603.PowhegPy8EG_CT10nloME_AZNLOCTEQ6L1_ZZllll_mll4.deriv.DAOD_HIGG8D1.e4475_s3126_r9364_r9315_p4133
mc16_13TeV.361602.PowhegPy8EG_CT10nloME_AZNLOCTEQ6L1_WZlvvv_mll4.deriv.DAOD_HIGG8D1.e4054_s3126_r9364_r9315_p4133
mc16_13TeV.361604.PowhegPy8EG_CT10nloME_AZNLOCTEQ6L1_ZZvvll_mll4.deriv.DAOD_HIGG8D1.e4475_s3126_r9364_r9315_p4133
mc16_13TeV.361600.PowhegPy8EG_CT10nloME_AZNLOCTEQ6L1_WWlqlv.deriv.DAOD_HIGG8D1.e4616_s3126_r9364_r9315_p4133
mc16_13TeV.361605.PowhegPy8EG_CT10nloME_AZNLOCTEQ6L1_ZZvvvv_mll4.deriv.DAOD_HIGG8D1.e4054_s3126_s3136_r9364_r9315_p4133
mc16_13TeV.361601.PowhegPy8EG_CT10nloME_AZNLOCTEQ6L1_WZlqlj_mll4.deriv.DAOD_HIGG8D1.e4475_s3126_r9364_r9315_p4133
mc16_13TeV.364286.Sherpa_222_NNPDF30NNLO_llvjj_ss_EW4.deriv.DAOD_HIGG8D1.e6055_e5984_s3126_r9364_r9315_p3983 mc16_13TeV.364285.Sherpa_222_NNPDF30NNLO_llvjj_ss_EW4.deriv.DAOD_HIGG8D1.e6055_e5984_s3126_r9364_r9315_p4133
mc16_13TeV.364740.MGPy8EG_NNPDF30NLO_A14NNPDF23LO_llvjj_EW6_OFPlus.deriv.DAOD_HIGG8D1.e7421_e5984_s3126_r9364_r9315_p4133
mc16_13TeV.364742.MGPy8EG_NNPDF30NLO_A14NNPDF23LO_llvjj_EW6_SFPlus.deriv.DAOD_HIGG8D1.e7421_e5984_s3126_r9364_r9315_p4133
mc16_13TeV.364253.Sherpa_222_NNPDF30NNLO_lllv.deriv.DAOD_HIGG8D1.e5916_s3126_r9364_r9315_p4133
mc16_13TeV.364250.Sherpa_222_NNPDF30NNLO_llll.deriv.DAOD_HIGG8D1.e5894_s3126_r9364_r9315_p4133
mc16_13TeV.364254.Sherpa_222_NNPDF30NNLO_llvv.deriv.DAOD_HIGG8D1.e5916_s3126_r9364_r9315_p4133
mc16_13TeV.364255.Sherpa_222_NNPDF30NNLO_llvvv.deriv.DAOD_HIGG8D1.e5916_s3126_r9364_r9315_p4133
mc16_13TeV.410155.aMcAtNloPythia8EvtGen_MEN30NLO_A14N23LO_ttW.deriv.DAOD_HIGG8D1.e5070_s3126_r9364_r9315_p4133
mc16_13TeV.410156.aMcAtNloPythia8EvtGen_MEN30NLO_A14N23LO_ttZnunu.deriv.DAOD_HIGG8D1.e5070_s3126_r9364_r9315_p4133
mc16_13TeV.410157.aMcAtNloPythia8EvtGen_MEN30NLO_A14N23LO_ttZqq.deriv.DAOD_HIGG8D1.e5070_s3126_r9364_r9315_p4133
mc16_13TeV.410218.aMcAtNloPythia8EvtGen_MEN30NLO_A14N23LO_ttee.deriv.DAOD_HIGG8D1.e5070_s3126_r9364_r9315_p4133
mc16_13TeV.410219.aMcAtNloPythia8EvtGen_MEN30NLO_A14N23LO_ttmumu.deriv.DAOD_HIGG8D1.e5070_s3126_r9364_r9315_p4133
mc16_13TeV.410220.aMcAtNloPythia8EvtGen_MEN30NLO_A14N23LO_ttautau.deriv.DAOD_HIGG8D1.e5070_s3126_r9364_r9315_p4133
mc16_13TeV.410276.aMcAtNloPythia8EvtGen_MEN30NLO_A14N23LO_ttee_mll_1_5.deriv.DAOD_HIGG8D1.e6087_e5984_s3126_r9364_r9315_p4133
mc16_13TeV.410277.aMcAtNloPythia8EvtGen_MEN30NLO_A14N23LO_ttmumu_mll_1_5.deriv.DAOD_HIGG8D1.e6087_e5984_s3126_r9364_r9315_p4133
mc16_13TeV.410278.aMcAtNloPythia8EvtGen_MEN30NLO_A14N23LO_ttautau_mll_1_5.deriv.DAOD_HIGG8D1.e6087_e5984_s3126_r9364_r9315_p4133
mc16_13TeV.410397.MadGraphPythia8EvtGen_ttbar_wbee_MEN30LO_A14N23LO.deriv.DAOD_HIGG8D1.e6086_e5984_s3126_r9364_r9315_p4133
mc16_13TeV.410398.MadGraphPythia8EvtGen_ttbar_wbmumu_MEN30LO_A14N23LO.deriv.DAOD_HIGG8D1.e6086_e5984_s3126_r9364_r9315_p4133
mc16_13TeV.410399.MadGraphPythia8EvtGen_ttbar_wbtautau_MEN30LO_A14N23LO.deriv.DAOD_HIGG8D1.e6086_e5984_s3126_r9364_r9315_p4133
mc16_13TeV.410658.PhPy8EG_A14_tchan_BW50_lept_top.deriv.DAOD_HIGG8D1.e6671_e5984_s3126_r9364_r9315_p4133
mc16_13TeV.410659.PhPy8EG_A14_tchan_BW50_lept_antitop.deriv.DAOD_HIGG8D1.e6671_e5984_s3126_r9364_r9315_p4133
mc16_13TeV.410644.PowhegPythia8EvtGen_A14_singletop_schan_lept_top.deriv.DAOD_HIGG8D1.e65271_e5984_s3126_r9364_r9315_p4133
mc16_13TeV.410645.PowhegPythia8EvtGen_A14_singletop_schan_lept_antitop.deriv.DAOD_HIGG8D1.e65271_e5984_s3126_r9364_r9315_p4133
mc16_13TeV.304014.MadGraphPythia8EvtGen_A14NNPDF23_3top_SM.deriv.DAOD_HIGG8D1.e4324_s3126_r9364_r9315_p4133
mc16_13TeV.410080.MadGraphPythia8EvtGen_A14NNPDF23_4topSM.deriv.DAOD_HIGG8D1.e4111_s3126_r9364_r9315_p4133
mc16_13TeV.410081.MadGraphPythia8EvtGen_A14NNPDF23_ttbarWW.deriv.DAOD_HIGG8D1.e4111_s3126_r9364_r9315_p4133
mc16_13TeV.364100.Sherpa_221_NNPDF30NNLO_Zmmumu_MAXHTPTV0_70_CVetoBVeto.deriv.DAOD_HIGG8D1.e5271_s3126_r9364_r9315_p4133
mc16_13TeV.364101.Sherpa_221_NNPDF30NNLO_Zmmumu_MAXHTPTV0_70_CFilterBVeto.deriv.DAOD_HIGG8D1.e5271_s3126_r9364_r9315_p4133
mc16_13TeV.364102.Sherpa_221_NNPDF30NNLO_Zmmumu_MAXHTPTV0_70_BFilter.deriv.DAOD_HIGG8D1.e5271_s3126_r9364_r9315_p4133
mc16_13TeV.364103.Sherpa_221_NNPDF30NNLO_Zmmumu_MAXHTPTV0_140_CVetoBVeto.deriv.DAOD_HIGG8D1.e5271_s3126_r9364_r9315_p4133
mc16_13TeV.364104.Sherpa_221_NNPDF30NNLO_Zmmumu_MAXHTPTV0_140_CFilterBVeto.deriv.DAOD_HIGG8D1.e5271_s3126_r9364_r9315_p4133
mc16_13TeV.364106.Sherpa_221_NNPDF30NNLO_Zmmumu_MAXHTPTV140_280_CVetoBVeto.deriv.DAOD_HIGG8D1.e5271_s3126_r9364_r9315_p4133
mc16_13TeV.364107.Sherpa_221_NNPDF30NNLO_Zmmumu_MAXHTPTV140_280_CFilterBVeto.deriv.DAOD_HIGG8D1.e5271_s3126_r9364_r9315_p4133
mc16_13TeV.364108.Sherpa_221_NNPDF30NNLO_Zmmumu_MAXHTPTV140_280_BFilter.deriv.DAOD_HIGG8D1.e5271_s3126_r9364_r9315_p4133
mc16_13TeV.364109.Sherpa_221_NNPDF30NNLO_Zmmumu_MAXHTPTV280_500_CVetoBVeto.deriv.DAOD_HIGG8D1.e5271_s3126_r9364_r9315_p4133
mc16_13TeV.364110.Sherpa_221_NNPDF30NNLO_Zmmumu_MAXHTPTV280_500_CFilterBVeto.deriv.DAOD_HIGG8D1.e5271_s3126_r9364_r9315_p4133
mc16_13TeV.364111.Sherpa_221_NNPDF30NNLO_Zmmumu_MAXHTPTV280_500_BFilter.deriv.DAOD_HIGG8D1.e5271_s3126_r9364_r9315_p4133
mc16_13TeV.364111.Sherpa_221_NNPDF30NNLO_Zmmumu_MAXHTPTV280_500_BFilter.deriv.DAOD_HIGG8D1.e5271_s3126_r9364_r9315_p4133
mc16_13TeV.364112.Sherpa_221_NNPDF30NNLO_Zmmumu_MAXHTPTV500_1000.deriv.DAOD_HIGG8D1.e5271_s3126_r9364_r9315_p4133
mc16_13TeV.364113.Sherpa_221_NNPDF30NNLO_Zmmumu_MAXHTPTV1000_E_CMS.deriv.DAOD_HIGG8D1.e5271_s3126_r9364_r9315_p4133
mc16_13TeV.364114.Sherpa_221_NNPDF30NNLO_Zee_MAXHTPTV0_70_CVetoBVeto.deriv.DAOD_HIGG8D1.e5299_s3126_r9364_r9315_p4133
mc16_13TeV.364115.Sherpa_221_NNPDF30NNLO_Zee_MAXHTPTV0_70_CFilterBVeto.deriv.DAOD_HIGG8D1.e5299_s3126_r9364_r9315_p4133
mc16_13TeV.364116.Sherpa_221_NNPDF30NNLO_Zee_MAXHTPTV0_70_BFilter.deriv.DAOD_HIGG8D1.e5299_s3126_r9364_r9315_p4133
mc16_13TeV.364117.Sherpa_221_NNPDF30NNLO_Zee_MAXHTPTV70_140_CVetoBVeto.deriv.DAOD_HIGG8D1.e5299_s3126_r9364_r9315_p4133
mc16_13TeV.364118.Sherpa_221_NNPDF30NNLO_Zee_MAXHTPTV70_140_CFilterBVeto.deriv.DAOD_HIGG8D1.e5299_s3126_r9364_r9315_p4133
mc16_13TeV.364119.Sherpa_221_NNPDF30NNLO_Zee_MAXHTPTV70_140_BFilter.deriv.DAOD_HIGG8D1.e5299_s3126_r9364_r9315_p4133
mc16_13TeV.364120.Sherpa_221_NNPDF30NNLO_Zee_MAXHTPTV140_280_CVetoBVeto.deriv.DAOD_HIGG8D1.e5299_s3126_r9364_r9315_p4133
mc16_13TeV.364121.Sherpa_221_NNPDF30NNLO_Zee_MAXHTPTV140_280_CFilterBVeto.deriv.DAOD_HIGG8D1.e5299_s3126_r9364_r9315_p4133
mc16_13TeV.364122.Sherpa_221_NNPDF30NNLO_Zee_MAXHTPTV140_280_BFilter.deriv.DAOD_HIGG8D1.e5299_s3126_r9364_r9315_p4133

```


mc16_13TeV.364535.Sherpa_222_NNPDF30NNLO_taunugamma_pty_140_E_CMS.deriv.DAOD_HIGG8D1.e5928_s3126_r9364_r9315_p4133
 mc16_13TeV.364535.Sherpa_222_NNPDF30NNLO_taunugamma_pty_140_E_CMS.deriv.DAOD_HIGG8D1.e5928_e5984_s3126_r9364_r9315_p4133
 mc16_13TeV.410560.MadGraphPythia8EvtGen_A14_Z_4fl_tchan_noAllHad.deriv.DAOD_HIGG8D1.e5803_s3126_r9364_r9315_p4133
 mc16_13TeV.410013.PowhegPythiaEvtGen_P2012_Wt_inclusive_top.deriv.DAOD_HIGG8D1.e3753_s3126_r9364_r9315_p4133
 mc16_13TeV.410014.PowhegPythiaEvtGen_P2012_Wt_inclusive_antitop.deriv.DAOD_HIGG8D1.e3753_s3126_r9364_r9315_p4133
 mc16_13TeV.410408.aMcAtNloPythia8EvtGen_tWZ_Ztoll_minDR1.deriv.DAOD_HIGG8D1.e6423_e5984_s3126_r9364_r9315_p4133
 mc16_13TeV.364242.Sherpa_222_NNPDF30NNLO_WWW_3l3v_EW6.deriv.DAOD_HIGG8D1.e5887_s3126_r9364_r9315_p4133
 mc16_13TeV.364243.Sherpa_222_NNPDF30NNLO_WWZ_4l2v_EW6.deriv.DAOD_HIGG8D1.e5887_s3126_r9364_r9315_p4133
 mc16_13TeV.364244.Sherpa_222_NNPDF30NNLO_WWZ_2l4v_EW6.deriv.DAOD_HIGG8D1.e5887_s3126_r9364_r9315_p4133
 mc16_13TeV.364245.Sherpa_222_NNPDF30NNLO_WZZ_5l1v_EW6.deriv.DAOD_HIGG8D1.e5887_s3126_r9364_r9315_p4133
 mc16_13TeV.364246.Sherpa_222_NNPDF30NNLO_WZZ_3l3v_EW6.deriv.DAOD_HIGG8D1.e5887_s3126_r9364_r9315_p4133
 mc16_13TeV.364247.Sherpa_222_NNPDF30NNLO_ZZZ_6l0v_EW6.deriv.DAOD_HIGG8D1.e5887_s3126_r9364_r9315_p4133
 mc16_13TeV.364248.Sherpa_222_NNPDF30NNLO_ZZZ_4l2v_EW6.deriv.DAOD_HIGG8D1.e5887_s3126_r9364_r9315_p4133
 mc16_13TeV.364249.Sherpa_222_NNPDF30NNLO_ZZZ_2l4v_EW6.deriv.DAOD_HIGG8D1.e5887_s3126_r9364_r9315_p4133
 mc16_13TeV.342284.Pythia8EvtGen_A14NNPDF23LO_WH125_inc.deriv.DAOD_HIGG8D1.e4246_s3126_r9364_r9315_p4133
 mc16_13TeV.342285.Pythia8EvtGen_A14NNPDF23LO_ZH125_inc.deriv.DAOD_HIGG8D1.e4246_s3126_r9364_r9315_p4133
 mc16_13TeV.341998.aMcAtNloHppEG_UEEE5_CTEQ6L1_CT10ME_tWH125_gamgam_yt_plus1.deriv.DAOD_HIGG8D1.e4394_e5984_s3126_r9364_r9315_p4133
 mc16_13TeV.410389.MadGraphPythia8EvtGen_A14NNPDF23_tggamma_nonallhadronic.deriv.DAOD_HIGG8D1.e6155_e5984_s3126_r9364_r9315_p4133
 mc16_13TeV.410470.PhPy8EG_A14_ttbar_hdamp258p75_nonallhad.deriv.DAOD_HIGG8D1.e6337_e5984_s3126_r9364_r9315_p4133
 mc16_13TeV.410472.PhPy8EG_A14_ttbar_hdamp258p75_dil.deriv.DAOD_HIGG8D1.e6348_e5984_s3126_r9364_r9315_p4133
 mc16_13TeV.346343.PhPy8EG_A14NNPDF23_NNPDF30ME_ttH125_allhad.deriv.DAOD_HIGG8D1.e7148_e5984_s3126_r9364_r9315_p4133
 mc16_13TeV.346344.PhPy8EG_A14NNPDF23_NNPDF30ME_ttH125_semilep.deriv.DAOD_HIGG8D1.e7148_e5984_s3126_r9364_r9315_p4133
 mc16_13TeV.346345.PhPy8EG_A14NNPDF23_NNPDF30ME_ttH125_dilep.deriv.DAOD_HIGG8D1.e7148_e5984_s3126_r9364_r9315_p4133

 mc16d:
 mc16_13TeV.364253.Sherpa_222_NNPDF30NNLO_lllv.deriv.DAOD_HIGG8D1.e5916_e5984_s3126_r10201_r10210_p4133
 mc16_13TeV.364250.Sherpa_222_NNPDF30NNLO_llll.deriv.DAOD_HIGG8D1.e5894_e5984_s3126_r10201_r10210_p4133
 mc16_13TeV.364254.Sherpa_222_NNPDF30NNLO_llvv.deriv.DAOD_HIGG8D1.e5916_e5984_s3126_r10201_r10210_p4133
 mc16_13TeV.364255.Sherpa_222_NNPDF30NNLO_lvvv.deriv.DAOD_HIGG8D1.e5916_e5984_s3126_r10201_r10210_p4133
 mc16_13TeV.410155.aMcAtNloPythia8EvtGen_MEN30NLO_A14N23LO_ttW.deriv.DAOD_HIGG8D1.e5070_e5984_s3126_r10201_r10210_p4133
 mc16_13TeV.410156.aMcAtNloPythia8EvtGen_MEN30NLO_A14N23LO_ttZnunu.deriv.DAOD_HIGG8D1.e5070_e5984_s3126_r10201_r10210_p4133
 mc16_13TeV.410157.aMcAtNloPythia8EvtGen_MEN30NLO_A14N23LO_ttZqq.deriv.DAOD_HIGG8D1.e5070_e5984_s3126_r10201_r10210_p4133
 mc16_13TeV.410218.aMcAtNloPythia8EvtGen_MEN30NLO_A14N23LO_ttee.deriv.DAOD_HIGG8D1.e5070_e5984_s3126_r10201_r10210_p4133
 mc16_13TeV.410219.aMcAtNloPythia8EvtGen_MEN30NLO_A14N23LO_ttmumu.deriv.DAOD_HIGG8D1.e5070_e5984_s3126_r10201_r10210_p4133
 mc16_13TeV.410220.aMcAtNloPythia8EvtGen_MEN30NLO_A14N23LO_ttautau.deriv.DAOD_HIGG8D1.e5070_e5984_s3126_r10201_r10210_p4133
 mc16_13TeV.410276.aMcAtNloPythia8EvtGen_MEN30NLO_A14N23LO_ttee_mll_1_5.deriv.DAOD_HIGG8D1.e6087_e5984_s3126_r10201_r10210_p4133
 mc16_13TeV.410277.aMcAtNloPythia8EvtGen_MEN30NLO_A14N23LO_ttmumu_mll_1_5.deriv.DAOD_HIGG8D1.e6087_e5984_s3126_r10201_r10210_p4133
 mc16_13TeV.410278.aMcAtNloPythia8EvtGen_MEN30NLO_A14N23LO_ttautau_mll_1_5.deriv.DAOD_HIGG8D1.e6087_e5984_s3126_r10201_r10210_p4133
 mc16_13TeV.410397.MadGraphPythia8EvtGen_ttbar_wbee_MEN30LO_A14N23LO.deriv.DAOD_HIGG8D1.e6086_e5984_s3126_r10201_r10210_p4133
 mc16_13TeV.410398.MadGraphPythia8EvtGen_ttbar_wbmumu_MEN30LO_A14N23LO.deriv.DAOD_HIGG8D1.e6086_e5984_s3126_r10201_r10210_p4133
 mc16_13TeV.410399.MadGraphPythia8EvtGen_ttbar_wbtautau_MEN30LO_A14N23LO.deriv.DAOD_HIGG8D1.e6086_e5984_s3126_r10201_r10210_p4133
 mc16_13TeV.410658.PhPy8EG_A14_ttchan_BW50_lept_top.deriv.DAOD_HIGG8D1.e6671_e5984_s3126_r10201_r10210_p4133
 mc16_13TeV.410659.PhPy8EG_A14_ttchan_BW50_lept_antitop.deriv.DAOD_HIGG8D1.e6671_e5984_s3126_r10201_r10210_p4133
 mc16_13TeV.410644.PowhegPythia8EvtGen_A14_singletop_schan_lept_top.deriv.DAOD_HIGG8D1.e6527_e5984_s3126_r10201_r10210_p4133
 mc16_13TeV.410645.PowhegPythia8EvtGen_A14_singletop_schan_lept_antitop.deriv.DAOD_HIGG8D1.e6527_s3126_r10201_r10210_p4133
 mc16_13TeV.304014.MadGraphPythia8EvtGen_A14NNPDF23_3top_SM.deriv.DAOD_HIGG8D1.e4324_e5984_s3126_r10201_r10210_p4133
 mc16_13TeV.410080.MadGraphPythia8EvtGen_A14NNPDF23_4topSM.deriv.DAOD_HIGG8D1.e4111_e5984_s3126_r10201_r10210_p4133
 mc16_13TeV.410081.MadGraphPythia8EvtGen_A14NNPDF23_ttbarWW.deriv.DAOD_HIGG8D1.e4111_e5984_s3126_r10201_r10210_p4133
 mc16_13TeV.364100.Sherpa_221_NNPDF30NNLO_Zmmumu_MAXHTPTV0_70_CVetoBVeto.deriv.DAOD_HIGG8D1.e5271_s3126_r10201_r10210_p4133
 mc16_13TeV.364101.Sherpa_221_NNPDF30NNLO_Zmmumu_MAXHTPTV0_70_CFilterBVeto.deriv.DAOD_HIGG8D1.e5271_s3126_r10201_r10210_p4133
 mc16_13TeV.364101.Sherpa_221_NNPDF30NNLO_Zmmumu_MAXHTPTV0_70_CFilterBVeto.deriv.DAOD_HIGG8D1.e5271_e5984_s3126_r10201_r10210_p4133
 mc16_13TeV.364102.Sherpa_221_NNPDF30NNLO_Zmmumu_MAXHTPTV0_70_BFilter.deriv.DAOD_HIGG8D1.e5271_s3126_r10201_r10210_p4133
 mc16_13TeV.364103.Sherpa_221_NNPDF30NNLO_Zmmumu_MAXHTPTV0_140_CVetoBVeto.deriv.DAOD_HIGG8D1.e5271_s3126_r10201_r10210_p4133
 mc16_13TeV.364104.Sherpa_221_NNPDF30NNLO_Zmmumu_MAXHTPTV0_140_CFilterBVeto.deriv.DAOD_HIGG8D1.e5271_s3126_r10201_r10210_p4133
 mc16_13TeV.364106.Sherpa_221_NNPDF30NNLO_Zmmumu_MAXHTPTV140_280_CVetoBVeto.deriv.DAOD_HIGG8D1.e5271_s3126_r10201_r10210_p4133
 mc16_13TeV.364107.Sherpa_221_NNPDF30NNLO_Zmmumu_MAXHTPTV140_280_CFilterBVeto.deriv.DAOD_HIGG8D1.e5271_s3126_r10201_r10210_p4133
 mc16_13TeV.364108.Sherpa_221_NNPDF30NNLO_Zmmumu_MAXHTPTV140_280_BFilter.deriv.DAOD_HIGG8D1.e5271_e5984_s3126_r10201_r10210_p4133
 mc16_13TeV.364108.Sherpa_221_NNPDF30NNLO_Zmmumu_MAXHTPTV140_280_BFilter.deriv.DAOD_HIGG8D1.e5271_s3126_r10201_r10210_p4133
 mc16_13TeV.364109.Sherpa_221_NNPDF30NNLO_Zmmumu_MAXHTPTV280_500_CVetoBVeto.deriv.DAOD_HIGG8D1.e5271_e5984_s3126_r10201_r10210_p4133
 mc16_13TeV.364109.Sherpa_221_NNPDF30NNLO_Zmmumu_MAXHTPTV280_500_CFilterBVeto.deriv.DAOD_HIGG8D1.e5271_s3126_r10201_r10210_p4133
 mc16_13TeV.364110.Sherpa_221_NNPDF30NNLO_Zmmumu_MAXHTPTV280_500_BFilter.deriv.DAOD_HIGG8D1.e5271_s3126_r10201_r10210_p4133
 mc16_13TeV.364111.Sherpa_221_NNPDF30NNLO_Zmmumu_MAXHTPTV280_500_BFilter.deriv.DAOD_HIGG8D1.e5271_e5984_s3126_r10201_r10210_p4133

mc16_13TeV.364192.Sherpa_221_NNPDF30NNLO_Wtaunu_MAXHTPTV140_280_BFilter.deriv.DAOD_HIGG8D1.e5340_e5984_s3126_r10201_r10210_p4133
 mc16_13TeV.364193.Sherpa_221_NNPDF30NNLO_Wtaunu_MAXHTPTV280_500_CVetoBVeto.deriv.DAOD_HIGG8D1.e5340_e5984_s3126_r10201_r10210_p4133
 mc16_13TeV.364193.Sherpa_221_NNPDF30NNLO_Wtaunu_MAXHTPTV280_500_CVetoBVeto.deriv.DAOD_HIGG8D1.e5340_e5984_s3126_s3136_r10201_r10210_p4133
 mc16_13TeV.364194.Sherpa_221_NNPDF30NNLO_Wtaunu_MAXHTPTV280_500_CFilterBVeto.deriv.DAOD_HIGG8D1.e5340_e5984_s3126_r10201_r10210_p4133
 mc16_13TeV.364194.Sherpa_221_NNPDF30NNLO_Wtaunu_MAXHTPTV280_500_CFilterBVeto.deriv.DAOD_HIGG8D1.e5340_s3126_r10201_r10210_p4133
 mc16_13TeV.364194.Sherpa_221_NNPDF30NNLO_Wtaunu_MAXHTPTV280_500_CFilterBVeto.deriv.DAOD_HIGG8D1.e5340_e5984_s3126_s3136_r10201_r10210_p4133
 mc16_13TeV.364195.Sherpa_221_NNPDF30NNLO_Wtaunu_MAXHTPTV280_500_BFilter.deriv.DAOD_HIGG8D1.e5340_e5984_s3126_r10201_r10210_p4133
 mc16_13TeV.364195.Sherpa_221_NNPDF30NNLO_Wtaunu_MAXHTPTV280_500_BFilter.deriv.DAOD_HIGG8D1.e5340_s3126_r10201_r10210_p4133
 mc16_13TeV.364196.Sherpa_221_NNPDF30NNLO_Wtaunu_MAXHTPTV500_1000.deriv.DAOD_HIGG8D1.e5340_e5984_s3126_s3136_r10201_r10210_p4133
 mc16_13TeV.364196.Sherpa_221_NNPDF30NNLO_Wtaunu_MAXHTPTV500_1000.deriv.DAOD_HIGG8D1.e5340_s3126_r10201_r10210_p4133
 mc16_13TeV.364197.Sherpa_221_NNPDF30NNLO_Wtaunu_MAXHTPTV1000_E_CMS.deriv.DAOD_HIGG8D1.e5340_e5984_s3126_r10201_r10210_p4133
 mc16_13TeV.364500.Sherpa_222_NNPDF30NNLO_eegamma_pty_7_15.deriv.DAOD_HIGG8D1.e5928_e5984_s3126_r10201_r10210_p4133
 mc16_13TeV.364501.Sherpa_222_NNPDF30NNLO_eegamma_pty_15_35.deriv.DAOD_HIGG8D1.e5928_e5984_s3126_r10201_r10210_p4133
 mc16_13TeV.364502.Sherpa_222_NNPDF30NNLO_eegamma_pty_35_70.deriv.DAOD_HIGG8D1.e5928_e5984_s3126_r10201_r10210_p4133
 mc16_13TeV.364503.Sherpa_222_NNPDF30NNLO_eegamma_pty_70_140.deriv.DAOD_HIGG8D1.e5928_e5984_s3126_r10201_r10210_p4133
 mc16_13TeV.364504.Sherpa_222_NNPDF30NNLO_eegamma_pty_140_E_CMS.deriv.DAOD_HIGG8D1.e5928_e5984_s3126_r10201_r10210_p4133
 mc16_13TeV.364505.Sherpa_222_NNPDF30NNLO_mumugamma_pty_7_15.deriv.DAOD_HIGG8D1.e5928_e5984_s3126_r10201_r10210_p4133
 mc16_13TeV.364506.Sherpa_222_NNPDF30NNLO_mumugamma_pty_15_35.deriv.DAOD_HIGG8D1.e5928_e5984_s3126_r10201_r10210_p4133
 mc16_13TeV.364507.Sherpa_222_NNPDF30NNLO_mumugamma_pty_35_70.deriv.DAOD_HIGG8D1.e5928_e5984_s3126_r10201_r10210_p4133
 mc16_13TeV.364508.Sherpa_222_NNPDF30NNLO_mumugamma_pty_70_140.deriv.DAOD_HIGG8D1.e5928_e5984_s3126_r10201_r10210_p4133
 mc16_13TeV.364509.Sherpa_222_NNPDF30NNLO_mumugamma_pty_140_E_CMS.deriv.DAOD_HIGG8D1.e5928_e5984_s3126_r10201_r10210_p4133
 mc16_13TeV.364510.Sherpa_222_NNPDF30NNLO_tautaugamma_pty_7_15.deriv.DAOD_HIGG8D1.e5928_e5984_s3126_r10201_r10210_p4133
 mc16_13TeV.364511.Sherpa_222_NNPDF30NNLO_tautaugamma_pty_15_35.deriv.DAOD_HIGG8D1.e5928_e5984_s3126_r10201_r10210_p4133
 mc16_13TeV.364512.Sherpa_222_NNPDF30NNLO_tautaugamma_pty_35_70.deriv.DAOD_HIGG8D1.e5928_e5984_s3126_r10201_r10210_p4133
 mc16_13TeV.364513.Sherpa_222_NNPDF30NNLO_tautaugamma_pty_70_140.deriv.DAOD_HIGG8D1.e5928_e5984_s3126_r10201_r10210_p4133
 mc16_13TeV.364513.Sherpa_222_NNPDF30NNLO_tautaugamma_pty_70_140.deriv.DAOD_HIGG8D1.e5928_e5984_s3126_r10201_r10210_p4133
 mc16_13TeV.364514.Sherpa_222_NNPDF30NNLO_tautaugamma_pty_140_E_CMS.deriv.DAOD_HIGG8D1.e5928_e5984_s3126_r10201_r10210_p4133
 mc16_13TeV.364521.Sherpa_222_NNPDF30NNLO_enugamma_pty_7_15.deriv.DAOD_HIGG8D1.e5928_e5984_s3126_r10201_r10210_p4133
 mc16_13TeV.364522.Sherpa_222_NNPDF30NNLO_enugamma_pty_15_35.deriv.DAOD_HIGG8D1.e5928_e5984_s3126_r10201_r10210_p4133
 mc16_13TeV.364523.Sherpa_222_NNPDF30NNLO_enugamma_pty_35_70.deriv.DAOD_HIGG8D1.e5928_e5984_s3126_r10201_r10210_p4133
 mc16_13TeV.364524.Sherpa_222_NNPDF30NNLO_enugamma_pty_70_140.deriv.DAOD_HIGG8D1.e5928_e5984_s3126_r10201_r10210_p4133
 mc16_13TeV.364525.Sherpa_222_NNPDF30NNLO_enugamma_pty_140_E_CMS.deriv.DAOD_HIGG8D1.e5928_e5984_s3126_r10201_r10210_p4133
 mc16_13TeV.364526.Sherpa_222_NNPDF30NNLO_munugamma_pty_7_15.deriv.DAOD_HIGG8D1.e5928_e5984_s3126_r10201_r10210_p4133
 mc16_13TeV.364527.Sherpa_222_NNPDF30NNLO_munugamma_pty_15_35.deriv.DAOD_HIGG8D1.e5928_e5984_s3126_r10201_r10210_p4133
 mc16_13TeV.364528.Sherpa_222_NNPDF30NNLO_munugamma_pty_35_70.deriv.DAOD_HIGG8D1.e5928_e5984_s3126_r10201_r10210_p4133
 mc16_13TeV.364529.Sherpa_222_NNPDF30NNLO_munugamma_pty_70_140.deriv.DAOD_HIGG8D1.e5928_e5984_s3126_r10201_r10210_p4133
 mc16_13TeV.364530.Sherpa_222_NNPDF30NNLO_munugamma_pty_140_E_CMS.deriv.DAOD_HIGG8D1.e5928_e5984_s3126_r10201_r10210_p4133
 mc16_13TeV.364531.Sherpa_222_NNPDF30NNLO_taunugamma_pty_7_15.deriv.DAOD_HIGG8D1.e5928_e5984_s3126_r10201_r10210_p4133
 mc16_13TeV.364532.Sherpa_222_NNPDF30NNLO_taunugamma_pty_15_35.deriv.DAOD_HIGG8D1.e5928_e5984_s3126_r10201_r10210_p4133
 mc16_13TeV.364533.Sherpa_222_NNPDF30NNLO_taunugamma_pty_35_70.deriv.DAOD_HIGG8D1.e5928_e5984_s3126_r10201_r10210_p4133
 mc16_13TeV.364534.Sherpa_222_NNPDF30NNLO_taunugamma_pty_70_140.deriv.DAOD_HIGG8D1.e5928_e5984_s3126_r10201_r10210_p4133
 mc16_13TeV.364535.Sherpa_222_NNPDF30NNLO_taunugamma_pty_140_E_CMS.deriv.DAOD_HIGG8D1.e5928_e5984_s3126_r10201_r10210_p4133
 mc16_13TeV.410560.MadGraphPythia8EvtGen_A14_Z_4fl_tchan_noAllHad.deriv.DAOD_HIGG8D1.e5803_e5984_s3126_r10201_r10210_p4133
 mc16_13TeV.410013.PowhegPythiaEvtGen_P2012_Wt_inclusive_top.deriv.DAOD_HIGG8D1.e3753_s3126_r10201_r10210_p4133
 mc16_13TeV.410014.PowhegPythiaEvtGen_P2012_Wt_inclusive_antitop.deriv.DAOD_HIGG8D1.e3753_s3126_r10201_r10210_p4133
 mc16_13TeV.410408.aMcAtNloPythia8EvtGen_tWZ_Tzoll_minDR1.deriv.DAOD_HIGG8D1.e6423_e5984_s3126_r10201_r10210_p4133
 mc16_13TeV.364242.Sherpa_222_NNPDF30NNLO_WWW_3l3v_EW6.deriv.DAOD_HIGG8D1.e5887_e5984_s3126_r10201_r10210_p4133
 mc16_13TeV.364243.Sherpa_222_NNPDF30NNLO_WWZ_4l2v_EW6.deriv.DAOD_HIGG8D1.e5887_e5984_s3126_r10201_r10210_p4133
 mc16_13TeV.364244.Sherpa_222_NNPDF30NNLO_WWZ_2l4v_EW6.deriv.DAOD_HIGG8D1.e5887_e5984_s3126_r10201_r10210_p4133
 mc16_13TeV.364245.Sherpa_222_NNPDF30NNLO_WZZ_5l1v_EW6.deriv.DAOD_HIGG8D1.e5887_e5984_s3126_r10201_r10210_p4133
 mc16_13TeV.364246.Sherpa_222_NNPDF30NNLO_WZZ_3l3v_EW6.deriv.DAOD_HIGG8D1.e5887_e5984_s3126_r10201_r10210_p4133
 mc16_13TeV.364247.Sherpa_222_NNPDF30NNLO_ZZZ_6lv_EW6.deriv.DAOD_HIGG8D1.e5887_e5984_s3126_r10201_r10210_p4133
 mc16_13TeV.364248.Sherpa_222_NNPDF30NNLO_ZZZ_4l2v_EW6.deriv.DAOD_HIGG8D1.e5887_e5984_s3126_r10201_r10210_p4133
 mc16_13TeV.364249.Sherpa_222_NNPDF30NNLO_ZZZ_2l4v_EW6.deriv.DAOD_HIGG8D1.e5887_e5984_s3126_r10201_r10210_p4133
 mc16_13TeV.342284.Pythia8EvtGen_A14NNPDF23LO_WH125_inc.deriv.DAOD_HIGG8D1.e4246_e5984_s3126_r10201_r10210_p4133
 mc16_13TeV.342285.Pythia8EvtGen_A14NNPDF23LO_ZH125_inc.deriv.DAOD_HIGG8D1.e4246_e5984_s3126_r10201_r10210_p4133
 mc16_13TeV.341998.aMcAtNloHppEG_UEEE5_CTEQ6L1_CT10ME_tWH125_gamgam_yt_plus1.deriv.DAOD_HIGG8D1.e4394_e5984_s3126_r10201_r10210_p4133
 mc16_13TeV.410470.PhPy8EG_A14_ttbar_hdamp258p75_nonallhad.deriv.DAOD_HIGG8D1.e6337_e5984_s3126_r10201_r10210_p4133
 mc16_13TeV.410472.PhPy8EG_A14_ttbar_hdamp258p75_dil.deriv.DAOD_HIGG8D1.e6348_e5984_s3126_r10201_r10210_p4133
 mc16_13TeV.346343.PhPy8EG_A14NNPDF23_NNPDF30ME_ttH125_allhad.deriv.DAOD_HIGG8D1.e7148_e5984_s3126_r10201_r10210_p4133
 mc16_13TeV.346344.PhPy8EG_A14NNPDF23_NNPDF30ME_ttH125_semilep.deriv.DAOD_HIGG8D1.e7148_e5984_a875_r10201_r10210_p4133
 mc16_13TeV.346345.PhPy8EG_A14NNPDF23_NNPDF30ME_ttH125_dilep.deriv.DAOD_HIGG8D1.e7148_e5984_a875_r10201_r10210_p4133

mc16e:
mc16_13TeV.361605.PowhegPy8EG_CT10nloME_AZNLOCTEQ6L1_ZZvvvv_mll4.deriv.DAOD_HIGG8D1.e4054_e5984_s3126_r10724_r10726_p4133
mc16_13TeV.361602.PowhegPy8EG_CT10nloME_AZNLOCTEQ6L1_WZlvvv_mll4.deriv.DAOD_HIGG8D1.e4054_e5984_s3126_r10724_r10726_p4133
mc16_13TeV.361601.PowhegPy8EG_CT10nloME_AZNLOCTEQ6L1_WZlvl1_mll4.deriv.DAOD_HIGG8D1.e4475_e5984_s3126_r10724_r10726_p4133
mc16_13TeV.361600.PowhegPy8EG_CT10nloME_AZNLOCTEQ6L1_WWlvv.deriv.DAOD_HIGG8D1.e4616_e5984_s3126_r10724_r10726_p4133
mc16_13TeV.361603.PowhegPy8EG_CT10nloME_AZNLOCTEQ6L1_ZZlIII_mll4.deriv.DAOD_HIGG8D1.e4475_e5984_s3126_r10724_r10726_p4133
mc16_13TeV.361604.PowhegPy8EG_CT10nloME_AZNLOCTEQ6L1_ZZvvll_mll4.deriv.DAOD_HIGG8D1.e4475_e5984_s3126_r10724_r10726_p4133
mc16_13TeV.364288.Sherpa_222_NNPDF30NNLO_llll_lowMIPtComplement.deriv.DAOD_HIGG8D1.e6096_s3126_r10724_p3983 mc16_13TeV.364287.Sherpa_222_NNPDF30NNLO_llvvjj_EW6.deriv.DAOD_HIGG8D1.e6055_e5984_s3126_r10724_r10726_p3983
mc16_13TeV.364285.Sherpa_222_NNPDF30NNLO_llvvjj_EW6.deriv.DAOD_HIGG8D1.e6055_s3126_r10724_p3983
mc16_13TeV.364284.Sherpa_222_NNPDF30NNLO_llvvjj_EW6.deriv.DAOD_HIGG8D1.e6055_s3126_r10724_p3983
mc16_13TeV.364283.Sherpa_222_NNPDF30NNLO_lllljj_EW6.deriv.DAOD_HIGG8D1.e6055_s3126_r10724_p3983
mc16_13TeV.364739.MGPy8EG_NNPDF30NLO_A14NNPDF23LO_lVlljjEW6_OFMinus.deriv.DAOD_HIGG8D1.e7421_e5984_s3126_r10724_r10726_p4133
mc16_13TeV.364742.MGPy8EG_NNPDF30NLO_A14NNPDF23LO_lVlljjEW6_SFPlus.deriv.DAOD_HIGG8D1.e7421_e5984_s3126_r10724_r10726_p4133
mc16_13TeV.364740.MGPy8EG_NNPDF30NLO_A14NNPDF23LO_lVlljjEW6_OFPlus.deriv.DAOD_HIGG8D1.e7421_e5984_s3126_r10724_r10726_p4133
mc16_13TeV.364741.MGPy8EG_NNPDF30NLO_A14NNPDF23LO_lVlljjEW6_SFMinus.deriv.DAOD_HIGG8D1.e7421_e5984_s3126_r10724_r10726_p4133
mc16_13TeV.364253.Sherpa_222_NNPDF30NNLO_llll.deriv.DAOD_HIGG8D1.e5916_e5984_s3126_r10724_r10726_p4133
mc16_13TeV.364250.Sherpa_222_NNPDF30NNLO_llll.deriv.DAOD_HIGG8D1.e5894_e5984_s3126_r10724_r10726_p4133
mc16_13TeV.364254.Sherpa_222_NNPDF30NNLO_llvv.deriv.DAOD_HIGG8D1.e5916_e5984_s3126_r10724_r10726_p4133
mc16_13TeV.364255.Sherpa_222_NNPDF30NNLO_llvv.deriv.DAOD_HIGG8D1.e5916_e5984_s3126_r10724_r10726_p4133
mc16_13TeV.410155.aMcAtNloPythia8EvtGen_MEN30NLO_A14N23LO_ttW.deriv.DAOD_HIGG8D1.e5070_e5984_s3126_r10724_r10726_p4133
mc16_13TeV.410156.aMcAtNloPythia8EvtGen_MEN30NLO_A14N23LO_ttZnunu.deriv.DAOD_HIGG8D1.e5070_e5984_s3126_r10724_r10726_p4133
mc16_13TeV.410157.aMcAtNloPythia8EvtGen_MEN30NLO_A14N23LO_ttZqq.deriv.DAOD_HIGG8D1.e5070_e5984_s3126_r10724_r10726_p4133
mc16_13TeV.410218.aMcAtNloPythia8EvtGen_MEN30NLO_A14N23LO_ttee.deriv.DAOD_HIGG8D1.e5070_e5984_s3126_r10724_r10726_p4133
mc16_13TeV.410219.aMcAtNloPythia8EvtGen_MEN30NLO_A14N23LO_ttmumu.deriv.DAOD_HIGG8D1.e5070_e5984_s3126_r10724_r10726_p4133
mc16_13TeV.410220.aMcAtNloPythia8EvtGen_MEN30NLO_A14N23LO_ttautau.deriv.DAOD_HIGG8D1.e5070_e5984_s3126_r10724_r10726_p4133
mc16_13TeV.410276.aMcAtNloPythia8EvtGen_MEN30NLO_A14N23LO_ttee_mll_1_5.deriv.DAOD_HIGG8D1.e6087_e5984_s3126_r10724_r10726_p4133
mc16_13TeV.410277.aMcAtNloPythia8EvtGen_MEN30NLO_A14N23LO_ttmumu_mll_1_5.deriv.DAOD_HIGG8D1.e6087_e5984_s3126_r10724_r10726_p4133
mc16_13TeV.410278.aMcAtNloPythia8EvtGen_MEN30NLO_A14N23LO_ttautau_mll_1_5.deriv.DAOD_HIGG8D1.e6087_e5984_s3126_r10724_r10726_p4133
mc16_13TeV.410397.MadGraphPythia8EvtGen_ttbar_wbee_MEN30LO_A14N23LO.deriv.DAOD_HIGG8D1.e6086_e5984_s3126_r10724_r10726_p4133
mc16_13TeV.410398.MadGraphPythia8EvtGen_ttbar_wbmumu_MEN30LO_A14N23LO.deriv.DAOD_HIGG8D1.e6086_e5984_s3126_r10724_r10726_p4133
mc16_13TeV.410399.MadGraphPythia8EvtGen_ttbar_wbtautau_MEN30LO_A14N23LO.deriv.DAOD_HIGG8D1.e6086_e5984_s3126_r10724_r10726_p4133
mc16_13TeV.410658.PhPy8EG_A14_tchan_BW50_lept_top.deriv.DAOD_HIGG8D1.e6671_e5984_s3126_s3136_r10724_r10726_p4133
mc16_13TeV.410659.PhPy8EG_A14_tchan_BW50_lept_antitop.deriv.DAOD_HIGG8D1.e6671_e5984_s3126_s3136_r10724_r10726_p4133
mc16_13TeV.410644.PowhegPythia8EvtGen_A14_singletop_schan_lept_top.deriv.DAOD_HIGG8D1.e6527_e5984_s3126_r10724_r10726_p4133
mc16_13TeV.410645.PowhegPythia8EvtGen_A14_singletop_schan_lept_antitop.deriv.DAOD_HIGG8D1.e6527_e5984_s3126_r10724_r10726_p4133
mc16_13TeV.304014.MadGraphPythia8EvtGen_A14NNPDF23_3top_SM.deriv.DAOD_HIGG8D1.e4324_e5984_s3126_r10724_r10726_p4133
mc16_13TeV.410080.MadGraphPythia8EvtGen_A14NNPDF23_4topSM.deriv.DAOD_HIGG8D1.e4111_e5984_s3126_r10724_r10726_p4133
mc16_13TeV.410081.MadGraphPythia8EvtGen_A14NNPDF23_ttbarWW.deriv.DAOD_HIGG8D1.e4111_e5984_s3126_r10724_r10726_p4133
mc16_13TeV.364100.Sherpa_221_NNPDF30NNLO_Zmmumu_MAXHTPTV_70_CVetoBVeto.deriv.DAOD_HIGG8D1.e5271_e5984_s3126_s3136_r10724_r10726_p4133
mc16_13TeV.364100.Sherpa_221_NNPDF30NNLO_Zmmumu_MAXHTPTV_70_CVetoBVeto.deriv.DAOD_HIGG8D1.e5271_e5984_s3126_r10724_r10726_p4133
mc16_13TeV.364101.Sherpa_221_NNPDF30NNLO_Zmmumu_MAXHTPTV_70_CFilterBVeto.deriv.DAOD_HIGG8D1.e5271_e5984_s3126_r10724_r10726_p4133
mc16_13TeV.364102.Sherpa_221_NNPDF30NNLO_Zmmumu_MAXHTPTV_70_BFilter.deriv.DAOD_HIGG8D1.e5271_e5984_s3126_s3136_r10724_r10726_p4133
mc16_13TeV.364102.Sherpa_221_NNPDF30NNLO_Zmmumu_MAXHTPTV_70_BFilter.deriv.DAOD_HIGG8D1.e5271_e5984_s3126_r10724_r10726_p4133
mc16_13TeV.364103.Sherpa_221_NNPDF30NNLO_Zmmumu_MAXHTPTV70_140_CVetoBVeto.deriv.DAOD_HIGG8D1.e5271_e5984_s3126_r10724_r10726_p4133
mc16_13TeV.364103.Sherpa_221_NNPDF30NNLO_Zmmumu_MAXHTPTV70_140_CVetoBVeto.deriv.DAOD_HIGG8D1.e5271_e5984_s3126_s3136_r10724_r10726_p4133
mc16_13TeV.364104.Sherpa_221_NNPDF30NNLO_Zmmumu_MAXHTPTV70_140_CFilterBVeto.deriv.DAOD_HIGG8D1.e5271_e5984_s3126_r10724_r10726_p4133
mc16_13TeV.364104.Sherpa_221_NNPDF30NNLO_Zmmumu_MAXHTPTV70_140_CFilterBVeto.deriv.DAOD_HIGG8D1.e5271_e5984_s3126_s3136_r10724_r10726_p4133
mc16_13TeV.364104.Sherpa_221_NNPDF30NNLO_Zmmumu_MAXHTPTV70_140_CFilterBVeto.deriv.DAOD_HIGG8D1.e5271_e5984_s3126_r10724_r10726_p4133
mc16_13TeV.364106.Sherpa_221_NNPDF30NNLO_Zmmumu_MAXHTPTV140_280_CVetoBVeto.deriv.DAOD_HIGG8D1.e5271_e5984_s3126_s3136_r10724_r10726_p4133
mc16_13TeV.364106.Sherpa_221_NNPDF30NNLO_Zmmumu_MAXHTPTV140_280_CVetoBVeto.deriv.DAOD_HIGG8D1.e5271_e5984_s3126_r10724_r10726_p4133
mc16_13TeV.364107.Sherpa_221_NNPDF30NNLO_Zmmumu_MAXHTPTV140_280_CFilterBVeto.deriv.DAOD_HIGG8D1.e5271_e5984_s3126_r10724_r10726_p4133
mc16_13TeV.364107.Sherpa_221_NNPDF30NNLO_Zmmumu_MAXHTPTV140_280_CFilterBVeto.deriv.DAOD_HIGG8D1.e5271_e5984_s3126_s3136_r10724_r10726_p4133
mc16_13TeV.364108.Sherpa_221_NNPDF30NNLO_Zmmumu_MAXHTPTV140_280_CFilterBVeto.deriv.DAOD_HIGG8D1.e5271_e5984_s3126_r10724_r10726_p4133
mc16_13TeV.364109.Sherpa_221_NNPDF30NNLO_Zmmumu_MAXHTPTV280_500_CVetoBVeto.deriv.DAOD_HIGG8D1.e5271_e5984_s3126_r10724_r10726_p4133
mc16_13TeV.364110.Sherpa_221_NNPDF30NNLO_Zmmumu_MAXHTPTV280_500_CFilterBVeto.deriv.DAOD_HIGG8D1.e5271_e5984_s3126_r10724_r10726_p4133
mc16_13TeV.364110.Sherpa_221_NNPDF30NNLO_Zmmumu_MAXHTPTV280_500_CFilterBVeto.deriv.DAOD_HIGG8D1.e5271_e5984_s3126_s3136_r10724_r10726_p4133
mc16_13TeV.364111.Sherpa_221_NNPDF30NNLO_Zmmumu_MAXHTPTV280_500_BFilter.deriv.DAOD_HIGG8D1.e5271_e5984_s3126_s3136_r10724_r10726_p4133
mc16_13TeV.364111.Sherpa_221_NNPDF30NNLO_Zmmumu_MAXHTPTV280_500_BFilter.deriv.DAOD_HIGG8D1.e5271_e5984_s3126_r10724_r10726_p4133
mc16_13TeV.364112.Sherpa_221_NNPDF30NNLO_Zmmumu_MAXHTPTV500_1000.deriv.DAOD_HIGG8D1.e5271_e5984_s3126_r10724_r10726_p4133
mc16_13TeV.364113.Sherpa_221_NNPDF30NNLO_Zmmumu_MAXHTPTV1000_E_CMS.deriv.DAOD_HIGG8D1.e5271_e5984_s3126_s3136_r10724_r10726_p4133
mc16_13TeV.364114.Sherpa_221_NNPDF30NNLO_Zee_MAXHTPTV0_70_CVetoBVeto.deriv.DAOD_HIGG8D1.e5299_e5984_s3126_s3136_r10724_r10726_p4133

mc16_13TeV.364196.Sherpa_221_NNPDF30NNLO_Wtaunu_MAXHTPTV500_1000.deriv.DAOD_HIGG8D1.e5340_e5984_s3126_s3136_r10724_r10726_p4133
 mc16_13TeV.364196.Sherpa_221_NNPDF30NNLO_Wtaunu_MAXHTPTV500_1000.deriv.DAOD_HIGG8D1.e5340_e5984_s3126_r10724_r10726_p4133
 mc16_13TeV.364197.Sherpa_221_NNPDF30NNLO_Wtaunu_MAXHTPTV1000_E_CMS.deriv.DAOD_HIGG8D1.e5340_e5984_s3126_s3136_r10724_r10726_p4133
 mc16_13TeV.364197.Sherpa_221_NNPDF30NNLO_Wtaunu_MAXHTPTV1000_E_CMS.deriv.DAOD_HIGG8D1.e5340_e5984_s3126_r10724_r10726_p4133
 mc16_13TeV.364500.Sherpa_222_NNPDF30NNLO_eegamma_pty_7_15.deriv.DAOD_HIGG8D1.e5928_e5984_s3126_r10724_r10726_p4133
 mc16_13TeV.364501.Sherpa_222_NNPDF30NNLO_eegamma_pty_15_35.deriv.DAOD_HIGG8D1.e5928_e5984_s3126_r10724_r10726_p4133
 mc16_13TeV.364502.Sherpa_222_NNPDF30NNLO_eegamma_pty_35_70.deriv.DAOD_HIGG8D1.e5928_e5984_s3126_r10724_r10726_p4133
 mc16_13TeV.364503.Sherpa_222_NNPDF30NNLO_eegamma_pty_70_140.deriv.DAOD_HIGG8D1.e5928_e5984_s3126_r10724_r10726_p4133
 mc16_13TeV.364504.Sherpa_222_NNPDF30NNLO_eegamma_pty_140_E_CMS.deriv.DAOD_HIGG8D1.e5928_e5984_s3126_r10724_r10726_p4133
 mc16_13TeV.364505.Sherpa_222_NNPDF30NNLO_mumugamma_pty_7_15.deriv.DAOD_HIGG8D1.e5928_e5984_s3126_r10724_r10726_p4133
 mc16_13TeV.364506.Sherpa_222_NNPDF30NNLO_mumugamma_pty_15_35.deriv.DAOD_HIGG8D1.e5928_e5984_s3126_r10724_r10726_p4133
 mc16_13TeV.364507.Sherpa_222_NNPDF30NNLO_mumugamma_pty_35_70.deriv.DAOD_HIGG8D1.e5928_e5984_s3126_r10724_r10726_p4133
 mc16_13TeV.364508.Sherpa_222_NNPDF30NNLO_mumugamma_pty_70_140.deriv.DAOD_HIGG8D1.e5928_e5984_s3126_r10724_r10726_p4133
 mc16_13TeV.364509.Sherpa_222_NNPDF30NNLO_mumugamma_pty_140_E_CMS.deriv.DAOD_HIGG8D1.e5928_e5984_s3126_r10724_r10726_p4133
 mc16_13TeV.364511.Sherpa_222_NNPDF30NNLO_tautaugamma_pty_15_35.deriv.DAOD_HIGG8D1.e5928_e5984_s3126_r10724_r10726_p4133
 mc16_13TeV.364512.Sherpa_222_NNPDF30NNLO_tautaugamma_pty_35_70.deriv.DAOD_HIGG8D1.e5928_e5984_s3126_r10724_r10726_p4133
 mc16_13TeV.364513.Sherpa_222_NNPDF30NNLO_tautaugamma_pty_70_140.deriv.DAOD_HIGG8D1.e5928_e5984_s3126_r10724_r10726_p4133
 mc16_13TeV.364514.Sherpa_222_NNPDF30NNLO_tautaugamma_pty_140_E_CMS.deriv.DAOD_HIGG8D1.e5928_e5984_s3126_r10724_r10726_p4133
 mc16_13TeV.364522.Sherpa_222_NNPDF30NNLO_enugamma_pty_15_35.deriv.DAOD_HIGG8D1.e5928_e5984_s3126_r10724_r10726_p4133
 mc16_13TeV.364523.Sherpa_222_NNPDF30NNLO_enugamma_pty_35_70.deriv.DAOD_HIGG8D1.e5928_e5984_s3126_r10724_r10726_p4133
 mc16_13TeV.364524.Sherpa_222_NNPDF30NNLO_enugamma_pty_70_140.deriv.DAOD_HIGG8D1.e5928_e5984_s3126_r10724_r10726_p4133
 mc16_13TeV.364525.Sherpa_222_NNPDF30NNLO_enugamma_pty_140_E_CMS.deriv.DAOD_HIGG8D1.e5928_e5984_s3126_r10724_r10726_p4133
 mc16_13TeV.364527.Sherpa_222_NNPDF30NNLO_munugamma_pty_15_35.deriv.DAOD_HIGG8D1.e5928_e5984_s3126_r10724_r10726_p4133
 mc16_13TeV.364528.Sherpa_222_NNPDF30NNLO_munugamma_pty_35_70.deriv.DAOD_HIGG8D1.e5928_e5984_s3126_r10724_r10726_p4133
 mc16_13TeV.364529.Sherpa_222_NNPDF30NNLO_munugamma_pty_70_140.deriv.DAOD_HIGG8D1.e5928_e5984_s3126_r10724_r10726_p4133
 mc16_13TeV.364530.Sherpa_222_NNPDF30NNLO_munugamma_pty_140_E_CMS.deriv.DAOD_HIGG8D1.e5928_e5984_s3126_r10724_r10726_p4133
 mc16_13TeV.364532.Sherpa_222_NNPDF30NNLO_taunugamma_pty_15_35.deriv.DAOD_HIGG8D1.e5928_e5984_s3126_r10724_r10726_p4133
 mc16_13TeV.364533.Sherpa_222_NNPDF30NNLO_taunugamma_pty_35_70.deriv.DAOD_HIGG8D1.e5928_e5984_s3126_r10724_r10726_p4133
 mc16_13TeV.364534.Sherpa_222_NNPDF30NNLO_taunugamma_pty_70_140.deriv.DAOD_HIGG8D1.e5928_e5984_s3126_r10724_r10726_p4133
 mc16_13TeV.364535.Sherpa_222_NNPDF30NNLO_taunugamma_pty_140_E_CMS.deriv.DAOD_HIGG8D1.e5928_e5984_s3126_r10724_r10726_p4133
 mc16_13TeV.410560.MadGraphPythia8EvtGen_A14_iZ_4fl_tchan_noAllHad.deriv.DAOD_HIGG8D1.e5803_e5984_s3126_r10724_r10726_p4133
 mc16_13TeV.410408.aMcAtNloPythia8EvtGen_tWZ_Ztoll_minDR1.deriv.DAOD_HIGG8D1.e6423_e5984_s3126_r10724_r10726_p4133
 mc16_13TeV.364242.Sherpa_222_NNPDF30NNLO_WWW_3l3v_EW6.deriv.DAOD_HIGG8D1.e5887_e5984_s3126_r10724_r10726_p4133
 mc16_13TeV.364243.Sherpa_222_NNPDF30NNLO_WWZ_4l2v_EW6.deriv.DAOD_HIGG8D1.e5887_e5984_s3126_r10724_r10726_p4133
 mc16_13TeV.364244.Sherpa_222_NNPDF30NNLO_WWZ_2l4v_EW6.deriv.DAOD_HIGG8D1.e5887_e5984_s3126_r10724_r10726_p4133
 mc16_13TeV.364245.Sherpa_222_NNPDF30NNLO_WZZ_5l1v_EW6.deriv.DAOD_HIGG8D1.e5887_e5984_s3126_r10724_r10726_p4133
 mc16_13TeV.364246.Sherpa_222_NNPDF30NNLO_WZZ_3l3v_EW6.deriv.DAOD_HIGG8D1.e5887_e5984_s3126_r10724_r10726_p4133
 mc16_13TeV.364247.Sherpa_222_NNPDF30NNLO_ZZZ_6l0v_EW6.deriv.DAOD_HIGG8D1.e5887_e5984_s3126_r10724_r10726_p4133
 mc16_13TeV.364248.Sherpa_222_NNPDF30NNLO_ZZZ_4l2v_EW6.deriv.DAOD_HIGG8D1.e5887_e5984_s3126_r10724_r10726_p4133
 mc16_13TeV.364249.Sherpa_222_NNPDF30NNLO_ZZZ_2l4v_EW6.deriv.DAOD_HIGG8D1.e5887_e5984_s3126_r10724_r10726_p4133
 mc16_13TeV.342284.Pythia8EvtGen_A14NNPDF23LO_WH125_inc.deriv.DAOD_HIGG8D1.e4246_e5984_s3126_r10724_r10726_p4133
 mc16_13TeV.342285.Pythia8EvtGen_A14NNPDF23LO_ZH125_inc.deriv.DAOD_HIGG8D1.e4246_e5984_s3126_r10724_r10726_p4133
 mc16_13TeV.341998.aMcAtNloHppEG_UEEEES_CTEQ6L1_CT10ME_iWH125_gamgam_yt_plus1.deriv.DAOD_HIGG8D1.e4394_e5984_s3126_r10724_r10726_p4133
 mc16_13TeV.410389.MadGraphPythia8EvtGen_A14NNPDF23_ttgamma_nonallhadronic.deriv.DAOD_HIGG8D1.e6155_e5984_s3126_r10724_r10726_p4133
 mc16_13TeV.410470.PhPy8EG_A14_ttbar_hdamp258p75_nonallhad.deriv.DAOD_HIGG8D1.e6337_e5984_s3126_r10724_r10726_p4133
 mc16_13TeV.410472.PhPy8EG_A14_ttbar_hdamp258p75_dil.deriv.DAOD_HIGG8D1.e6348_e5984_s3126_r10724_r10726_p4133
 mc16_13TeV.346343.PhPy8EG_A14NNPDF23_NNPDF30ME_ttH125_allhad.deriv.DAOD_HIGG8D1.e7148_e5984_s3126_r10724_r10726_p4133
 mc16_13TeV.346343.PhPy8EG_A14NNPDF23_NNPDF30ME_ttH125_allhad.deriv.DAOD_HIGG8D1.e7148_e5984_a875_r10724_r10726_p4133
 mc16_13TeV.346344.PhPy8EG_A14NNPDF23_NNPDF30ME_ttH125_semilep.deriv.DAOD_HIGG8D1.e7148_e5984_a875_r10724_r10726_p4133
 mc16_13TeV.346344.PhPy8EG_A14NNPDF23_NNPDF30ME_ttH125_semilep.deriv.DAOD_HIGG8D1.e7148_e5984_s3126_r10724_r10726_p4133
 mc16_13TeV.346345.PhPy8EG_A14NNPDF23_NNPDF30ME_ttH125_dilep.deriv.DAOD_HIGG8D1.e7148_e5984_a875_r10724_r10726_p4133
 mc16_13TeV.346345.PhPy8EG_A14NNPDF23_NNPDF30ME_ttH125_dilep.deriv.DAOD_HIGG8D1.e7148_e5984_s3126_r10724_r10726_p4133